MICROCOPY RESOLUTION TEST CHART

NATIONAL BUREAU OF STANDARDS 1963-A

THE BUCKLING OF COMPOSITE CYLINDRICAL

PANELS CONSIDERING ENVIRONMENTAL EFFECTS

THESIS

Anthony D. Straw

AFIT/GAE/AA/85D-15

DTIC
ELECTE
FEB 1 2 1986
S
B
D

DEPARTMENT OF THE AIR FORCE

AIR UNIVERSITY

AIR FORCE INSTITUTE OF TECHNOLOGY

Wright-Patterson Air Force Base, Ohio

AFIT/GAE/AA/85D-15

THE BUCKLING OF COMPOSITE CYLINDRICAL

PANELS CONSIDERING ENVIRONMENTAL EFFECTS

THESIS

Anthony D. Straw

AFIT/GAE/AA/85D-15

DTIC
ELECTE
FEB 1 2 1986

S D

B

THE BUCKLING OF COMPOSITE

CYLINDRICAL PANELS CONSIDERING

ENVIRONMENTAL EFFECTS
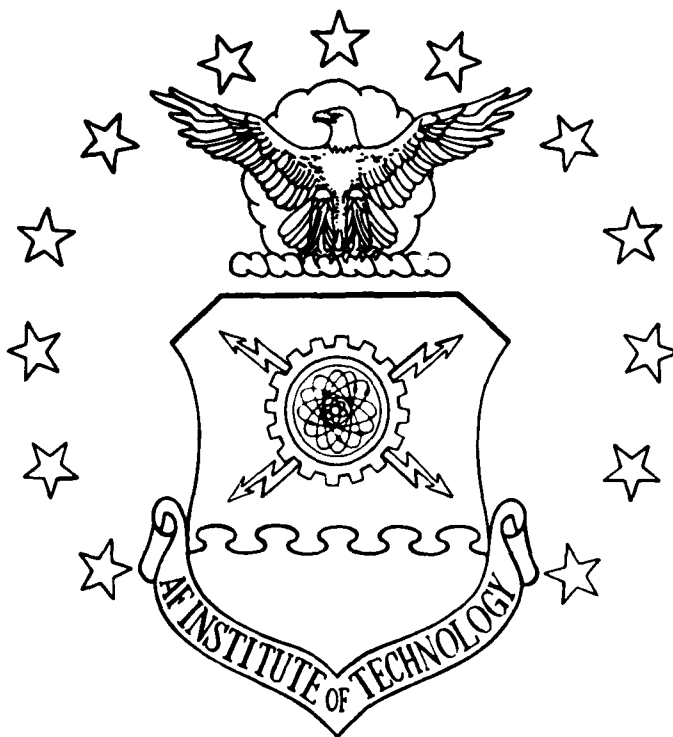
THESIS

Presented to the Faculty of the School of Engineering

of the Air Force Institute of Technology

Air University

In Partial Fulfillment of the

Requirements for the Degree of

Master of Science in Aeronautical Engineering

Anthony D. Straw, B.S.

December 1985

Acknowledgements

I would like to thank my advisor and committee chairman, Dr. Anthony Palazotto, for his professional guidance and instruction during the preparation of this thesis and throughout my time at AFIT. I am also thankful for the support and help I received from my remaining committee members, Capt Ronald Hinrichsen and Dr. Peter Torvik. I would like to extend a special note of appreciation to Dr. Peter Torvik, for his assistance in getting me accepted into AFIT so I could continue my education.

I would like to thank Dr. Donald Paul, from the Air Force Flight Dynamics Laboratory, for sponsoring this project and coming up with the computer time necessary to accomplish the work in this thesis.

I am grateful to the management of the Foreign Technology Division, particularly Mr. James Bartley, for allowing me the opportunity to pursue this degree under the Long-Term Full-Time Training Program.

But above all else, I would like to thank my wife, Barb, and daughter, Krisi, for their support and understanding throughout this endeavor.

A-1

Table of Contents

iv

List of Figures

LIST OF TABLES

Symbols

A_{ij}	Extensional stiffnesses
B_{ij}	Coupling stiffnesses
C	Moisture concentration
C_0, C_1, C_2	Moisture concentration initial conditions
D_{ij}	Bending stiffnesses
E_1	Longitudinal modulus of elasticity
E_2	Transverse modulus of elasticity
F	Degrees Fahrenheit
G_{12}	Shear modulus of elasticity
h	Laminate thickness
K	Diffusion coefficient
κ_x, κ_y, κ_{xy}	Curvatures
M_x, M_y, M_{xy}	Moment resultants
N_x, N_y, N_{xy}	Force resultants
$\overline{N}_x$	Bifurcation load for axial loading
$\overline{N}_{xy}$	Bifurcation load for shear loading
Q_{ij}	Reduced stiffnesses
$\overline{Q}_{ij}$	Transformed reduced stiffnesses
R, r	Panel's radius
RU, RV, RW	Rotations about the x, y, and z coordinate axes
t	Time
t^*	Dimensionless time
T_g	Glass transition temperature

u, v, w U, V, W	Displacements in the x, y, z directions, respectively
x, y, z	Spacial coordinates
X, Y, Z	Structural coordinate directions
1, 2, 3	Lamina principle axis directions
α	Angle of intersection of two flat plates
β, ϕ	Rotation
γ	Shear strain
ϵ	Normal strain
θ	Ply orientation
ν	Poisson's ratio
σ	Normal stress
τ	Shear stress
( ),( )	Comma denotes partial differentiation with respect to the subscript
( )^o	Zero superscript denotes a middle surface value
[ ]s	Denotes a ply orientation that is symmetric with respect to the middle surface

Abstract

An analytical study was conducted to determine the influence of
moisture, temperature, and curvature on the bifurcation load of
cylindrical, composite panels subjected to a simple shear loading. Two
laminate ply orientations, $[0/45/-45/90]_s$ and $[45/-45]_{2s}$, were analyzed
for six radii, four temperatures, and two initial moisture conditions.
The eight-ply composite panels were assumed to be manufactured from a
graphite/epoxy, AS/3501-5. To evaluate the influence of moisture and
temperature, the transverse modulus, E_2, and shear modulus, G_{12}, were
degraded based on experimental test data for the AS/3501-5 system. Each
ply orientation, for a 12 in. panel radius, was evaluated at 20
time/temperature conditions that ranged from 80 to 300°F, and moisture
concentrations ranging from a zero moisture content to an equilibrium
moisture distribution. The investigation of curvature was conducted
only for the $[45/-45]_{2s}$ laminate and at a limited number of
time/temperature conditions.

The bifurcation loads were determined using the STAGS-C1 finite
elements shell analysis program. This analysis used the prebuckled
linear displacement option to calculate the bifurcation loads. An
increase in temperature and moisture absorption was found to cause a
reduction in the panels bifurcation load ranging from a maximum of 25.6
percent for the $[0/45/-45/90]_s$ laminate to 34.5 percent for the
$[45/-45]_{2s}$ laminate for the panels with a 12 in. radius. This reduction

in the bifurcation load is significantly influenced by the change in curvature at elevated temperatures and moisture content. The maximum reduction in the bifurcation load varied from 34.5 percent for a 12 in. panel radius to 11.9 percent for a 10,000 in. panel radius a decrease of 22.6 percent for the $[45/-45]_{2s}$ laminate.

THE BUCKLING OF COMPOSITE

CYLINDRICAL PANELS CONSIDERING

ENVIRONMENTAL EFFECTS

I. Introduction

Background

Composite materials' high strength to weight ratio makes it
particularly well suited for aircraft structural use. The desire to
improve the efficiency of the structural design through the application
of composites in order to tailor the component's strength and stiffness
to match the load and stiffness requirements results in components with
unique structural responses. The USAF's forward swept aircraft design
is an excellent example of the materials' advantage in that, through
proper composite "tailoring", the problem of aeroelastic divergence can
be practically avoided without the enormous weight gain associated with
conventional metals. One difficulty in such applications of composites
is the inability to use conventional, classical structural design
practices to predict the structural response of composite laminates.
The fact that their stiffness can be oriented to preferred directions
make them complex structures to analyze.

In a semimonocoque design, thin skin panels along with fuselage
frames and longerons or wing skins with spars and ribs are used to

1

achieve an efficient structure. In such a design, the accurate
determination of the buckling load of curved skin panels is necessary to
prevent premature structural failure. It is stated in Ref. [1] that,
"Numerous papers concerning the instability of laminated, anisotropic
plates and shells can be found in the open literature. Buckling of
curved panels has, however, received little attention." This is
especially the case for shear buckling of curved panels. Some recent
work has been carried out on curved panels in order to evaluate their
buckling characterisitcs under compression loads [2-5]. From the
standpoint of shear instability of cylindrical composite panels, Harper
looked at shear buckling of circular cylindrical shells [6] and Whitney
examined shear buckling of symmetric and unsymmetric angle-ply,
graphite/epoxy curved plates[1].

Another aspect related to composite material research is the
consideration of moisture and temperature effects on the overall
structural characteristics. Snead and Palazotto examined the effects of
moisture and temperature on the instability of cylindrical composite
panels loaded in axial compression [7]. These influences, sometimes
referred to as hygrothermal effects, fall in the general category of
environmental influences. Hygrothermal effects have been found to
significantly degrade the mechanical properties of most organic matrix
compounds [7-21].

Purpose

The purpose of this thesis is to analytically evaluate the

2

instability of composite cylindrical panels subject to simple shear loading, using the STAGS-C1 finite element shell analysis program. The influence of moisture, temperature, and curvature on the panel's bifurcation load will be investigated using this finite element program.

Scope

The cylindrical panels evaluated in this thesis are 12 in. by 12 in., eight-ply laminates made of graphite/epoxy. The panel's thickness, width, and height are held constant while the radius, ply orientation, laminate temperature, and initial surface moisture conditions are varied. Six radii, two ply orientations, and a simple support boundary condition are investigated. During the investigation of the environmental influences, four temperatures and two surface moisture conditions, at five time values, are evaluated.

II. <u>Theory</u>

<u>Classical Laminated Plate Theory</u>

The analysis of any composite structure requires an understanding
of classical laminate plate theory (CLPT). A brief overview of the
basic principles will be presented here. For a more detailed analysis
of CLPT one should refer to any introductory text on composite
materials [22-23]. For a single orthotropic layer, the fiber oriented
reference system is shown in Figure 2.1. It will be the standard
used in this thesis.
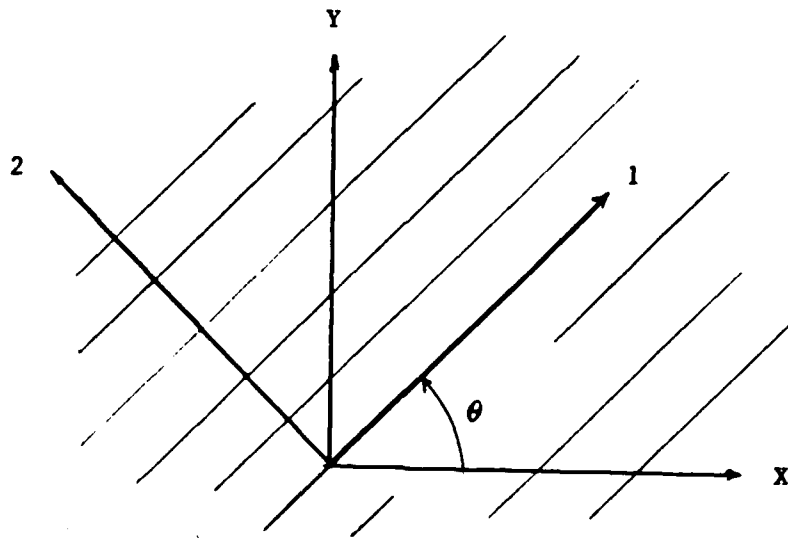
Figure 2.1 Definition of Coordinate System

The plane stress constitutive relations for an othotropic lamina can be written as:

$$\left\{\begin{matrix} \sigma_1 \\ \sigma_2 \\ \tau_{12} \end{matrix}\right\} = \begin{bmatrix} Q_{11} & Q_{12} & 0 \\ Q_{12} & Q_{22} & 0 \\ 0 & 0 & Q_{66} \end{bmatrix} \left\{\begin{matrix} \epsilon_1 \\ \epsilon_2 \\ \gamma_{12} \end{matrix}\right\} \qquad (1)$$

Where the Q_{ij}'s are the reduced stiffnesses and are defined in terms of the engineering constants as:

$$\begin{aligned}
Q_{11} &= E_1/(1-\nu_{12}\nu_{21}) \\
Q_{12} &= \nu_{12}E_2/(1-\nu_{12}\nu_{21}) = \nu_{21}E_1/(1-\nu_{12}\nu_{21}) \\
Q_{22} &= E_2/(1-\nu_{12}\nu_{21}) \\
Q_{66} &= G_{12}
\end{aligned} \qquad (2)$$

where

$$\begin{aligned}
\nu_{12} &= -\frac{\epsilon_2}{\epsilon_1} \\
\nu_{21} &= -\frac{\epsilon_1}{\epsilon_2} \\
G_{12} &= -\frac{\tau_{12}}{\gamma_{12}}
\end{aligned} \qquad (3)$$

In any other coordinate system with the fiber axis oriented at some angle θ with respect to the structural axes, the stresses are:

$$\left\{\begin{matrix} \sigma_x \\ \sigma_y \\ \tau_{xy} \end{matrix}\right\} = \begin{bmatrix} \overline{Q}_{11} & \overline{Q}_{12} & \overline{Q}_{16} \\ \overline{Q}_{12} & \overline{Q}_{22} & \overline{Q}_{26} \\ \overline{Q}_{16} & \overline{Q}_{26} & \overline{Q}_{66} \end{bmatrix} \left\{\begin{matrix} \epsilon_x \\ \epsilon_y \\ \gamma_{xy} \end{matrix}\right\} \qquad (4)$$

5

Where the $\overline{Q}_{ij}$'s are the transformed reduced stiffnesses:

$$\overline{Q}_{11} = Q_{11}\cos^4\theta + 2(Q_{12} + 2Q_{66})\sin^2\theta \cos^2\theta + Q_{22}\sin^4\theta$$

$$\overline{Q}_{12} = (Q_{11} + Q_{22} - 4Q_{66})\sin^2\theta \cos^2\theta + Q_{12}(\sin^4\theta + \cos^4\theta)$$

$$\overline{Q}_{22} = Q_{11}\sin^4\theta + 2(Q_{12} + 2Q_{66})\sin^2\theta \cos^2\theta + Q_{22}\cos^4\theta$$

$$\overline{Q}_{16} = (Q_{11} - Q_{12} - 2Q_{66})\sin\theta \cos^3\theta + (Q_{12} - Q_{22} + 2Q_{66})$$
$$\sin^3\theta \cos\theta \qquad\qquad (5)$$

$$\overline{Q}_{26} = (Q_{11} - Q_{12} - 2Q_{66})\sin^3\theta \cos\theta + (Q_{12} - Q_{22} + 2Q_{66})$$
$$\sin\theta \cos^3\theta$$

$$\overline{Q}_{66} = (Q_{11} + Q_{22} - 2Q_{12} - 2Q_{66})\sin^2\theta \cos^2\theta + Q_{66}(\sin^4\theta + \cos^4\theta)$$

To extend the stress-strain relationship to a multilayered laminate, two assumptions must be made. First, the laminate is assumed to have perfect bonds between the lamina so that no interlamina slipping can occur. Secondly, the Kirchhoff-Love hypothesis applies. This hypothesis states that normals to the mid-surface remain plane and normal to that surface after bending. These assumptions lead to the strain-curvature relationship for a laminate.

$$\left\{ \begin{array}{c} \epsilon_x \\ \epsilon_y \\ \gamma_{xy} \end{array} \right\} = \left\{ \begin{array}{c} \epsilon_x^o \\ \epsilon_y^o \\ \gamma_{xy}^o \end{array} \right\} + Z \left\{ \begin{array}{c} \kappa_x \\ \kappa_y \\ 2\kappa_{xy} \end{array} \right\} \qquad\qquad (6)$$

Where the o superscript indicates the mid-surface strains, the κ's are mid-surface curvatures and Z (See Figure 2.2) represents a distance from the panel's mid-surface.

6
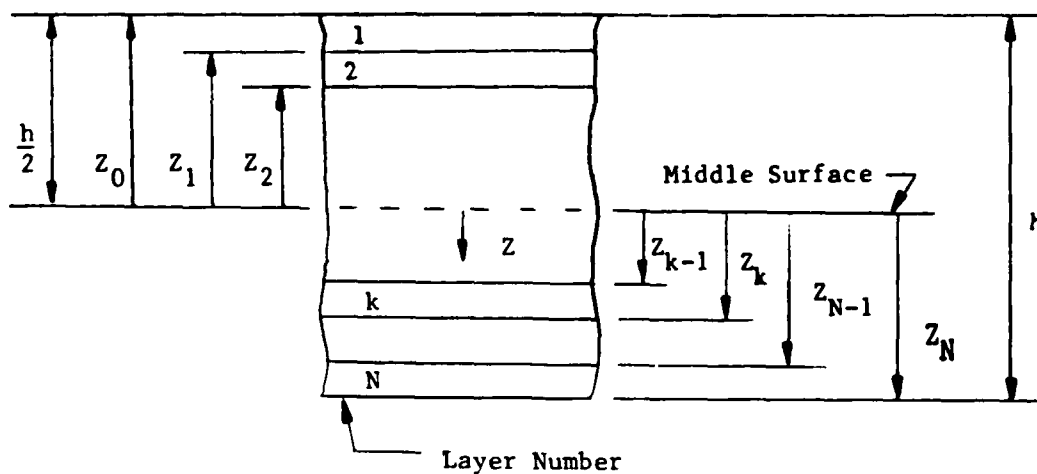
Figure 2.2 Geometry of an N-Layered Laminate

For a cylindrical panel with moderately large displacements and also moderately large rotations of tangents to its mid-surface, the above strains and curvatures are given by Sanders' kinematic relations without initial imperfections [24] as

$$\epsilon_x^o = u_{,x} + \frac{1}{2}\phi_x + \frac{1}{2}\phi^2$$

$$\epsilon_y^o = v_{,y} + \frac{w}{r} + \frac{1}{2}\phi_y^2 - \frac{1}{2}\phi^2$$

$$\gamma_{xy}^o = v_{,x} + u_{,y} + \phi_x \phi_y$$

$$\kappa_x = \phi_{x,x}$$

$$\kappa_y = \phi_{y,y}$$

$$2\kappa_{xy} = \phi_{y,x} + \phi_{x,y} + \frac{\phi}{r}$$

(7)

Where u, v, and w are the axial, circumferential, and radial components of displacement, respectively, of the panel's mid-surface. The ϕ's are

rotational components and are expressed in terms of the displacements as:

$$\phi_x = - w,_x$$

$$\phi_y = - w,_y + \frac{v}{r} \tag{8}$$

$$\phi = \frac{1}{2}(v,_x - u,_y)$$

where r is the panel's radius of curvature.

If Eq. (6) is substituted into Eq. (4), the stresses in the kth layer can be expressed in terms of the laminate mid-surface strains and curvatures as:

$$\begin{Bmatrix} \sigma_x \\ \sigma_y \\ \tau_{xy} \end{Bmatrix}_k = \begin{bmatrix} \overline{Q}_{11} & \overline{Q}_{12} & \overline{Q}_{16} \\ \overline{Q}_{12} & \overline{Q}_{22} & \overline{Q}_{26} \\ \overline{Q}_{16} & \overline{Q}_{26} & \overline{Q}_{66} \end{bmatrix}_k \left\{ \begin{Bmatrix} \epsilon_x^o \\ \epsilon_y^o \\ \gamma_{xy}^o \end{Bmatrix} + z \begin{Bmatrix} \kappa_x \\ \kappa_y \\ 2\kappa_{xy} \end{Bmatrix} \right\} \tag{9}$$

The resultant forces and moments acting on a laminate can now be found by integration of the above stresses in each lamina through the laminate thickness. Denoting the in-plane ply stress by σ_i, then

$$(N_i, M_i) = \int_{-t/2}^{t/2} \sigma_i (1,z) \, dz \tag{10}$$

where N_i and M_i are the force and moment per unit length (width) of the cross-section of the laminite as shown in Figure 2.3.
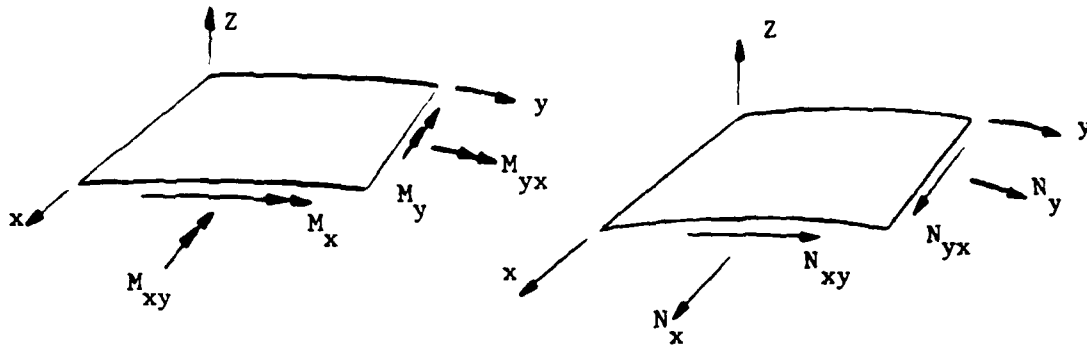
Figure 2.3   Forces and Moments on a Laminate

The forces and moments shown in Figure 2.3 can be written as:

$$
\begin{Bmatrix} N_x \\ N_y \\ N_{xy} \end{Bmatrix} = \int_{-h/2}^{h/2} \begin{Bmatrix} \sigma_x \\ \sigma_y \\ \tau_{xy} \end{Bmatrix}_k dZ = \sum_{n=1}^{N} \int_{Z_{k-1}}^{Z_k} \begin{Bmatrix} \sigma_x \\ \sigma_y \\ \tau_{xy} \end{Bmatrix}_k dZ
\tag{11}
$$

and

$$
\begin{Bmatrix} M_x \\ M_y \\ M_{xy} \end{Bmatrix} = \int_{-h/2}^{h/2} Z \begin{Bmatrix} \sigma_x \\ \sigma_y \\ \tau_{xy} \end{Bmatrix}_k dZ = \sum_{n=1}^{N} \int_{Z_{k-1}}^{Z_k} Z \begin{Bmatrix} \sigma_x \\ \sigma_y \\ \tau_{xy} \end{Bmatrix}_k dZ
\tag{12}
$$

where N is the total number of laminae, and Z_k and Z_{k-1} are defined in Figure 2.2.

The integration indicated by Eq's. (11) and (12) can be rearranged to take advantage of the fact that the stiffness matrix, $[\overline{Q}_{ij}]$, for each lamina is constant within that layer. Therefore, the stiffness

9

matrix can be removed from behind the integration but remains within the summation sign. Also note that mid-plane strains and curvatures are independent of Z and can also be removed from the integration and summation. Thus, the force and moment resultants can be written as:

$$\begin{Bmatrix} N_x \\ N_y \\ N_{xy} \end{Bmatrix} = \begin{bmatrix} A_{11} & A_{12} & A_{16} \\ A_{12} & A_{22} & A_{26} \\ A_{16} & A_{26} & A_{66} \end{bmatrix} \begin{Bmatrix} \epsilon_x^o \\ \epsilon_y^o \\ \gamma_{xy}^o \end{Bmatrix} + \begin{bmatrix} B_{11} & B_{12} & B_{16} \\ B_{12} & B_{22} & B_{26} \\ B_{16} & B_{26} & B_{66} \end{bmatrix} \begin{Bmatrix} \kappa_x \\ \kappa_y \\ \kappa_{xy} \end{Bmatrix} \qquad (13)$$

$$\begin{Bmatrix} M_x \\ M_y \\ M_{xy} \end{Bmatrix} = \begin{bmatrix} B_{11} & B_{12} & B_{16} \\ B_{12} & B_{22} & B_{26} \\ B_{16} & B_{26} & B_{66} \end{bmatrix} \begin{Bmatrix} \epsilon_x^o \\ \epsilon_y^o \\ \gamma_{xy}^o \end{Bmatrix} + \begin{bmatrix} D_{11} & D_{12} & D_{16} \\ D_{12} & D_{22} & D_{26} \\ D_{16} & D_{26} & D_{66} \end{bmatrix} \begin{Bmatrix} \kappa_x \\ \kappa_y \\ \kappa_{xy} \end{Bmatrix} \qquad (14)$$

where:

$$A_{ij} = \sum_{k=1}^{N} (\overline{Q}_{ij})_k (Z_k - Z_{k-1})$$

$$B_{ij} = \frac{1}{2} \sum_{k=1}^{N} (\overline{Q}_{ij})_k (Z_k^2 - Z_{k-1}^2) \qquad (15)$$

$$D_{ij} = \frac{1}{3} \sum_{k=1}^{N} (\overline{Q}_{ij})_k (Z_k^3 - Z_{k-1}^3)$$

The A_{ij}'s are called extensional stiffnesses, the B_{ij}'s are called bending-extensional coupling stiffnesses, and the D_{ij}'s are called bending stiffness. For a linear analysis the mid-surface strains and curvatures can be expressed in terms of the displacements by substituting Eq. (8) into Eq. (7) to yield

10

$$\begin{Bmatrix} \epsilon_x^o \\ \epsilon_y^o \\ \gamma_{xy}^o \\ \kappa_x \\ \kappa_y \\ 2\kappa_{xy} \end{Bmatrix} = \begin{Bmatrix} u,_x \\ v,_y + \dfrac{w}{r} \\ v,_x + u,_y - w,_x \dfrac{v}{r} \\ - w,_{xx} \\ - w,_{yy} + \dfrac{v,_y}{r} \\ - w,_{yx} + \dfrac{v,_x}{r} - w_{xy} + \dfrac{1}{2}(v,_x - u,_y)/r \end{Bmatrix} \tag{16}$$

where the non-linear terms have been left-off.

STAGS-C1 Theory

The Structural Analysis of General Shells (STAGS-C1) is a computer code developed by the Lockhead Palo Alto Research Laboratory to analyze general shells under various static, thermal, and mechanical loading [25-26]. The approach used by STAGS-C1 to solve these problems is an energy-based finite element analysis. According to the energy method, a system's total potential energy is used to derive its equilibrium equations from which stability can be determined by the solution to an eigenvalue problem.

A shell's total potential energy, V, is equal to its internal strain energy minus the product of the external forces and their respective deflections. This can be written as [27]:

$$V = \frac{1}{2}\langle d \rangle^T [K]\langle d \rangle - d^T \langle R1 \rangle \tag{17}$$

11

where $\langle d \rangle$ is the vector of nodal degrees of freedom of the structure,
[K] is the structural stiffness matrix, and $\langle R1 \rangle$ is the structural applied
load vector.

An element's strain energy, U, is given by [24]:

$$U = \frac{1}{2} \int_{area} \langle \epsilon \rangle_o^T \begin{bmatrix} [A] & [B] \\ [B] & [D] \end{bmatrix} \langle \epsilon \rangle_o dA \qquad (18)$$

where $\langle \epsilon \rangle_o$ is the mid-plane strain and curvature vector given by Eq. (7)
and [A], [B],[D] are the 3 x 3 stiffness matrices given by Eq's. (13)
and (14).

In general, the strain vector $\langle \epsilon \rangle_o$ is a function of the mid-surface
displacements (u, v, and w), the first order partial derivatives of u,
v, and w with respect to x and y, and the second order partial
derivatives of w with respect to x and y. Bauld [24] carried out the
integration of Eq. (18) using the terms from Eq. (7) for $\langle \epsilon \rangle_o$ and found
that the expression for strain energy is comprised of three distinct
parts. The first part is quadratic, the second part is cubic, and the
third part is quartic in displacements. This result can be written in
terms of the appropriate element shape functions and nodal degrees of
freedom.

By using a similar finite element analysis on the element's external
forces the element's external potential energy can be obtained. This
combined with the strain energy gives the total system potential energy
Eq. (17) and can be written in the form given by Bauld [24] as:

$$V = (1/2H_{rs} + 1/6N1_{rs} + 1/12N2_{rs})d_r d_s - R_s d_s \qquad (19)$$

where the structural nodal degrees of freedom are replaced by the displacement vector, d. H_{rs} is the system's linear stiffness matrix with no dependence on the displacement vector, d. $N1_{rs}$ and $N2_{rs}$ are matrices with linear and quadratic dependence, respectively, on displacement. R_s is the surface force vector.

The principle of total potential energy states that the equilibrium configuration of a conservative mechanical system corresponds to a stationary value of the total potential energy of the system [27]. Therefore, taking the first variation of Eq. (19) and setting it equal to zero, one obtains a set of nonlinear, algebraic equations of the form:

$$(H_{rs} + 1/2N1_{rs} + 1/3N2_{rs})d_s - R_r = 0 \qquad (20)$$

The loss of stability (collapse), results when the second variation of the system's total potential energy ceases to be positive definite, or:

$$DET(H_{rs} + N1_{rs} + N2_{rs}) = 0 \qquad (21)$$

Equation (21) is used by STAGS-C1 to solve the eigenvalue problem of the form [28]:

$$[H] + \lambda[I] + \lambda^2[J] = 0 \qquad (22)$$

13

Where [I] and [J] represent nonlinear stiffness matrices in unknown displacements and products of displacements, respectively. For a linear analysis, λ, is the proportionality constant of a convenient load level used in the equilibrium Eq's. (20) to solve for the unknown displacements. Also the J matrix, which arises from the prebuckling rotations, is omitted. The quantities H, I, J, or equivalently, H_{rs}, $N1_{rs}$, and $N2_{rs}$ are calculated once based on the equilibrium displacements. Finally, the load proportionality parameter, λ, is incremented until a sign change on the left side of Eq. (21) occurs, signifying bifurcation.

III.   Finite Element Modeling

This thesis will evaluate the stability of cylindrical composite
panels that are subjected to a simple shear load. Such a panel would be
representative of an aircraft fuselage skin panel. The STAGS-C1
requires the user to input the type of shell surface geometry. To model
the cylindrical panels and to allow for different radii of curvature,
the STAGS-C1 cylindrical shell geometry was selected. (See Figure 3.1).
In Figure 3.1 U, V, and W represent the displacements in the X, Y, and Z
directions, respectively and RU, RV, and RW represent the rotations
about the X, Y, and Z coordinate axes, respectively.
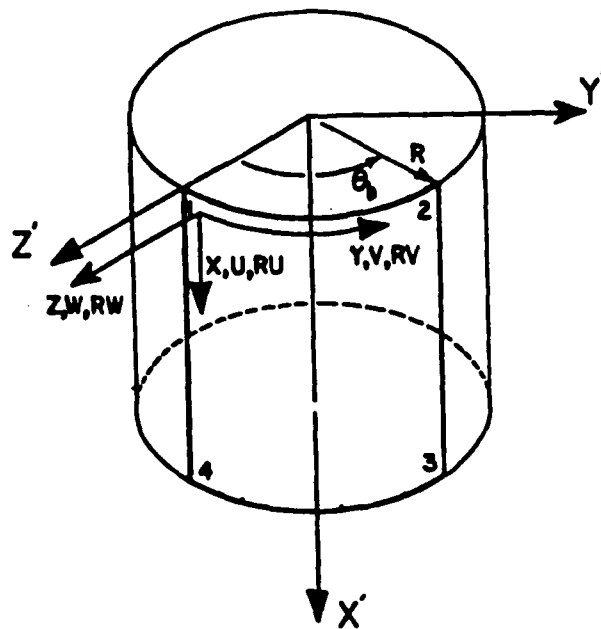
Figure 3.1   STAGS-C1 Cylindrical Shell Geometry

15

This study also required the equivalant of a flat plate. To model this, using the cylindrical shell geometry model, a study was run to determine what value of R would correspond to ∞. For a symmetric laminate, a radius of 10,000 in. gave values within 0.02 percent of STAGS-C1 flat plate geometry.

Boundary Conditions and Loading

The boundary conditions used in the bifurcation analysis were selected to represent simple shear in a flat plate. The boundary conditions (See Figure 3.1) assumed that the structure's ring frames and stringers were effective in restraining out-of-plane deflections (W), also the top and bottom frames restrained the rotational movement about the X-axis (RU) and the two sides stringers restrained the rotational movement about the Y-axis (RV). The boundary conditions are summarized in Table 1, where 0 represents a fixed displacement and 1 represents a free displacement along the panel's edges. These values were used for both the pre- and post-buckle boundary conditions.

Table 2.1

Panel Boundary Conditions

	U	V	W	RU	RV	RW
Top	1	1	0	0	1	1
Right Side	1	1	0	1	0	1
Bottom	0	0	0	0	1	1
Left Side	1	1	0	1	0	1

To input a simple shear load into the panel, line loads (N_{xy} and N_{yx}) were applied to all four edges (See Figure 3.2). They were assumed to act uniformly along all sides of the panel which in a flat plate would represent a simple shear loading.
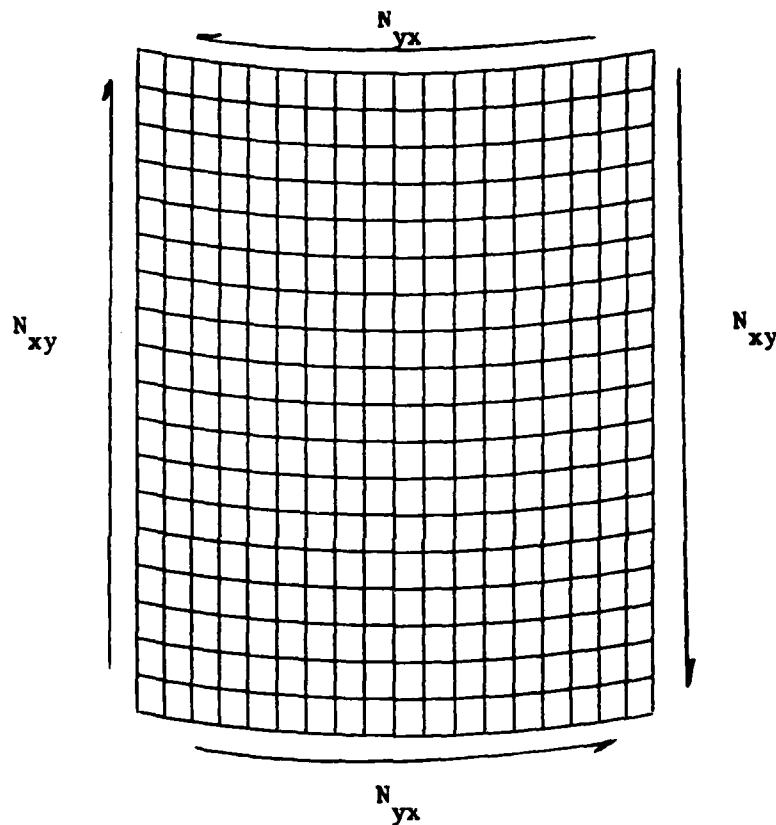
Figure 3.2 Finite Element Grid

Grid Size

The determination of a finite element grid size is a trade-off between cost and accuracy. Nelson [29] found that to obtain accurate results, there should be at least five node points per each half sine

wave of the buckled pattern in the circumferential direction. Several
papers [2, 3,and 7] indicate that for the panel used in this analysis
a grid of 0.5 x 0.5 in. elements represent a good trade-off between
accuracy and computer economics. For the 12.0 x 12.0 in. panel, used in
this analysis, a 0.5 x 0.5 in. element would correlate to a mesh of 24 x
24 elements or a total of 576 elements and 625 nodes. Due to the large
number of computer runs needed to complete this analysis, it was decided
to increase the element size to 2/3 x 2/3 in. which correlates to a mesh
of 18 x 18 elements or a total of 324 elements and 361 nodes. (See
Figure 3.2) Computer runs showed that this still gave five nodes per
each half sine wave and reduced the cost per run by 2.3 times. To
varify that this reduction would still yield valid results, a
convergence study was run which showed that the difference between the
bifurcation loads for the 324 elements and 576 elements is approximately
0.24 percent which was well within engineering accuracy.

Finite Element Selection

The STAGS-C1 finite elements program, as used in this analysis, uses
flat elements to model curved surfaces. Figure 3.3 illustrates how a
cylindrical surface can be modeled with flat elements. The use of flat
elements presents conformity problems which are important when dealing
with nonlinear and stability problems. Compatibility problems develop
for both the rotational and displacement degrees of freedom at the nodes.

The rotational problem is dealt with by assuming that the angle of
intersection α is small, and, as a consequence, the normal rotation β_z

18
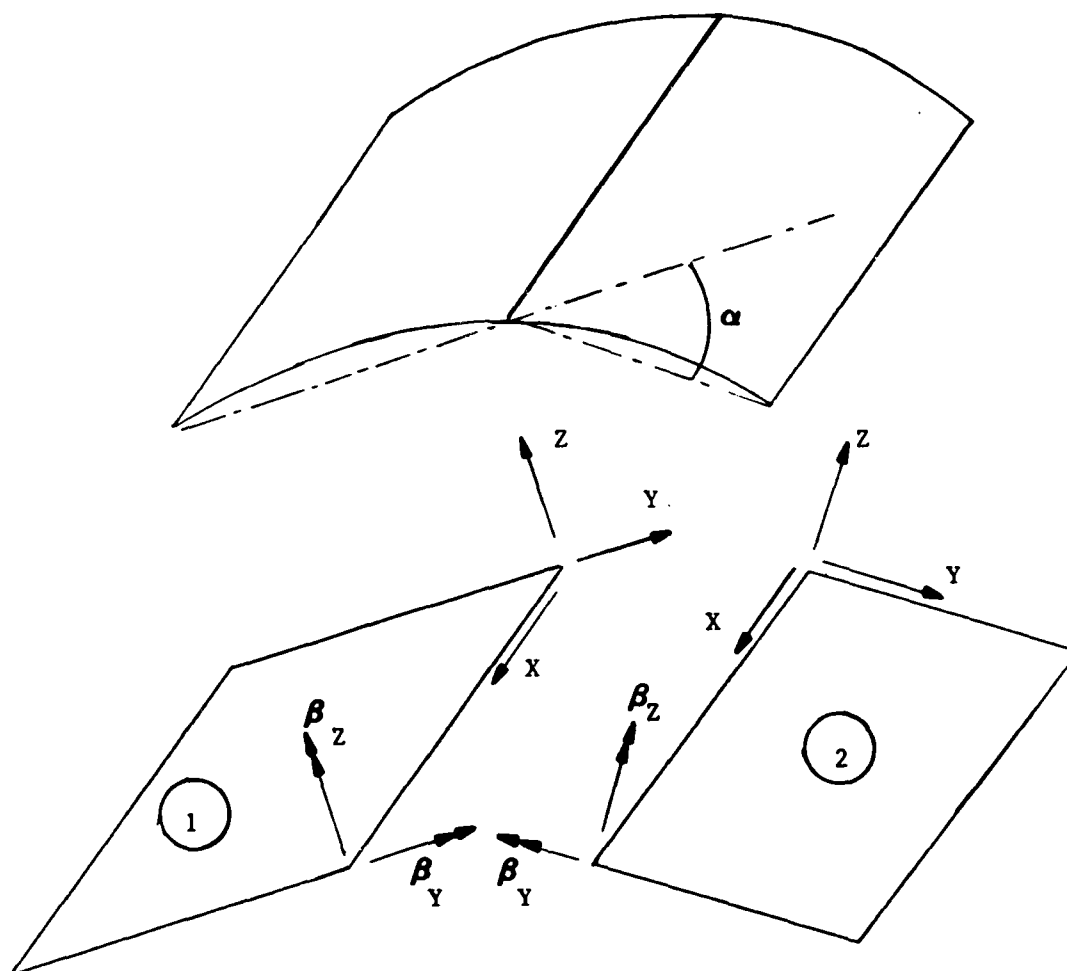
Figure 3.3 Modeling of Cylindrical Shell with Flat Plates

is ignored while the conformity constraint is satisfied by letting $\beta_y^{(1)} = \beta_y^{(2)}$.

Complete displacement compatability along the common boundary requires that:

$$(v^{(1)} - v^{(2)}) \cos (\alpha/2) - (w^{(1)} + w^{(2)}) \sin (\alpha/2) = 0$$
$$(w^{(1)} - w^{(2)}) \cos (\alpha/2) + (v^{(1)} + v^{(2)}) \sin (\alpha/2) = 0 \tag{23}$$

Where v and w are the displacements in the y and z directions, respectively. These conditions will not be met if v and w are not represented by polynomials of the same order. To satisfy this requirement, additional degrees of freedom are added to the element to raise the order of the polynomials representing the inplane deformation. Since w is represented by a cubic polynomial, because the strain energy expression includes second order derivatives of the transverse displacement w, it is necessary that u and v also be represented by cubic polynomials. This is achieved by the use of two rotations at each corner node, $- v_{,x}$ and $u_{,y}$, and tangential displacements at mid-side nodes. The difference between these two rotations yields a shear strain at each corner node, which is introduced as an additional degree of freedom. Thus, each element has a total of 32 degrees of freedom. In STAGS-C1 this element is referred to as the SH411. (See Figure 3.4)

A somewhat simpler version of the SH411 element, the SH410 element, is also included for thin shell analysis. This element excludes the

20
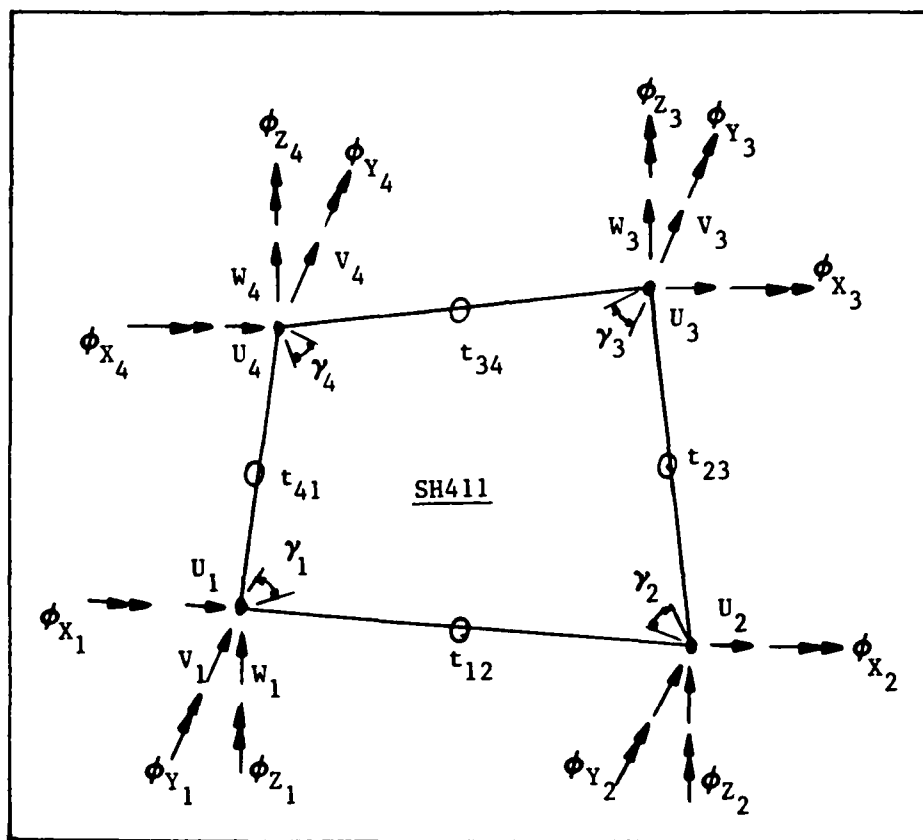
Figure 3.4   SH411 Element

21
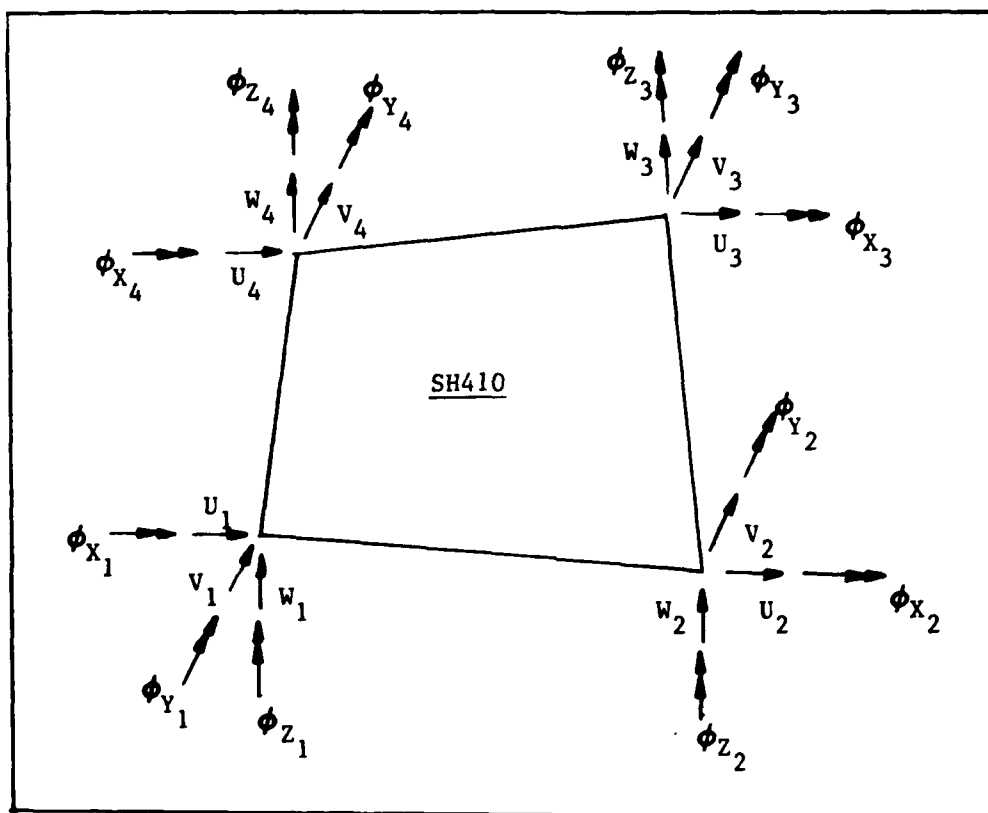
Figure 3.5   SH410 Element

mid-side tangential displacements and uses only an average normal rotation at each of the corner nodes. This restricts u to a linear function in the x-direction and v to a linear function in the y-direction. Also the shear strain is suppressed at the corner nodes. (See Figure 3.5) Because of this the SH410 element is an incompatible element, but it still yields valid results for some problems. For a more thorough explanation of these elements development, the reader should refer to Reference [30] and [31].

To help assist in the decision of which element to use, a small convergence study was conducted for both elements (See Figure 3.6 and 3.7). The geometric radius was selected to be 24 in. for the 12 in. x 12 in. panel. Figure 3.6 showes the differences between the eigenvalues for the SH411 and SH410 elements verses the number of elements in the grid. The SH410 converges to a slightly higher value (about 1.6 percent higher at 324 elements) than the SH411. The reason for this is that the SH410 produces a stiffer element than the SH411 due to it's incompatibility. Figure 3.7 shows a 8.2 percent difference in the bifurcation load, $\overline{N}_{xy}$, at 324 elements. The values for $\overline{N}_{xy}$ were calculated by multipuling the eigenvalues by the internal resulting force N_{xy}. This force was calculated by STAGS based on the applied load and the element selected. For this analysis a unit line load N_{xy} was applied to the boundaries. Therefore, the difference between the SH410 and SH411 values in Figure 3.7 was due to the differences in the elements and how STAGS distributed the load through the panel. Since the SH410 suppresses the shear strain at the nodes, it requires a higher shear load to produce bifurcation.

23
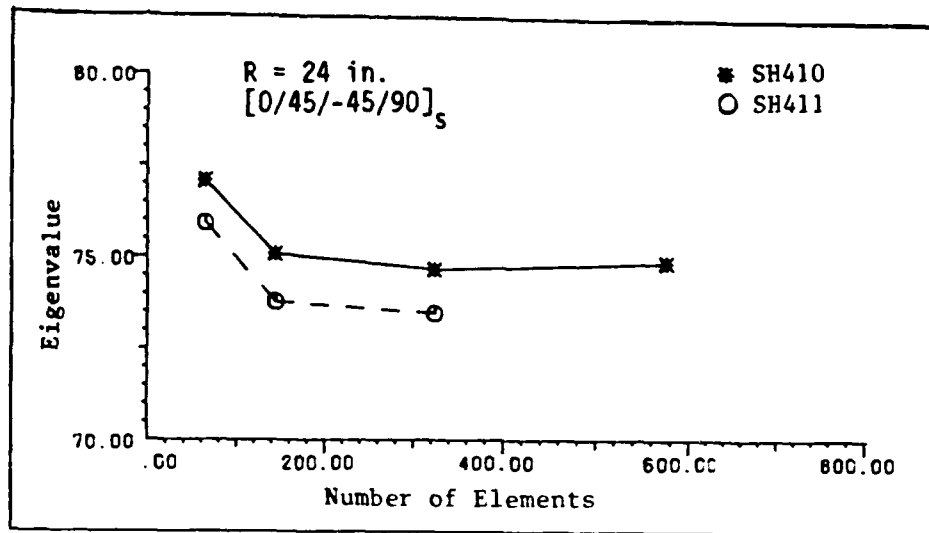
Figure 3.6 Convergence Comparison for the Eigenvalue
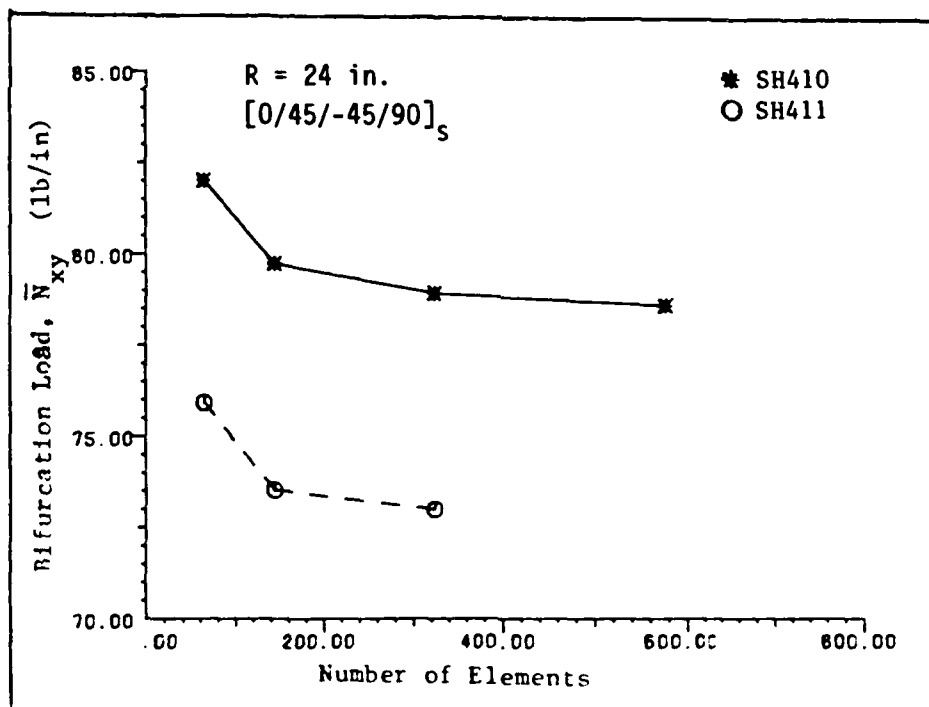
Figure 3.7 Convergence Comparison for the Bifurcation Load, $\overline{N}_{xy}$

24

Even though the SH410 element does not perform as well as the SH411, it was selected for use in this analysis when evaluating the influence of hygrothermal and curvature effects. Part of this reason is cost. The SH411 cost between 2 and 2.5 times that of SH410 run. The other reason is that this analysis is interested in the trends, so when the bifurcation load is normalized with respect to the room temperature and zero moisture values, the differences in the bifurcation load reduces to a ratio of the eigenvalues and the error divides out.

Bifurcation Analysis Method

STAGS-C1 has two buckling analysis modes. One uses a linear, pre-buckling displacements state and is referred to in the STAGS-C1 manual as the bifurcation analysis with a linear stress state. The second method uses a geometric pre-buckling, nonlinear displacement calculation and is referred to as the bifurcation analysis with a non-linear displacement state. For this study the bifurcation analysis with a linear stress state will be used. This method will calculate the pre-buckling displacements and rotations, stress resultants, strains, and stresses as desired. It also predicts the bifurcation eigenvalue and the shape of the eigenvector. It does not yield any post-buckling information.

Validation of Model

To check the boundary conditions, loading, and how well STAGS predicts buckling with bending-extensional coupling, the finite element

25

model was compared to a Galerkin solution obtained by Whitney [1]. In his paper, he presented an analytical solution for the buckling of anisotropic cylindrical plates under arbitrary combinations of axial load, internal pressure, and in-plane shear load. He used the Donnell equations, as they are applied to laminated cylindrical shallow panels, in conjunction with the Galerkin method to determine the critical buckling loads. Two of his solutions were selected to check the finite element model. One related to the effects of bending-twisting coupling and the second related to the effects of bending-extensional coupling.

This comparison considered two 12-layer angle-ply laminates with the stacking geometries $[+45_3/-45_3]_s$ and $[+45_6/-45_6]$ under pure in-plane shear loading. The panels were 18 x 18 in. square with a thickness of h = 0.06 in. In order to keep the same number of elements, the grid spacing was increased to 1 in. x 1 in., which still gave five nodes per half sine wave. The buckling boundary conditions also had to be changed in STAGS to the simple support boundary conditions referred to as BC-1 to correlate to Whitney's work. These boundary conditions are:

At x = 0, 18 in.

$$N_n = M_n = V = W = 0$$

(24)

and at y = 0, 18 in.

$$N_n = M_n = U = W = 0$$

The Galerkin method satisfies the natural boundary conditions. Whitney also used the following ply properties for his laminates:

26

$$E_1/E_2 = 14.0, \quad G_{12}/E_2 = 0.5, \quad \nu_{12} = 0.25 \qquad (25)$$

which are typical properties of current graphite/epoxy composite materials. These values had to be modified somewhat for input into the STAGS program to give:

$$E_1 = 14 \times 10^6 \text{ psi}$$
$$E_2 = 1 \times 10^6 \text{ psi}$$
$$G_{12} = 0.5 \times 10^6 \text{ psi} \qquad (26)$$
$$\nu_{12} = 0.25$$

which yeilds Whitney's ratios.

Figure 3.8 shows the comparison for the model studying the effects of bending-twisting coupling. The two sets of curves correspond to a + or − shear load. The symmetric lay-up $[+45_3/-45_3]_s$ eliminates all B_{ij}'s from Eqn's (13) an (14) along with A_{16} and A_{26}, but leaves in the bending-twisting coupling terms D_{16} and D_{26}. Since Whitney used the Donnell equations as shown

$$
\begin{Bmatrix}
\epsilon_x^o \\
\epsilon_y^o \\
\gamma_{xy}^o \\
\kappa_x \\
\kappa_y \\
2\kappa_{xy}
\end{Bmatrix}
=
\begin{Bmatrix}
u_{,x} \\
v_{,y} + w/R \\
v_{,x} + u_{,y} \\
- w_{,xx} \\
- w_{,yy} \\
- 2w_{,xy}
\end{Bmatrix}
\qquad (27)
$$

He had to restrain the radius parameter in order to keep the assumptions used by the Donnell equations valid. The smallest radius
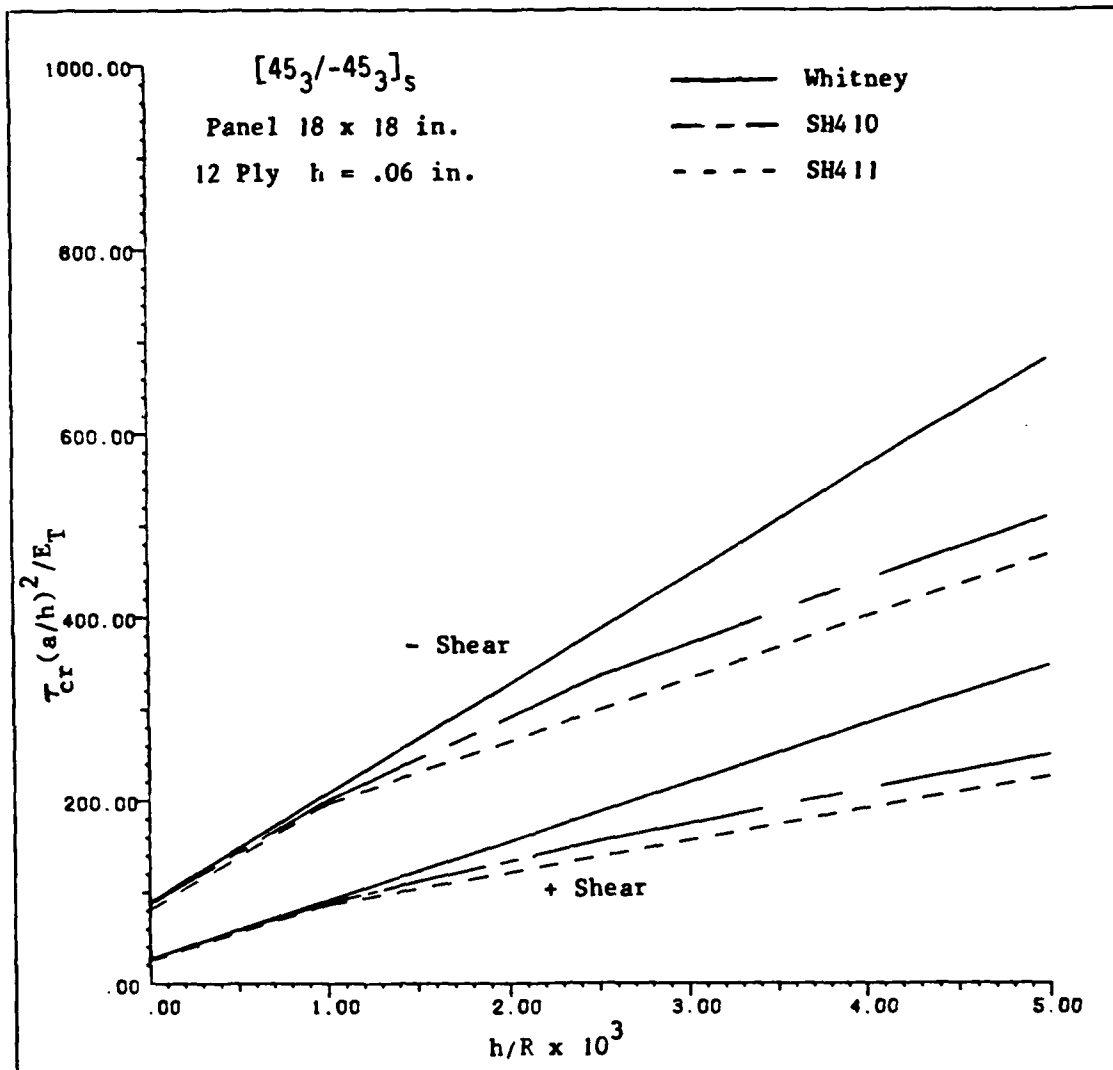
Figure 3.8 STAGS-C1 Finite Element vs Whitney's Galerkin, $[45_3/-45_3]_s$

28

he investigated was for an R = 60 in., which correlates to a h/R x 10^3 of 1.0. Whitney's work was extrapolated linearly down to a radius of 12 in. for comparison purposes. This is possible because Donnell's equations are linear in R. Both STAGS elements SH410 and SH411 correlate to what Whitney found in the range from R = 60 to ∞. What differences were found came about because Whitney was able to input a pure shear load, N_{xy}, into his equations and zero out all remaining resultant forces and moments. With STAGS the input of a pure shear load also generates some additional resultant forces and moments which contribute to reduce the bifurcation load. The deviation between the extrapolated Whitney and STAGS solutions is primarily due to the use in STAGS of the general shell equations:

$$
\begin{Bmatrix}
\epsilon^o_x \\
\epsilon^o_y \\
\gamma^o_{xy} \\
\kappa_x \\
\kappa_y \\
2\kappa_{xy}
\end{Bmatrix}
=
\begin{Bmatrix}
u,_x \\
v,_y + w/R \\
v,_x + u,_y - \underline{w,_x\, v/R} \\
- w,_{xx} \\
- w,_{yy} - \underline{w,_y/R} \\
- 2w,_{xy} + \underline{v,_x/2R} + \underline{(v,_x - u,_y)/2R}
\end{Bmatrix}
\tag{16}
$$

The underlined terms are functions of the radius which are not found in Donnell's equation and come into play as the radius decreases. The use of the Donnell equation for a radius of 12 in. would introduce an error from 34 - 39 percent if compared to the SH410 element and from 45 - 54 percent if compared to the SH411 element.

Figures 3.9, 3.10, 3.11 show the comparison for the model studying
the effects of bending-extensional coupling with Figure 3.11 being a
combination of Figures 3.9 and 3.10. The unsymmetric lay-up
$[+45_6/-45_6]$ eliminates A_{16}, A_{26}, D_{16}, and D_{26} along with all the B_{ij}'s
except B_{16} and B_{26}, the bending-extensional coupling terms, from Eqn's
(13) and (14). One can see that similar conclusions can be reached
from these curves. The main difference is that the prebuckle
displacements, forces, and moments play a much more important role in
this lay-up no matter what the curvature since they can not be removed
from the STAGS runs. Again, using the Donnell equation for a radius of
12 in. would introduce an error of around 59 percent if compared to
the SH410 element and around 79 percent if compared to the SH411
element. Again, if the correct value for the bifurcation load is
needed the SH411 should be used as found in the bending-twisting
components and the convergence test.

The influence of hygrothermal effects can develop bending –
extensional coupling in symmetric lay-ups. This analysis indicates
that the model selected for this thesis should give a good indication of
the influence of hygrothermal and curvature effects on cylindrical
composite panels loaded in shear if the curvature is greater than
R = 60 in. Also since the bifurcation load, $\overline{N}_{xy}$, will be normalized in
this thesis for analysis of the effects of hygrothermal and curvature,
the use of the SH410 instead of the SH411 will not influence the
outcome of the analysis when comparing a curvature down to R = 12 in.

30
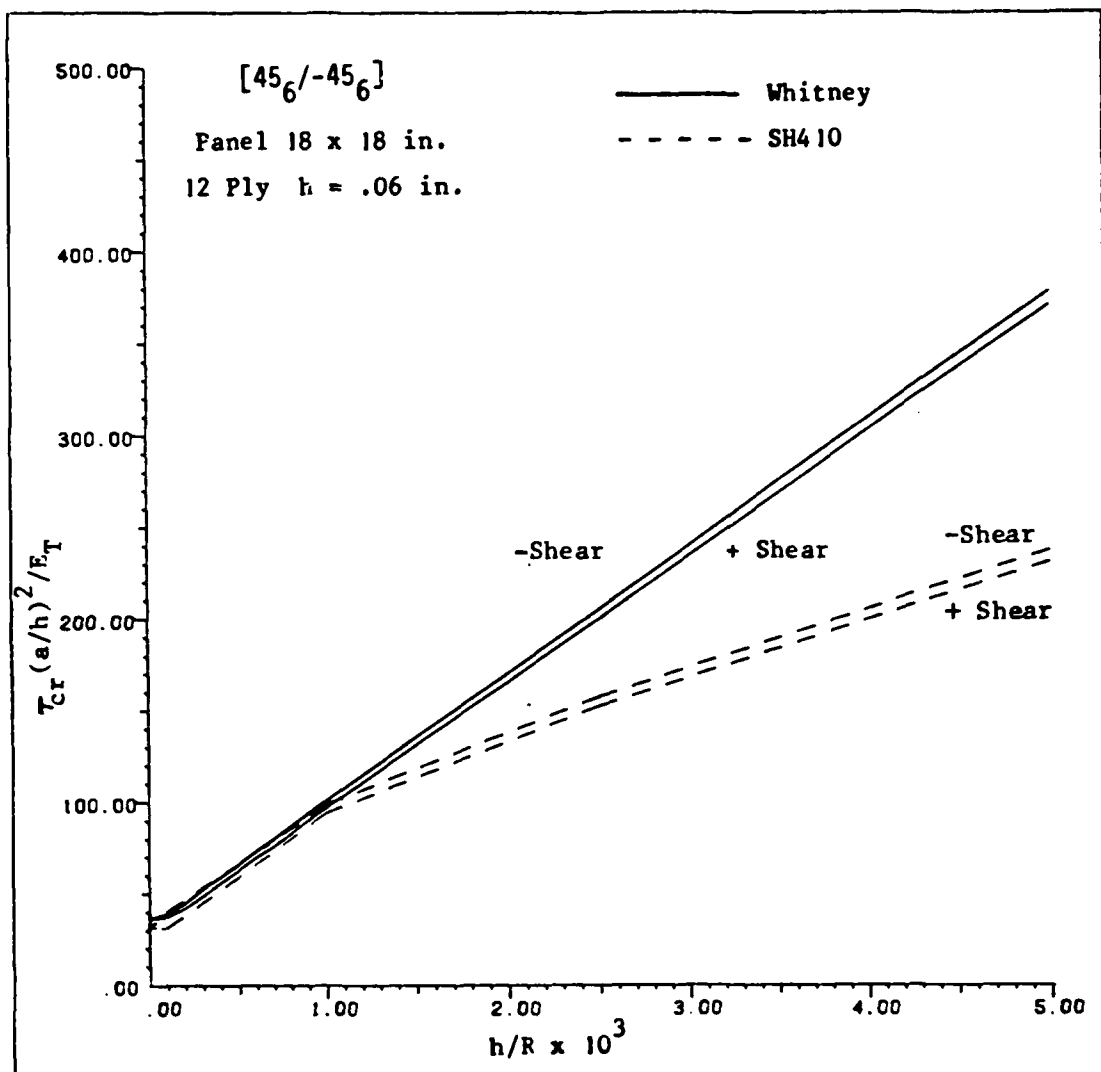
Figure 3.9 STAGS-C1 Finite Element (SH410) vs Whitney's
Galerkin, $[45_6/-45_6]$

31
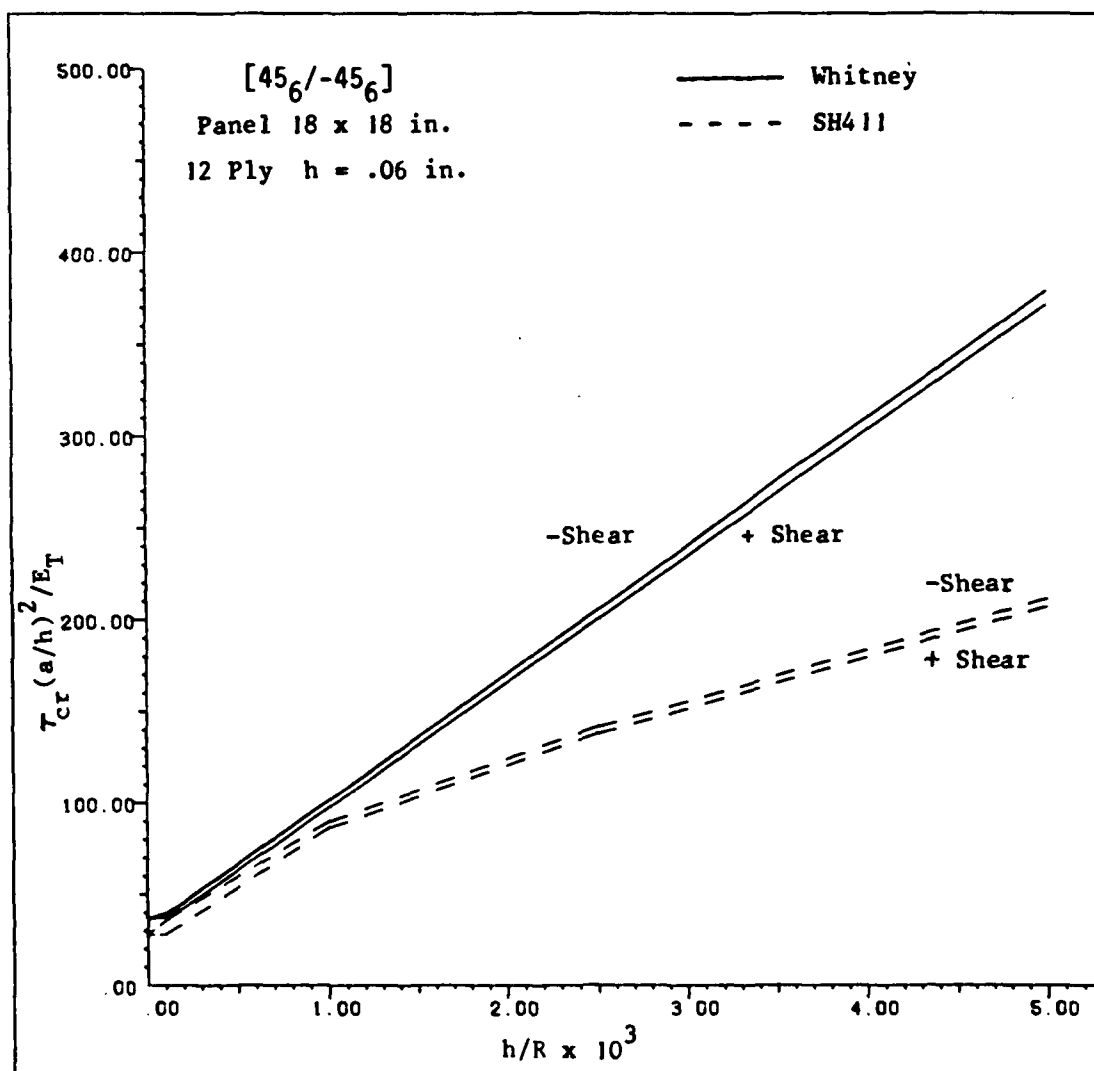
Figure 3.10 STAGS-C1 Finite Element (SH411) vs Whitney's
Galerkin, $[45_6/-45_6]$

32
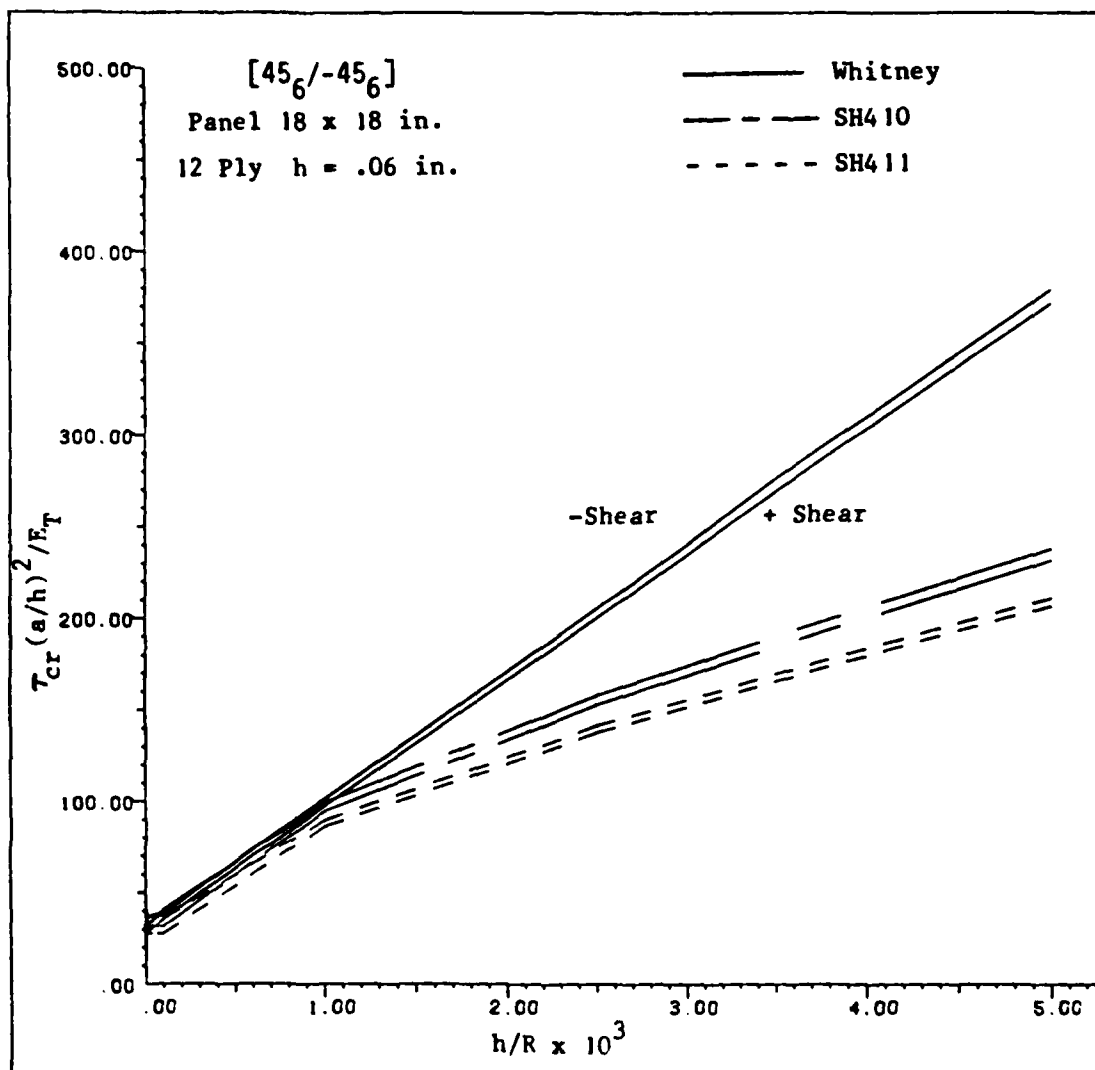
Figure 3.11   STAGS-C1 Finite Element vs Whitney's Galerkin, $[45_6/-45_6]$

33

IV.   Evaluation of Moisture and Temperature Conditions

Due to their excellent performance characteristics, advanced
composite materials have been gaining wide use in aerospace structures.
However, it is recognized that absorption of moisture and exposure to
thermal environments can have undersirable effects on the mechanical
properties of such materials [7-21]. Shirrell, Halpin, and Browning
[19] reported that, unless these effects are accounted for in designing
a system, the service life and reliability of a polymeric matrix
composite may be compromised. Moisture absorption affects the composite
in several different ways. Firstly, the resin swells causing a change
in the residual stresses of the composite and possibly micro-crack
formation. Secondly, the resin may be plasticized thus causing an
increase in the elongation of the resin near failure. This also has an
effect on the damping of the material. This plasticization is the
result of the lowering of the glass transition temperature T_g. The
glass transition temperature is actually a temperature range below which
the resin is essentially brittle and above which it behaves rubbery.
Thirdly, the interface between fiber and resin may be affected thus
influencing the composites' strength and toughness. The fibers are not
affected by either moisture absorption or moderate thermal environments
which might be encountered during a normal aircraft service life.
These changes in the resin have been found to result in a decrease in
the tensile properties [13] and a reduction in the transverse and shear
moduli [12 and 15] of the composite material. Also a slight increase in
the longitudinal elastic modulus was reported in Reference [12].

34

Advanced resinous composites can absorb water through the following mechanisms:

1. the fiber - matrix interface (capillary);

2. cracks and voids in the composite; and,

3. the resin (diffusion).

Of these three, the primary mechanism of water penetration in large well-fabricated composite structures is a rapid surface absorption followed by diffusion of the water through the resin [19].

Prediction of Moisture Absorption

The testing of composite materials to determine their mechanical properties is usually done at known temperatures and moisture concentrations. Since the primary mechanism for absorption of moisture is through diffusion, Fick's second law of diffusion [32] which, under certain circumstances has been shown to correlate with test data [12], will be used as the model for diffusion in this analysis. Fick developed this equation in 1855 by drawing an anology between heat conduction in a solid and diffusion through a solid. Fick's second law is:

$$\frac{\partial C}{\partial t} = K \frac{\partial^2 C}{\partial z^2} \qquad (28)$$

where C is the concentration of the diffusing substance through the thickness of the laminate as a function of time and distance through

35

the thickness, Z is the space coordinate measured normal to the
surface, K is the diffusion constant, and t is time.

The solution of this partial differential equation, with boundary
and initial conditions pertinent to the problem of diffusion, is shown
below. This is the same solution used by Snead and Palazotto [7] and is
slightly different from that form found in Section 4.3.3 of Reference [32].

$$C(Z,t) = C_1 + (C_2 - C_1) \frac{Z}{h} + \frac{2}{\pi} \sum_{n=1}^{\infty} \frac{C_2 \cos(n\pi - C_1)}{n} \sin(\frac{n\pi Z}{h}) \quad *$$

$$\exp\left[\frac{-Kt}{h^2}\right] n^2 \pi^2 + \frac{4C_0}{\pi} \sum_{m=0}^{\infty} \frac{1}{2m+1} \sin \frac{(2m+1)\pi Z}{h} \quad * \qquad (29)$$

$$\exp\left[\frac{-Kt}{h^2} (2m+1)^2 \pi^2\right]$$

Where C is as previously defined, C_0 is the initial, uniform moisture
concentration through the thickness of the laminate, C_1 and C_2 are the
initial moisture concentration conditions at the inside (-z) and outside
(+z) surface of the laminate, respectively, and h is the thickness of
the laminate.

The moisture concentration distribution through the thickness can be
determined by using this series solution with a known diffusion constant
and prescribed initial conditions. Then the reduced mechanical
properties of each ply can be obtained from appropriate test data by
assuming that the effective moisture concentration of each ply can be

36

approximated by the calculated moisture concentration at the middle of
that ply.

This series solution is a combination of a steady state moisture
distribution (the first two terms) and a transient moisture
distribution (the last two terms) which decreases with increasing time.
Therefore, the accuracy of this series approximation is dependent upon
the number of terms used during the two summations. Snead [7] wrote a
computer program which was used in this analysis to calculated the
solution to the series approximation. To insure an accurate solution,
the program carries out the summation until there is no change from the
previous answer. For the CDC computer, this is equivalent to 14
significant digits of accuracy. A version of Snead's computer program
is shown in Appendix A.

The use of Fick's equation has certain limitations which must be
considered. The series solution of Fick's equation was derived assuming
a constant moisture diffusion coefficient K. In reality the diffusion
coefficient is a function of the laminate's temperature and moisture
concentration. The diffusion of moisture into a composite can be
assumed to take place at a constant temperature in simple cases since
the process is relatively slow, requiring many months or years before
the laminate achieves a state of equilibrium moisture concentration.

The accuracy of Fick's equation to model moisture diffusion in
composites is also affected by rapid temperature changes. The rapid
thermal heating of the laminate to temperature near the material's T_g

37

has been found to increase the rate of moisture weight gain above that which is predicted by Fick's equation [11, 12, 14, and 17]. This increase is believed to be due to the development of surface crazing and cracking brought about by the rapid heating and resin swelling [12].

Fick's equation has been generally accepted as a good initial approximation of the moisture concentration distribution through a composite laminate, for simple cases, when the restrictions of no rapid heating, surface crazing or cracking, and assuming that a constant K are observed [12, 16, 18, and 19]. These are the assumptions being made for this analysis.

AS/3501-5 Mechanical Properties

The material properties required by STAGS-C1 as input parameters are the composite's longitudinal modulus E_1, transverse modulus E_2, shear modulus G_{12}, and Poisson's ratio ν_{21}. Poisson's ratio ν_{12} relates the strain in the 2 direction to the strain in the 1 direction when stressed in the 1 direction. Snead and Palazotto [7] used the experimentally – measured data for the graphite/epoxy system, AS/3501-5, found in Figure 8.18 of Reference 22 to determine the elastic moduli as a function of temperature and moisture concentration. The values of E_2 and G_{12} used in his work from which intermediate values are linearly interpolated, are shown in Table 4.1. For a better perspective, Figure 4.1 shows this data in graphical form. The material properties as calculated by Snead and Palazotto will be used in this work in order to correlate the findings.

38

TABLE 4.1

Values of Transverse and Shear Moduli
for AS/3501-5 [15]

Transverse Modulus, E_2 (psi)

Moisture Concentration (percent)	Temperature			
	80°F	200°F	250°F	300°F
0.0	1.41375E06	1.09475E06	1.015E06	1.015E06
0.050	1.305E06	0.9135E06	0.6235E06	0.522E06
1.050	1.2615E06	0.841E06	0.4785E06	0.290E06

Shear Modulus, G_{12} (psi)

0.0	0.8555E06	0.7830E06	0.6815E06	0.6525E06
1.050	0.8555E06	0.6597E06	0.3915E06	0.1522E06
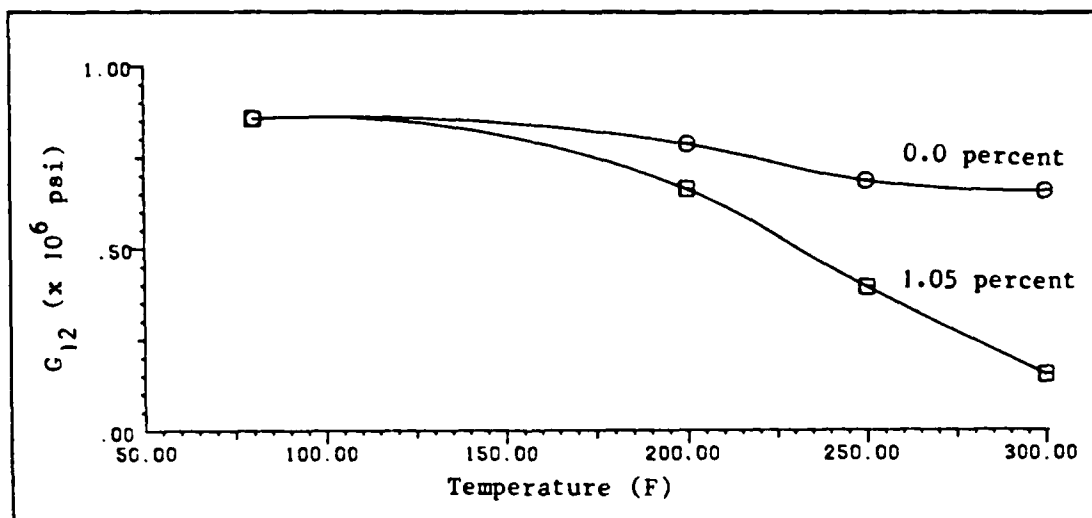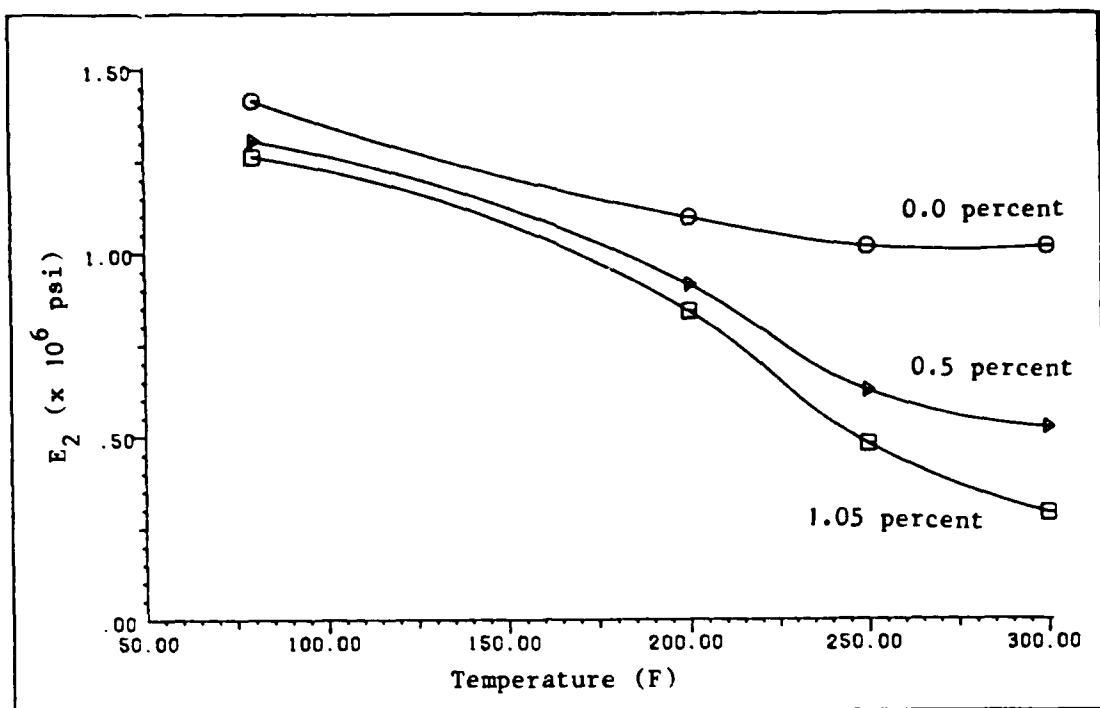
Figure 4.1 E_2 and G_{12} Degradation vs Temperature at Constant Values of Moisture Concentration

40

The moisture and temperature influences on the transverse and shear moduli are clearly evident in the experimental data for AS/3501-5 shown in Table 4.1 and Figure 4.1. The transverse modulus E_2 shows degradation both at room temperature and elevated temperatures while the shear modulus G_{12} only shows degradation at elevated temperatures. Also visable is the change in the T_g caused by the absorbed moisture. The resulting plasticization of the resin is shown by the increased degradation in the moduli with increasing moisture concentration at each elevated temperature. The longitudinal modulus E_1 is dominated by the fiber stiffnesses and hence is not significantly influenced by changes in moisture and temperature as are the matrix dominated E_2 and G_{12} moduli. Therefore, E_1, is assumed to be contant and has a value of 18.85×10^6 psi for AS/3501-5. Also for this work the value of ν_{12} was assumed to be a constant, $\nu_{12} = 0.3$.

Moisture Conditions

The series solution, Eq. (28), to the Fick's equation requires three moisture concentration coefficients C_0, C_1, and C_2 to determine the moisture concentration through the laminate's thickness as a function of time. These moisture concentrations, measured as a percentage of the weight gained by the composite, correspond to the initial moisture concentration in the laminate, the moisture concentration at the interior (-Z) surface, and the moisture concentration at the exterior (+Z) surface, respectively, for the cylindical panel. Table 4.2 lists the three moisture concentration conditions considered by Snead and Palazotto [7].

41

Table 4.2

Snead and Palazotto's Moisture Conditions

Cond. No.	C_0	C_1	C_2
1	0.00	0.00	0.0105
2	0.00	0.0105	0.00
3	0.00	0.0105	0.0105

They used a surface moisture concentration of 0.0105 to correspond to the material test data, Table 4.1, that was available for a saturation moisture concentration of 1.05 percent. (Note: The concentration of 1.05 percent relates to an environment which has a 75 percent relative humidity.) Conditions 1 and 2, in Table 4.2, result in an unsymmetric degradation of the E_2 and G_{12} moduli resulting in an unsymmetric laminate, which will introduce bending-extension coupling. Condition 3, in Table 4.2, is symmetric and will not produce any bending-extension coupling. Snead and Palazotto found that conditions 1 and 2 produced similar results to each other, therefore, only one unsymmetric condition was examined in this thesis along with one symmetric condition. Table 4.3 shows these moisture conditions.

Table 4.3

Moisture Conditions

Cond. No.	C_0	C_1	C_2
1	0.00	0.00	0.0105
2	0.00	0.0105	0.0105

42

Along with the coefficients C_0, C_1, and C_2, in Eq. (29), it is standard to use a dimensionless time t*, where $t* = K$ (in^2/sec) x $t(sec)/h^2(in)^2$. This eliminates the need to pick a specific diffusion coefficient, K and time. The dimensionless times used in this analysis are 0.0, 0.001, 0.01, 0.1, and 0.5. These values represent from zero moisture absorption to a steady-state distribution, respectively. Table 4.4 shows how t* corresponds to real time given a specific K and laminate thickness h.

Table 4.4

Relation Between Real and Dimensionless Time

Real Time (sec)	Real Time (days)	Dimensionless Time t*
0.0	0.0	0.0
3.045E04	0.35	0.001
3.045E05	3.52	0.01
3.045E06	35.24	0.1
1.527E07	176.24	0.5

Note: These times were calculated using K = 0.52537E-10 (in^2/sec) for an 8-ply, 0.04 thick, AS/3501-5 laminate.

The parametric equation used to determine the value of K = 0.52537E-10 (in^2/sec) in Table 4.4 was

$$K(in^2/sec) = 6.51 \exp(-5722/T) (0.03937)^2 \qquad (30)$$

where T is the laminate temperature in degrees Kelvin. This equation was taken from Reference [22]. Figure 4.2 shows the moisture
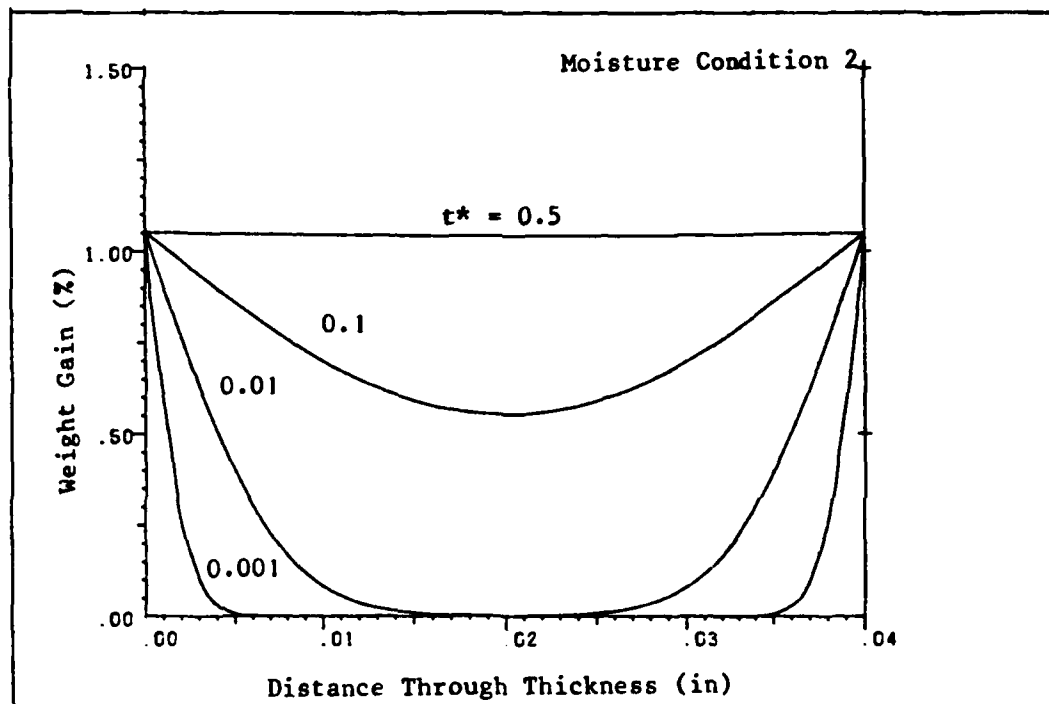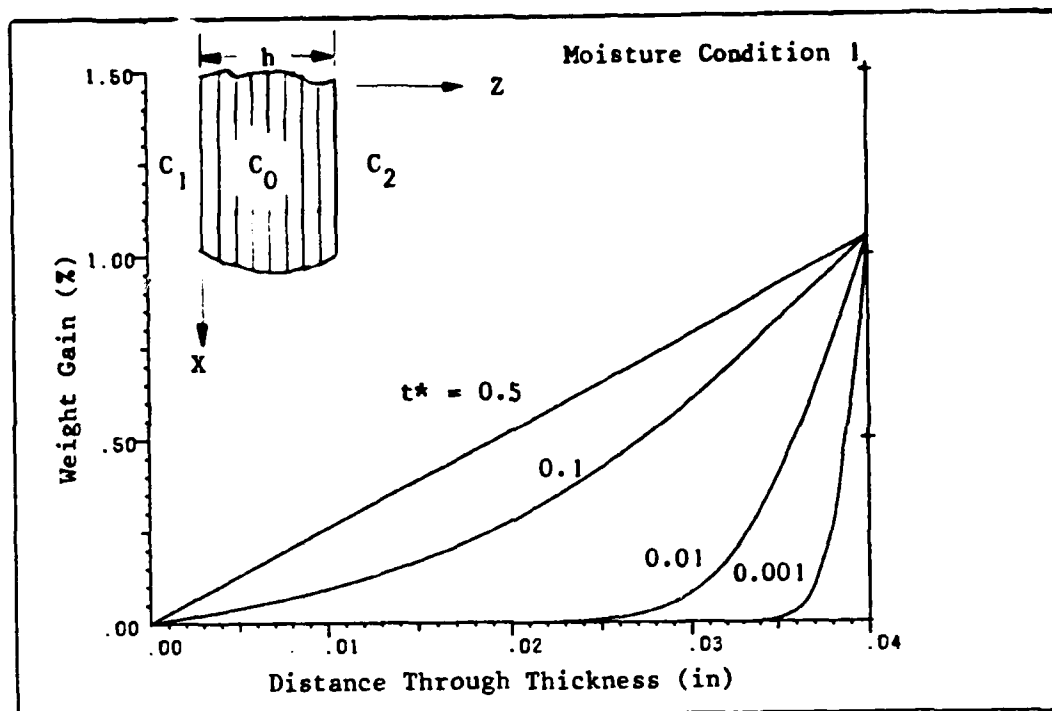
Figure 4.2 Moisture Concentration Distribution for Moisture
Condition 1 and 2

distribution through the thickness for the five time values and moisture conditions 1 and 2. This figure shows that the panel will absorb moisture nonsymmetrically, for moisture condition 1. This means that, as time increases, the panel will reach a steady state condition, $t^* = 0.5$, where each lamina has a different moisture content. The symmetric nature of moisture condition 2 is also shown, and as time increases, the panel will reach a steady state condition, $t^* = 0.5$, where each lamina has the same moisture content. The moisture distribution is shown as a continuous function in Figure 4.2, however, as mentioned previously, the moisture concentration is calculated at the center of each ply and then assumed to be constant through the ply thickness in this analysis.

Temperature Conditions

For this analysis the laminate was assumed to be at a constant temperature. This is possible since the moisture diffusion process is much slower than that of thermal diffusion. Crank [32] indicated a factor of 10^6 for the time difference. Four different temperatures; 80, 200, 250 and 300°F; were used in this analysis to evaluate the influence of a wide range of temperatures on a composite panel. This range varies from room temperature to the operational survice limit. The service limit for graphite/epoxy is approximatelly 300°F. These temperatures were selected because the material test data, Figure 4.1, was taken at these four temperatures.

Laminate Ply Orientations

Two eight-ply laminates will be evaluated. The two ply orientations chosen are the $[0/45/-45/90]_s$ and the $[45/-45]_{2s}$, which correspond to two of the three orientations investigated by Snead and Palazotto [7].

V. Results and Discussion

For the hygrothermal investigation carried out within this study, a combination of moisture conditions, temperatures, and times generates a matrix of 40 cases for each given laminate per radius. These 40 cases are broken into two sets of 20 cases; 20 cases for each moisture condition. Because of the large number of cases to be evaluated, all 40 cases were run for only the radius of 12 in. for both laminates. In the analysis of curvature, the radii 36, 48, 96, and 10,000 in. were run for only the $[45/-45]_{2s}$ laminate, with a limited number of temperature and time steps. This reduced the number of cases, but still provided adequate information to analyze the effects of curvature on the bifurcation load. In this last mentioned analysis, moisture condition 1 was evaluated at 300°F and time steps 0.00 and 0.5, while moisture condition 2 was evaluated at 80, 200, and 300°F for all five time steps. A matrix of the case numbers and corresponding conditions is shown in Table 5.1 and a list of the bifurcation loads, $\bar{N}_{xy}$, for these cases can be found in Appendix B.

The computation of the moisture concentration distribution and the reduction in the transverse and shear moduli is done by the computer program listed in Appendix A. This computer program also generated the input deck for the STAGS-C1 program, and is a modification of the computer program written by Snead [7]. It was modified to allow for shear loading and changes in curvature.

Table 5.1

Moisture, Temperature, and Radius Conditions Evaluated

Case No.	Moisture Condition	Temperature	Radius (in.)	Laminate
1-20	1	a,b,c,d	12	$[0/45/-45/90]_s$
21-40	1	a,b,c,d	12	$[45/-45]_{2s}$
41-60	2	a,b,c,d	12	$[0/45/-45/90]_s$
61-80	2	a,b,c,d	12	$[45/-45]_{2s}$
81-91	2	a,b,c,d	24	$[45/-45]_{2s}$
92-93	1	d	24	$[45/-45]_{2s}$
300-305	2	a,d	36	$[45/-45]_{2s}$
100-110	2	a,b,d	48	$[45/-45]_{2s}$
111-112	1	d	48	$[45/-45]_{2s}$
121-128	2	a,b,d	96	$[45/-45]_{2s}$
131-132	1	d	96	$[45/-45]_{2s}$
141-147	2	a,b,d	10,000	$[45/-45]_{2s}$

Note: The cases with a R = 12 in. were run for all five times and four temperatures, however, the remaining cases were run at a mixture of time steps and temperatures depending on the moisture condition and radius.

Notation:

Moisture Condition	Temperature (°F)
1 — $c_0 = c_1 = 0.00$ $\quad c_2 = 0.0105$	a -- 80.0
	b -- 200.0
2 — $c_0 = 0.0$ $\quad c_1 = c_2 = 0.0105$	c -- 250.0
	d -- 300.0

Reduction in Bifurcation Load

The evaluation of the data for a panel loaded in shear indicates that the degradation of the E_2 and G_{12} moduli due to moisture and temperature effects results in a reduction of the panel's bifurcation load, $\overline{N}_{xy}$. Figures 5.1 and 5.3 show the results of the STAGS-C1 runs for the two 12 in. by 12 in. panels, with a radius of 12 in., while Figures 5.2 and 5.4 show the results found by Snead and Palazotto [7] for a similar panel acting under compressive loads. In these plots $\overline{N}_{xy_{orig}}$ and $\overline{N}_{x_{orig}}$ represents the bifurcation loads for a panel at 80°F, and a dimensionless time of $t^* = 0.00$ when loaded in shear and axial compression, respectively. These values are unaffected by either temperature or moisture degradations. The actual shear buckling values are shown in tabular form along with individual plots for each time and temperature series in Appendix B.

As was expected, the panel's bifurcation load decreased with increasing temperature and absorbed moisture. Comparing Figure 5.1 to Figure 5.2 shows a similarity in the trends for the reduced bifurcation loads for the [0/45/-45/90]$_s$ laminate considering shear and compression. A point should be made that even though the percent reductions are similar the actual values for the bifurcation loads, Table 5.2, differ considerably, i.e., for room temperature, zero moisture $\overline{N}_x$ = 514.8 lb/in compared to $\overline{N}_{xy}$ = 123.4 lb/in for the [0/45/-45/90]$_s$ laminate. The difference in Figures 5.1 and 5.2 is that the curves for the shear loading are shifted down below those for axial

49
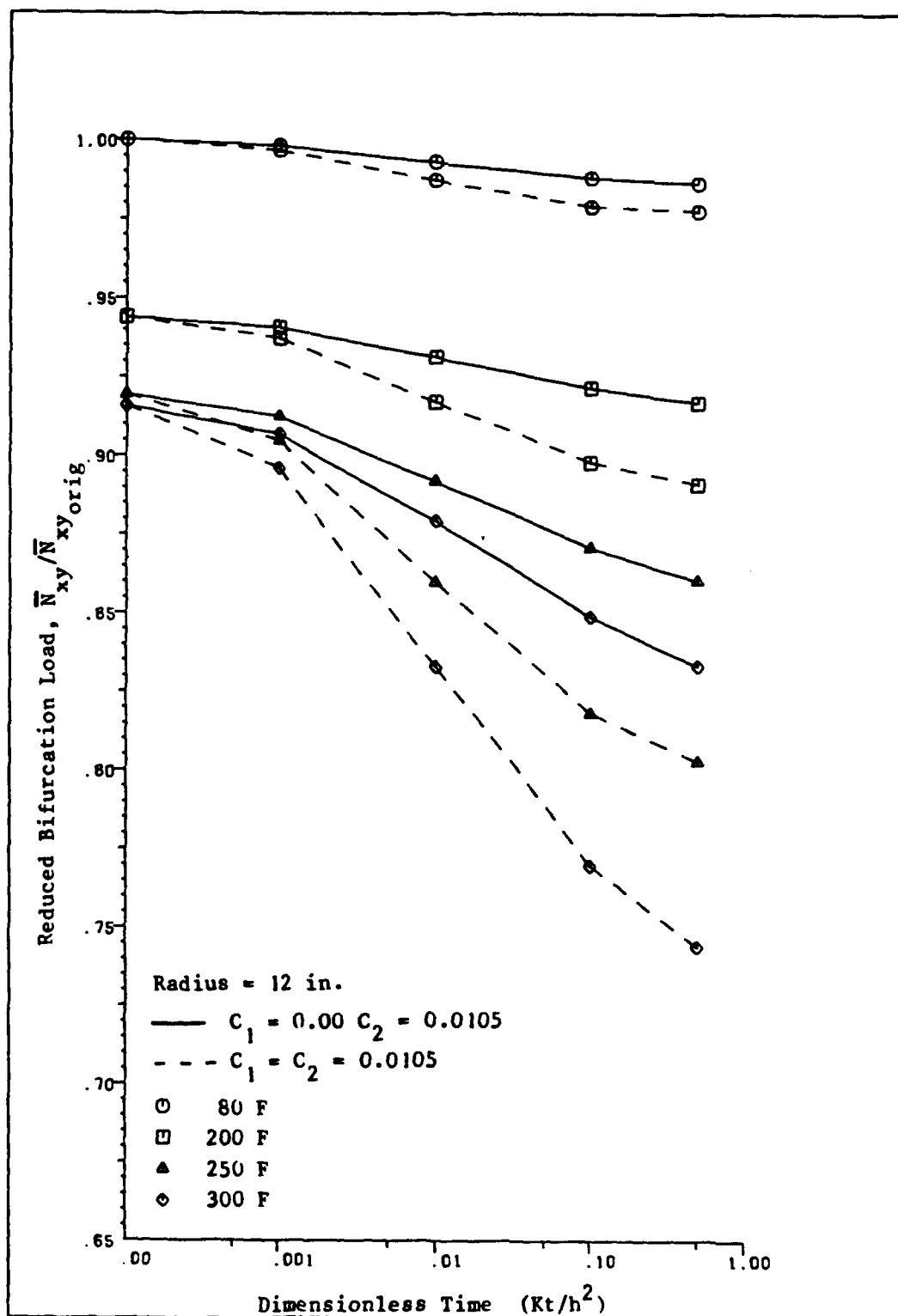
Figure 5.1   Degradation in $\overline{N}_{xy}$ for the $[0/45/-45/90]_s$ Laminate

50
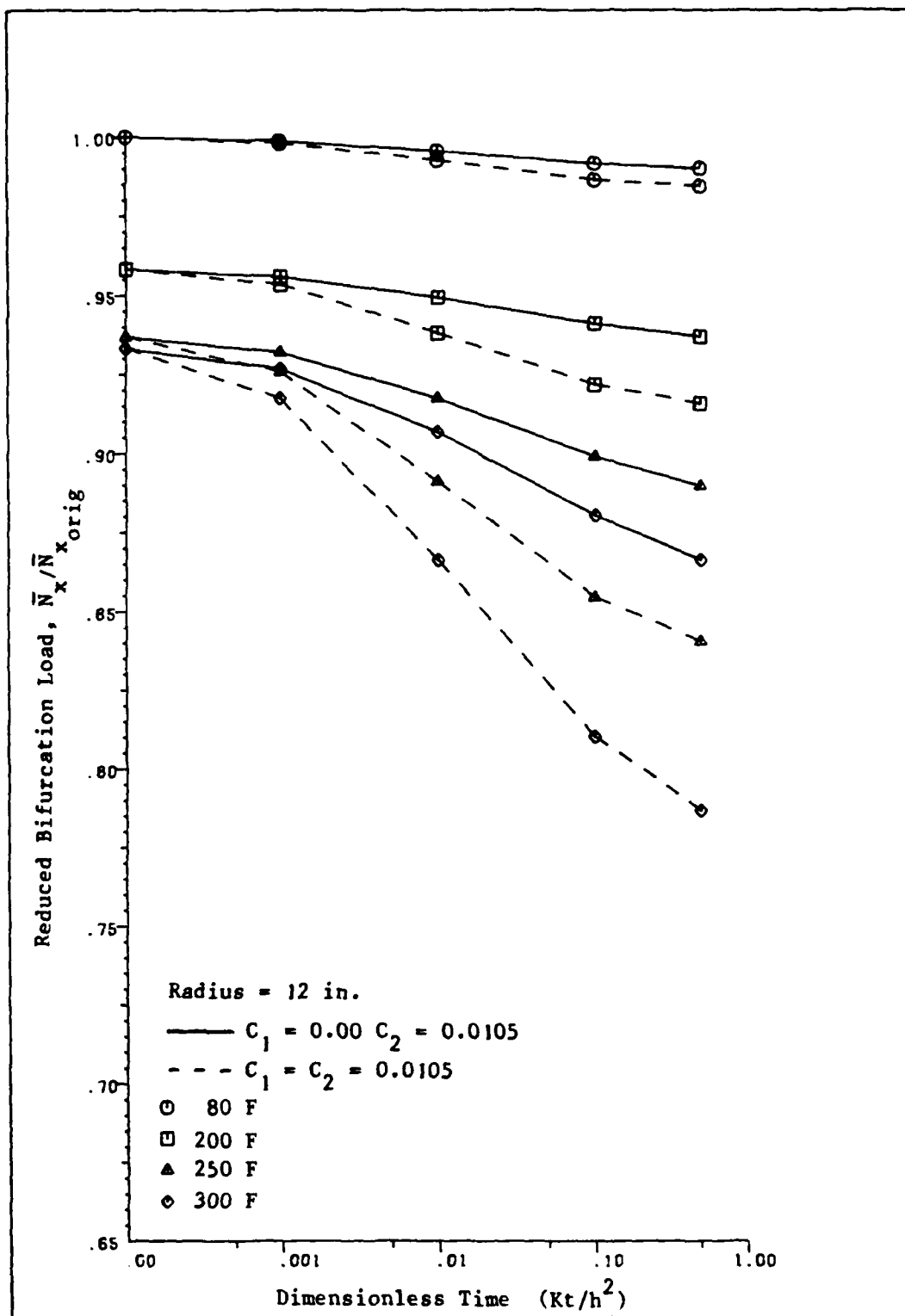
Figure 5.2 Degradation in $\overline{N}_x$ for the $[0/45/-45/90]_s$ Laminate
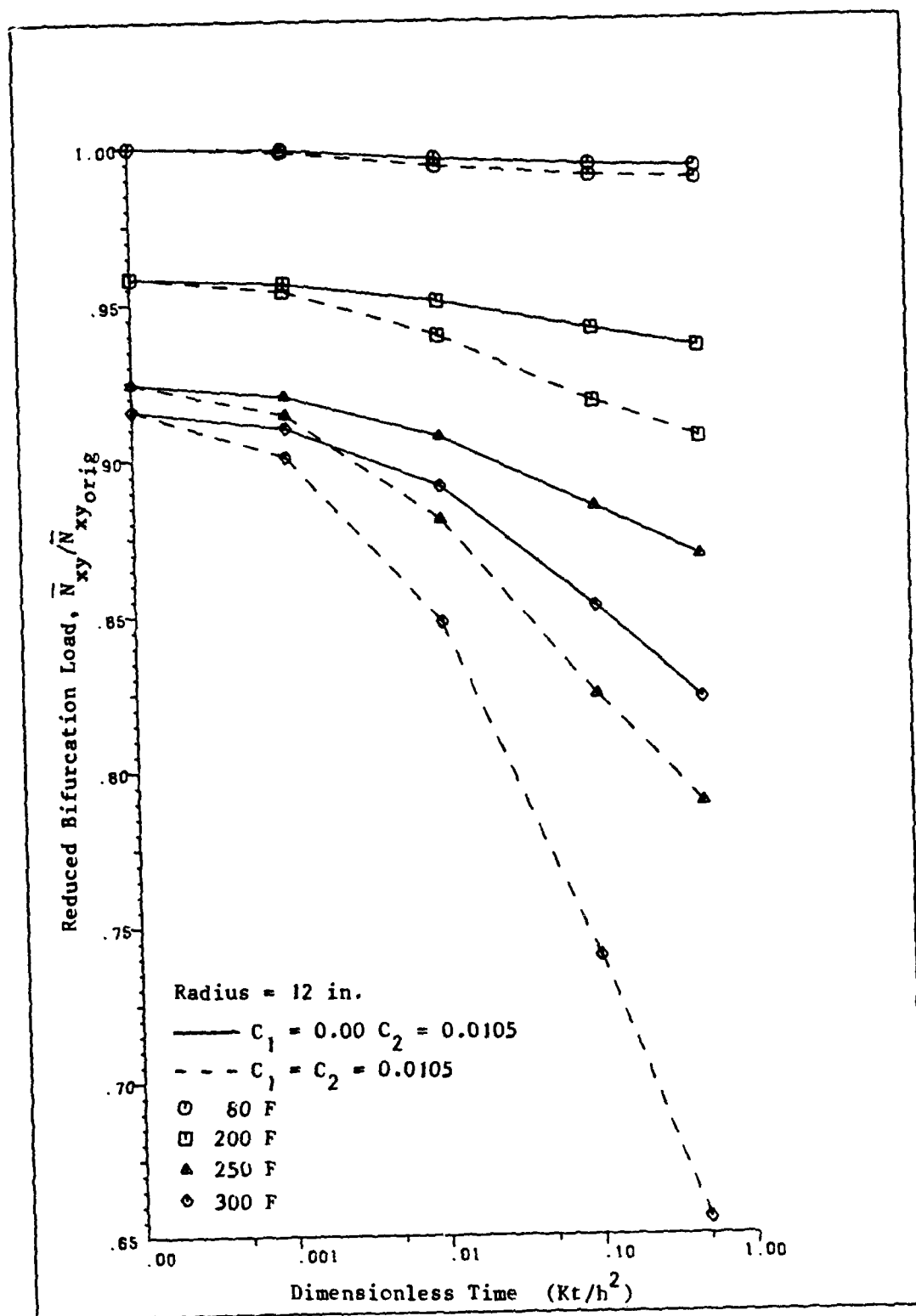
Figure 5.3 Degradation in $\bar{N}_{xy}$ for the $[45/-45]_{2s}$ Laminate

52
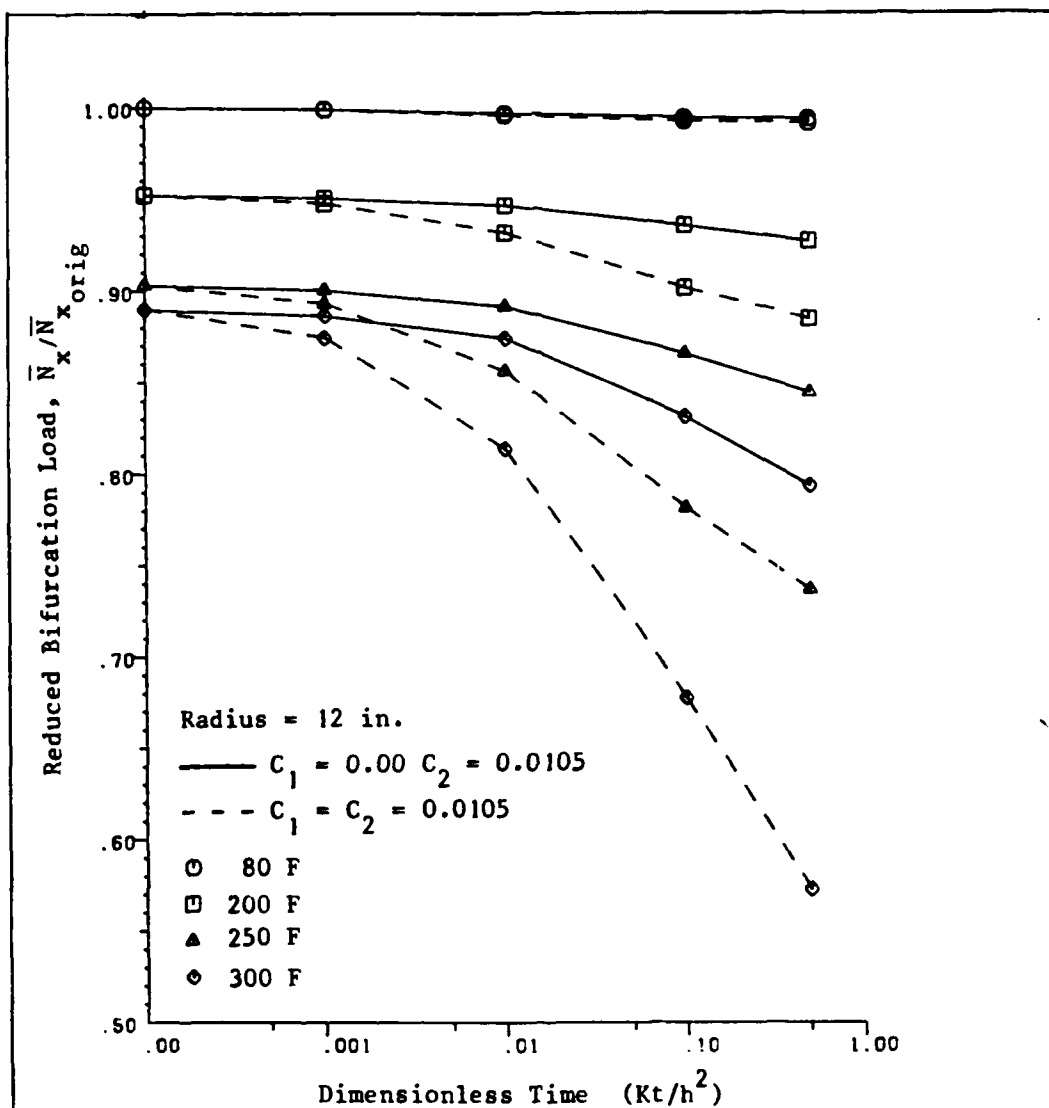
Figure 5.4 Degradation in $\overline{N}_x$ for the $[45/-45]_{2s}$ Laminate

53

Table 5.2

Comparison of Bifurcation Loads (lb/in) at 80°F, $t^* = 0.00$, and R = 12 in.

Laminate	Axial Compression [7]	Shear
$[0/45/-45/90]_s$	514.8	123.4
$[45/-45]_{2s}$	428.9	160.9

loading. For example at a temperature of 300°F and moisture condition 2, the reduction in shear was 26 percent while for axial compression it was 21 percent, a difference of 5 percent. A similar analogue can be drawn from Figures 5.3 and 5.4 for the $[45/-45]_s$ laminate, except that the curves for the shear loadings are shifted up above those for an axial load. For example at a $T = 300°F$ and moisture condition 2, the reduction for shear was 35 percent while for axial compression it was 43 percent a difference of 8 percent. To illustrate this better, Figures 5.5 thru 5.8 show these comparisons for each moisture condition and laminate. Figures 5.5 thru 5.8 also show that the laminates perform as designed. That is, the rate of reduction for the $[45/-45]_{2s}$ laminate loaded in shear was less than that for the $[0/45/-45/90]_s$ laminate loaded in shear while the rate of reduction for the $[0/45/-45/90]_s$ laminate loaded in compression was less than that for the $[45/-45]_{2s}$ laminate loaded in compression for a given temperature and moisture conditions.

As with Snead and Palazotto's [7] work, the reductions in the
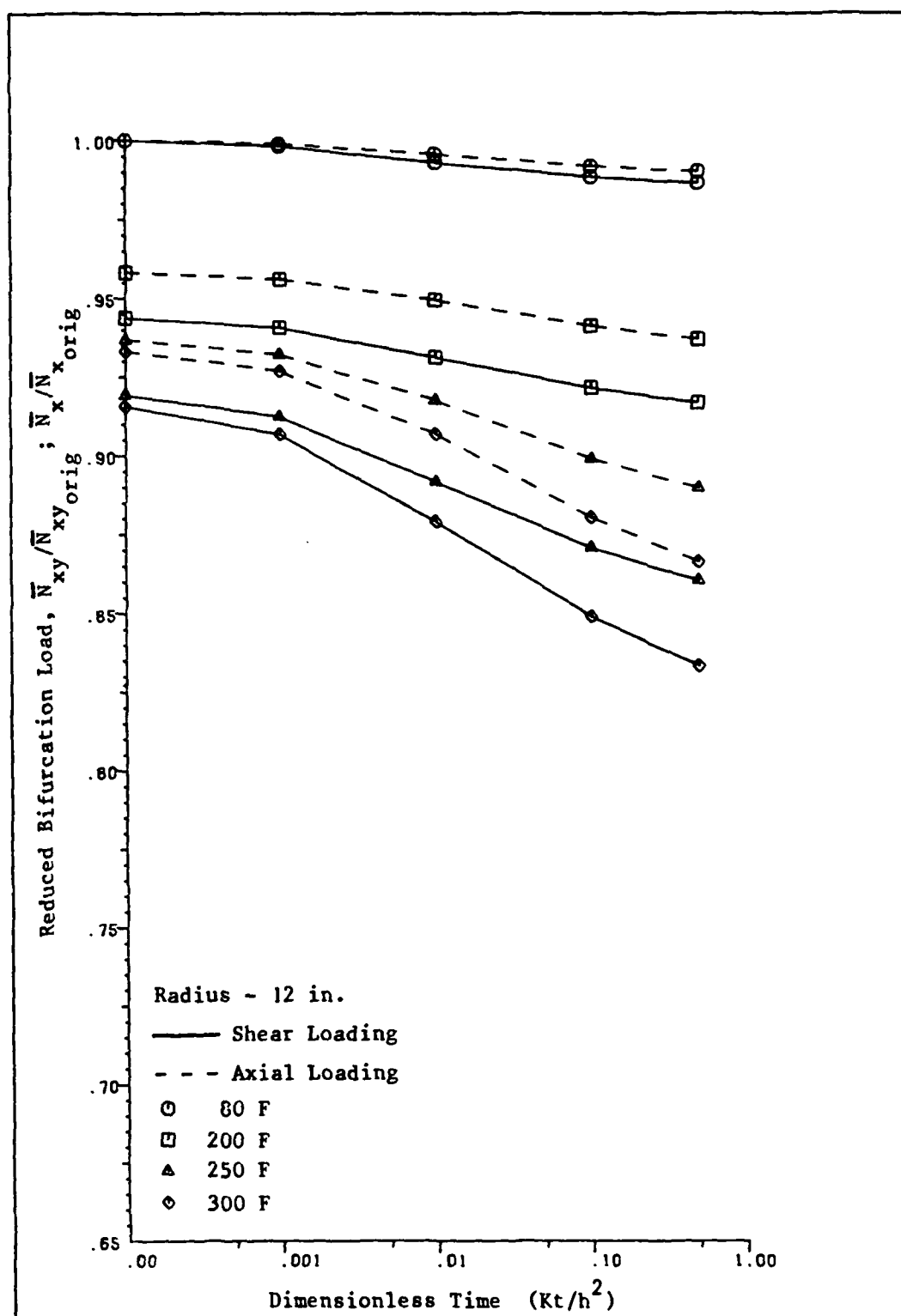
Figure 5.5 Axial vs Shear Loading for Moisture Condition 1,
[0/45/-45/90]$_s$

55
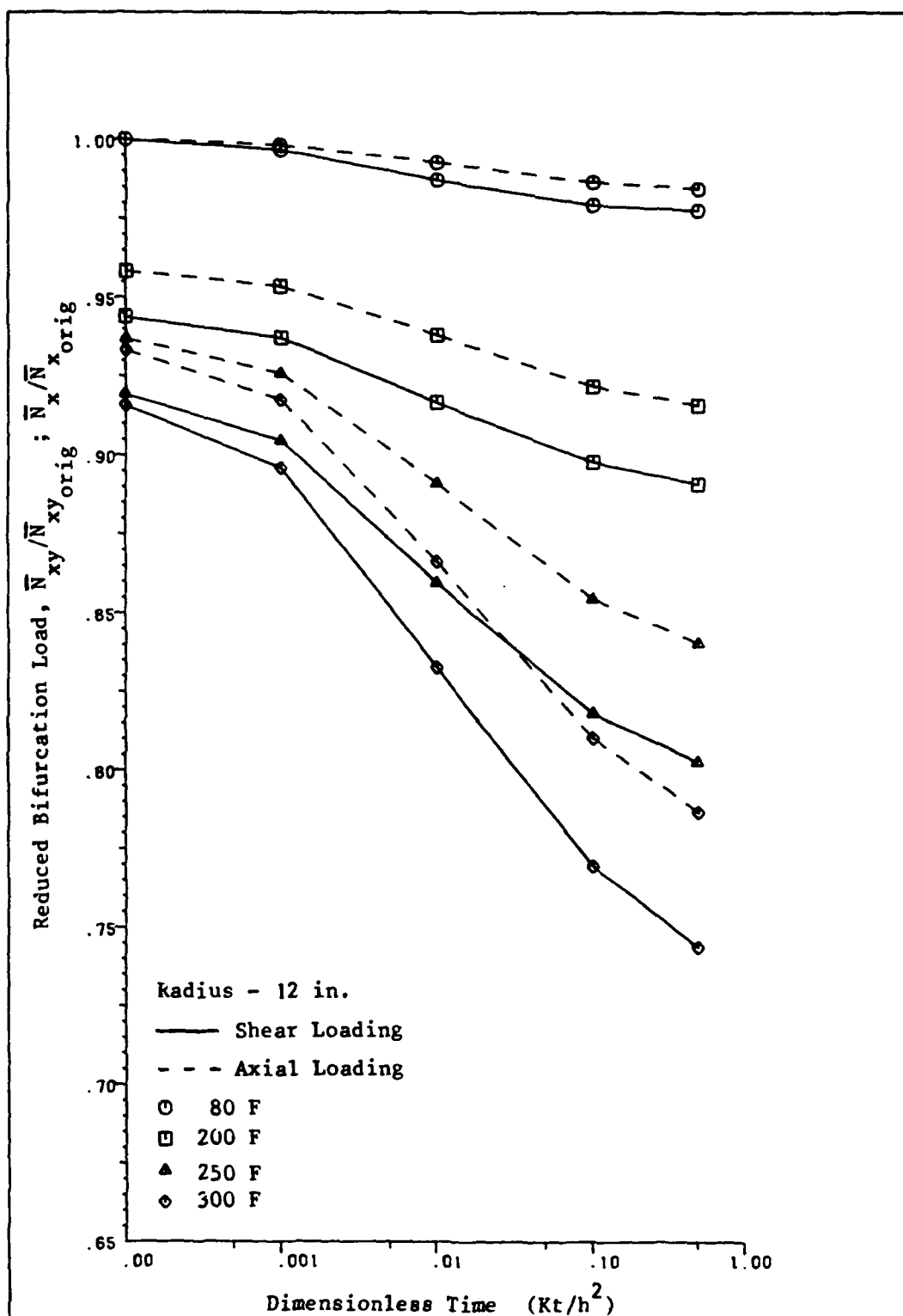
Figure 5.6 Axial vs Shear Loading for Moisture Condition 2,
[0/45/-45/90]$_s$

56
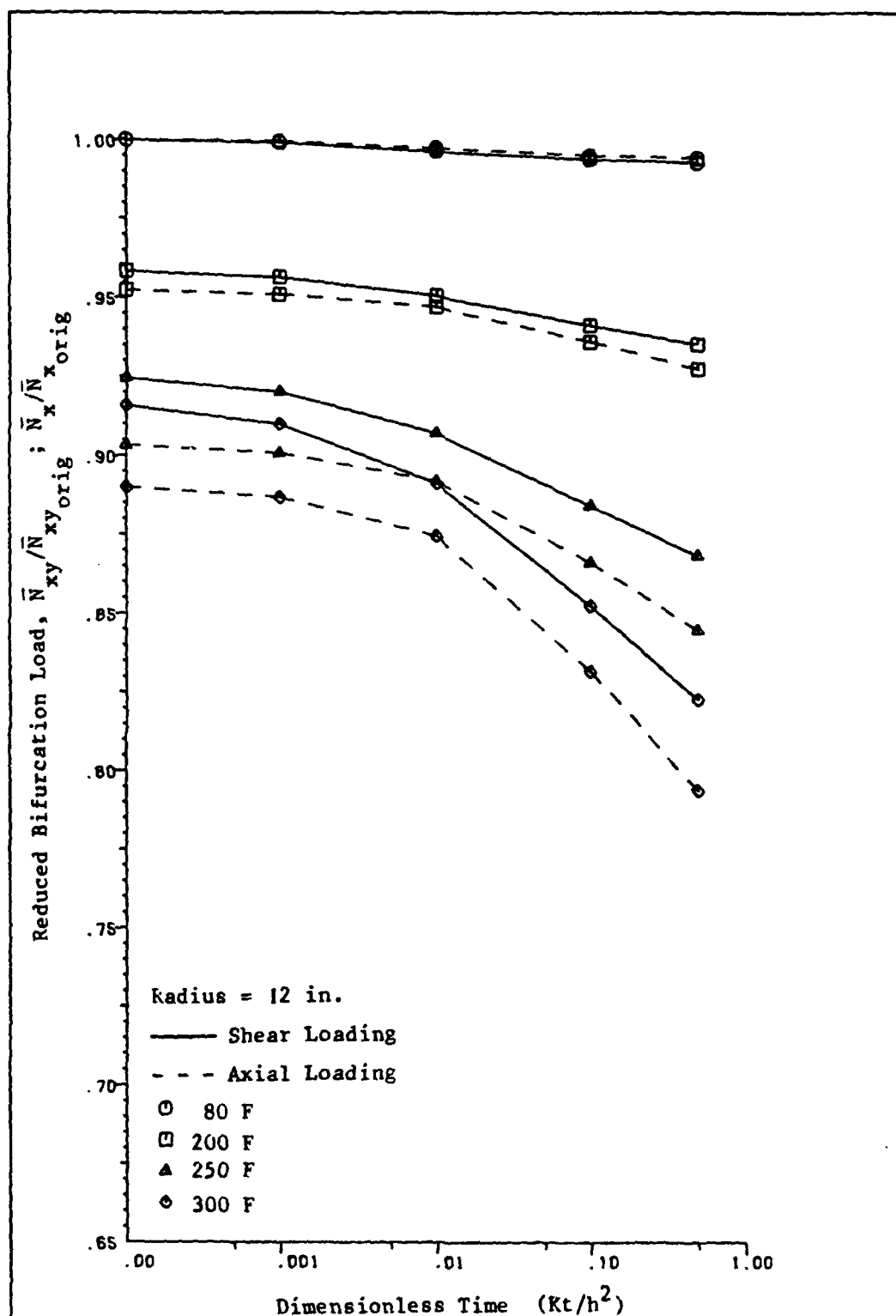
Figure 5.7   Axial vs Shear Loading for Moisture Condition 1,
$[45/-45]_{2s}$

57
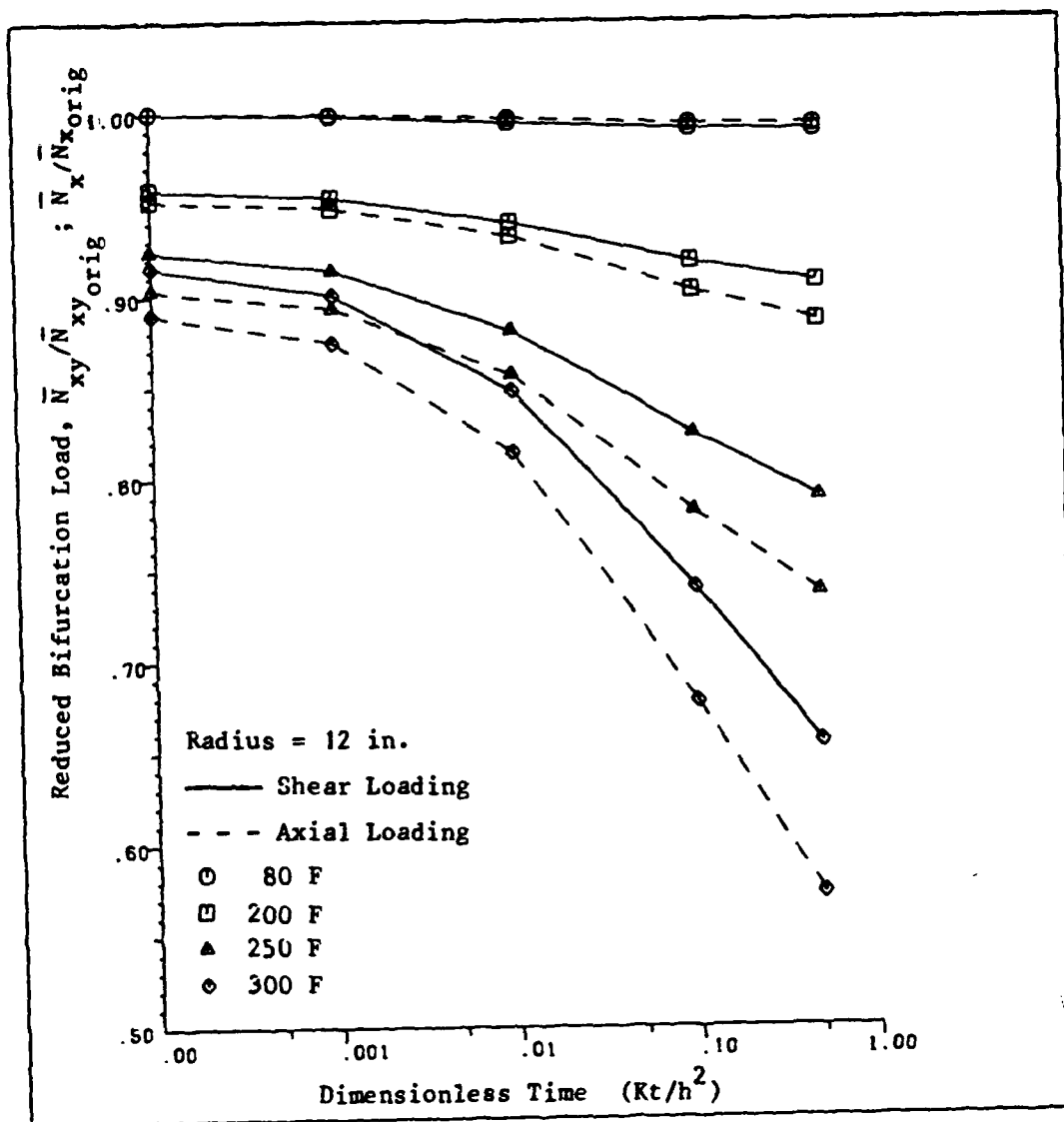
Figure 5.8 Axial vs Shear Loading for Moisture Condition 2, $[45/-45]_{2s}$

58

bifurcation loads are significant considering that dimensional changes due to resin swelling were not included. The maximum reduction in $\overline{N}_{xy}$ for each laminate and moisture condition is summarized in Table 5.3 for the radius of 12 in.

Table 5.3

Percent Reduction in Bifurcation Load, $\overline{N}_{xy}$
at 300°F, t* = 0.5, and R = 12 in.

Laminate	Moisture Condition	
	1	2
[0/45/-45/90]$_S$	16.7	25.6
[+45/-45]$_{2s}$	17.8	34.5

Another similarity to Snead and Palazotto's [7] work is that for mositure condition 1 the reduction in the bifurcation load, $\overline{N}_{xy}$, was not as great as it was for moisture condition 2 even though moisture condition 1 causes the initially symmetric laminate to become unsymmetric, which introduces bending – extension coupling. The symmetric moisture condition 2 has a much greater influence on both laminates. This is due to an over all general reduction in the material properties as moisture is absorbed into the panel symmetrically.

Effects of Curvature

The [45/-45]$_{2s}$ laminate was examined at six different radii (12, 24, 36, 48, 96, and 10,000 in.), considering moisture condition 2, to evaluate the effects of curvature on the bifurcation load. This laminate was selected because, in comparison to the [0/45/-45/90]$_S$

59
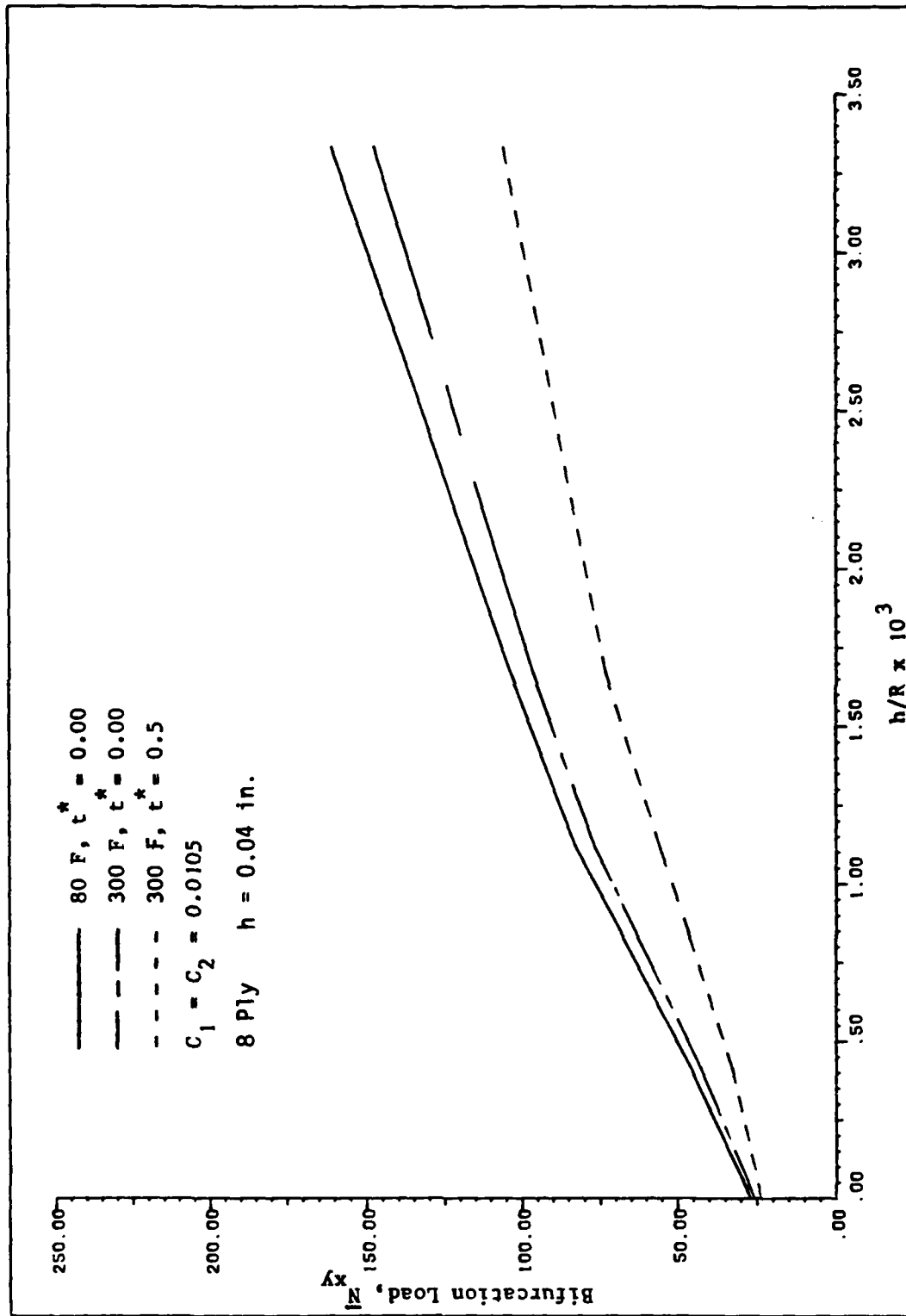
Figure 5.9 Curvature Effects on the Bifurcation Load, $\bar{N}_{xy}$ $[45/-45]_{2s}$ Laminate

laminate, it exhibits a greater reduction in the reduced bifurcation load for a given moisture content and temperature. Figure 5.9 shows the general overall effects of curvature on the bifurcation load. That is, as the panel's radius increases the bifurcation load, $\overline{N}_{xy}$ decreases. Also shown in this figure are the effects of temperature and moisture absorption on the bifurcation load. Though the only temperature shown is 300°F with times absorption set at $t^* = 0.0$ and 0.5, it can be stated that for any given radius the increase in temperature and moisture content reduces the bifurcation load. A better illustration of the effects of curvature is shown in Figure 5.10. This figure shows that curvature does influence the percent reduction in the bifurcation load. This is different from Snead and Palazotto's [7] findings. They investigated three radii, 12, 24, and 48 in. and came to the conclusion that for a panel under axial loading the reduction in the panels' bifurcation load, $\overline{N}_x$, did not significantly vary from those for the 12 in. radius panel. They therefore concluded that the results obtained for the 12 in. radius panel should be valid for any radius. Figure 5.11 shows how this conclusion can be reached by only examining panels of radii 12, 24, and 48 in. If the radii 96 and 10,000 in. are added to their work, the effects of curvature become apparent. The overall effect of curvature is to decrease the influence of temperature and moisture on the panels bifurcation load. This means that using the reduced bifurcation load results for the 12 in. radius, or any other radius, as a valid approximation for another radius will yield invalid results. Thus in general, the effects of curvature must be accounted for. One needs to compare results for the reduced bifurcation load for

61
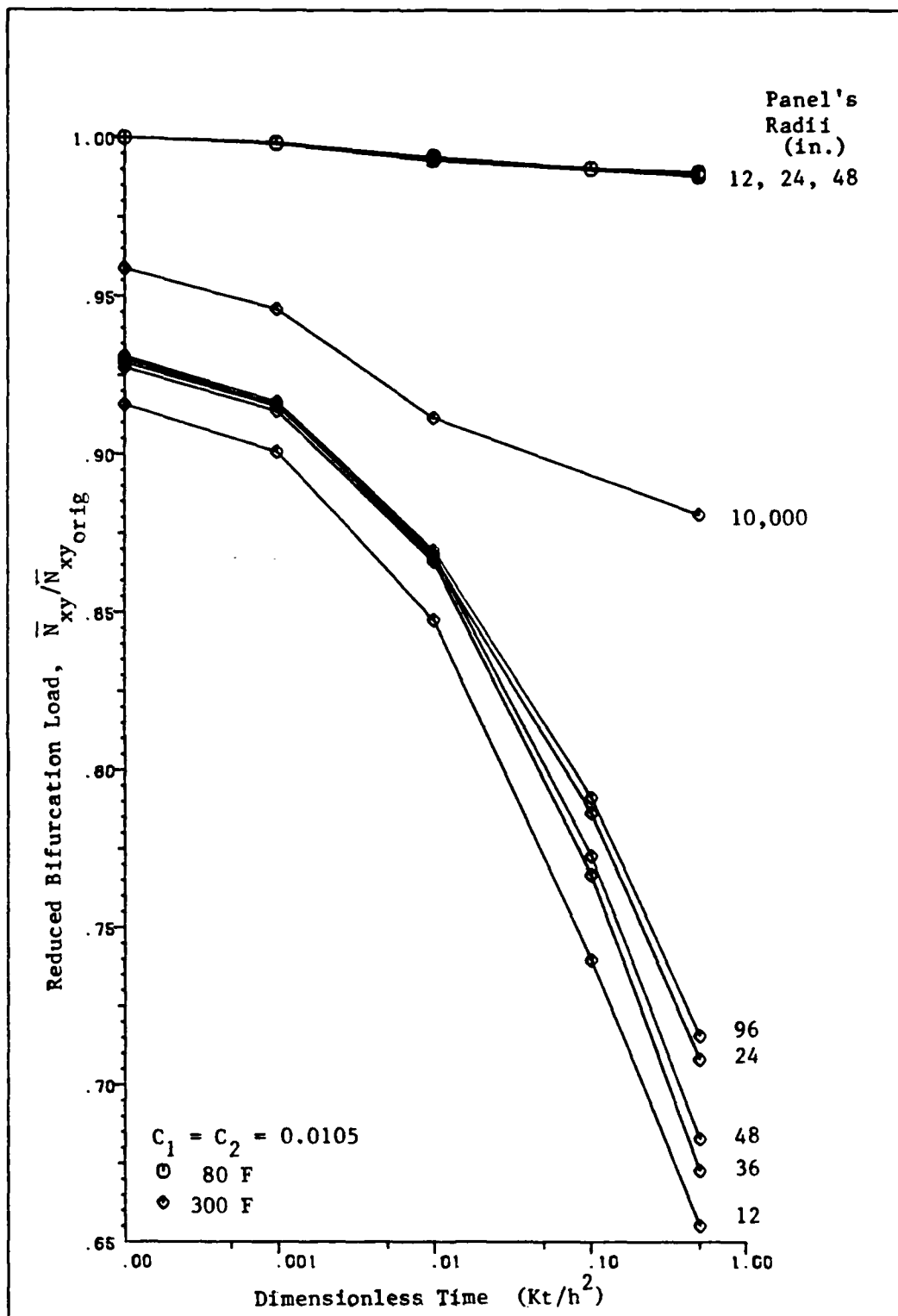
Figure 5.10 Effects of Curvature on Degradation in N_{xy} for the $[45/-45]_{2s}$ Laminate

62
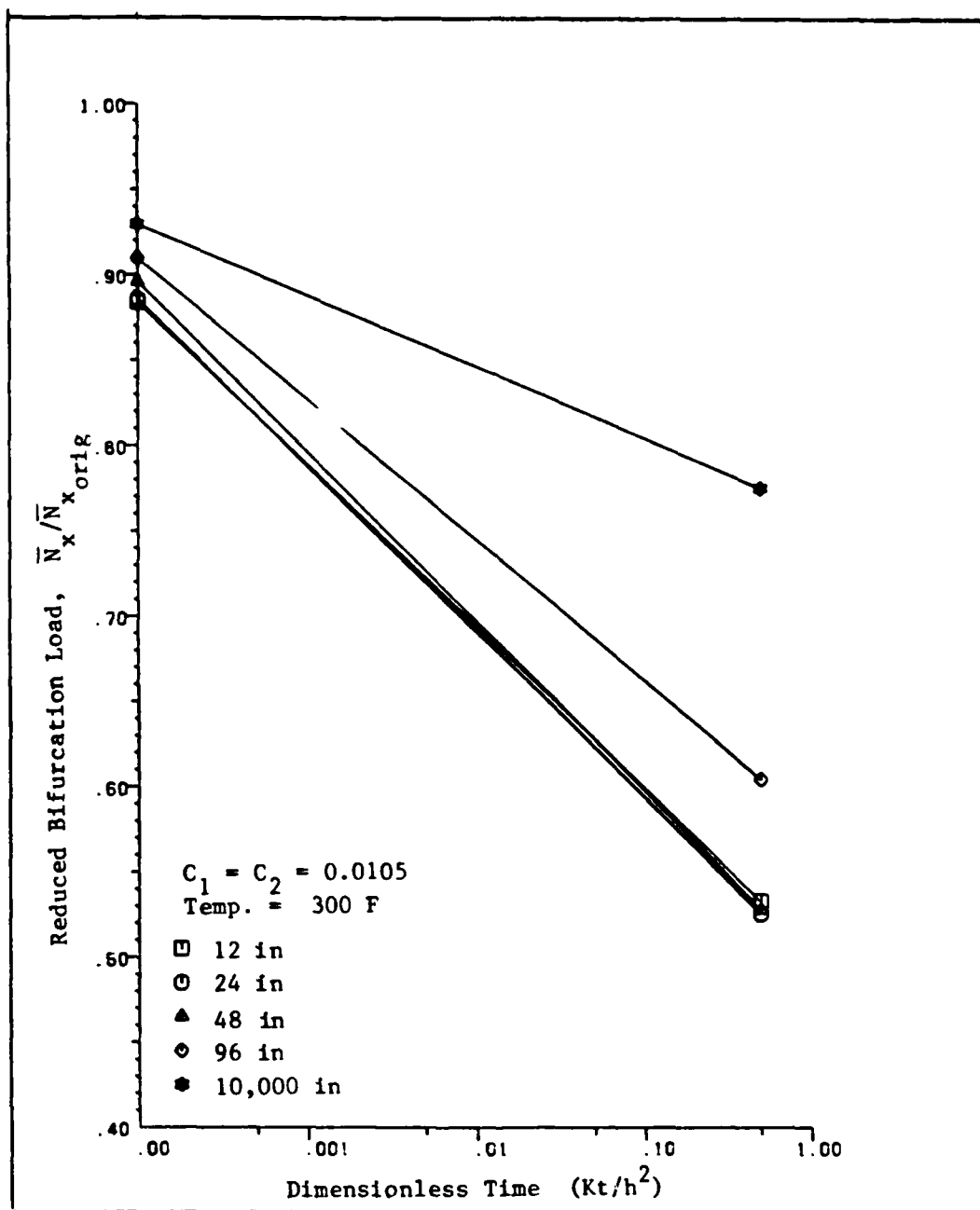
Figure 5.11 Effects of Curvature on Degradation in $\overline{N}_x$ for the [45/-45]$_{2s}$ Laminate
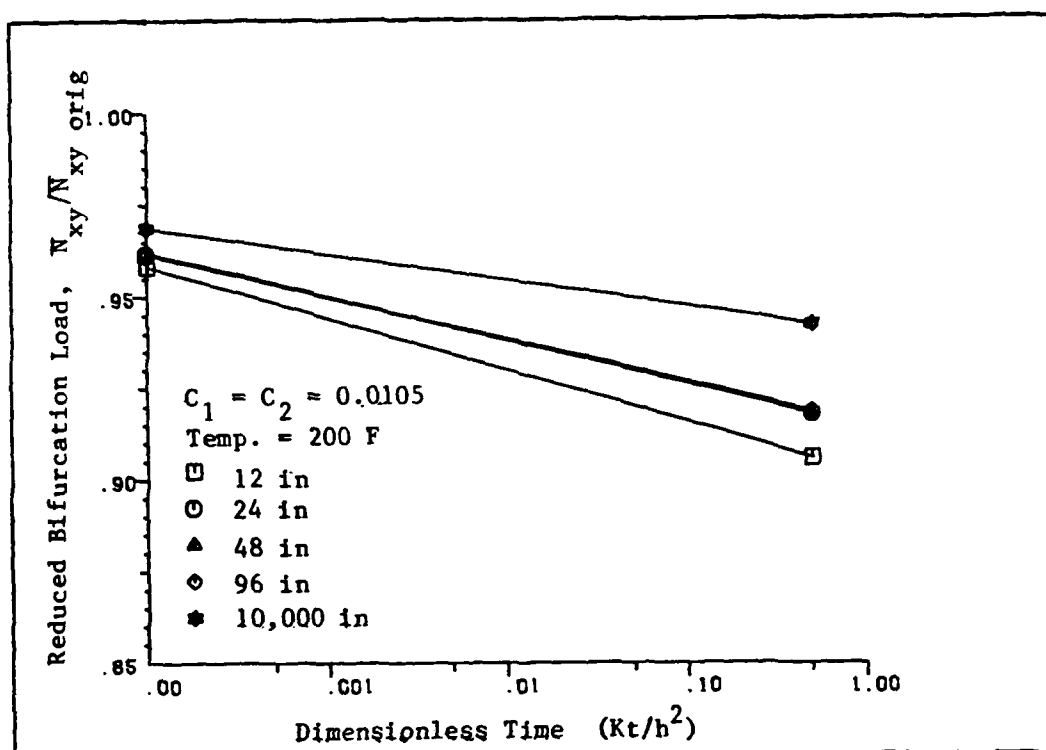
Figure 5.12   Effects of Curvature on Degradation in $\overline{N}_{xy}$ for the $[45/-45]_{2s}$ Laminate at $200°F$

the same radius of curvature. Note that although only a few points are plotted in Figure 5.11 the trend is still quite visible.

Looking at Figures 5.10 and 5.12, one can see that the influence of curvature is also a function of the laminate's temperature. These figures are plots of the reduced bifurcation load for the $[45/-45]_{2s}$ laminate for moisture condition 2. Figure 5.10 has the plots for temperatures 80 and 300°F, while Figure 5.12 is a plot for the temperature of 200°F. It is apperent from these plots that for a temperature of 80°F the effects of curvature can be neglected, and that as the temperature increases to 300°F the effects of curvature becomes more important and cannot be neglected. As the temperature increases, the effects of curvature tends to decrease the influence of moisture and temperature on the reduced bifurcation load. This difference can be seen best by comparing the maximum reduction in the bifurcation loads for the panels of radius 12 in. and 10,000 in. The 12 in. panel has a 35 percent reduction in the bifurcation load while the 10,000 in. panel has only a 12 percent reduction. This is a 23 percent decrease in the effects of moisture and temperature on the reduced bifurcation load. This reduction is also apparent at intermediate temperatures, (Figure 5.12) but to a lesser extent. Examination of the same panel but at moisture condition 1 also shows the effect of curvature on the reduced bifurcation load (See Figure 5.13). However, the overall effect is not as drastic as it is for moisture condition 2. Note that this plot is for the worst case only, which is at a temperature of 300°F.
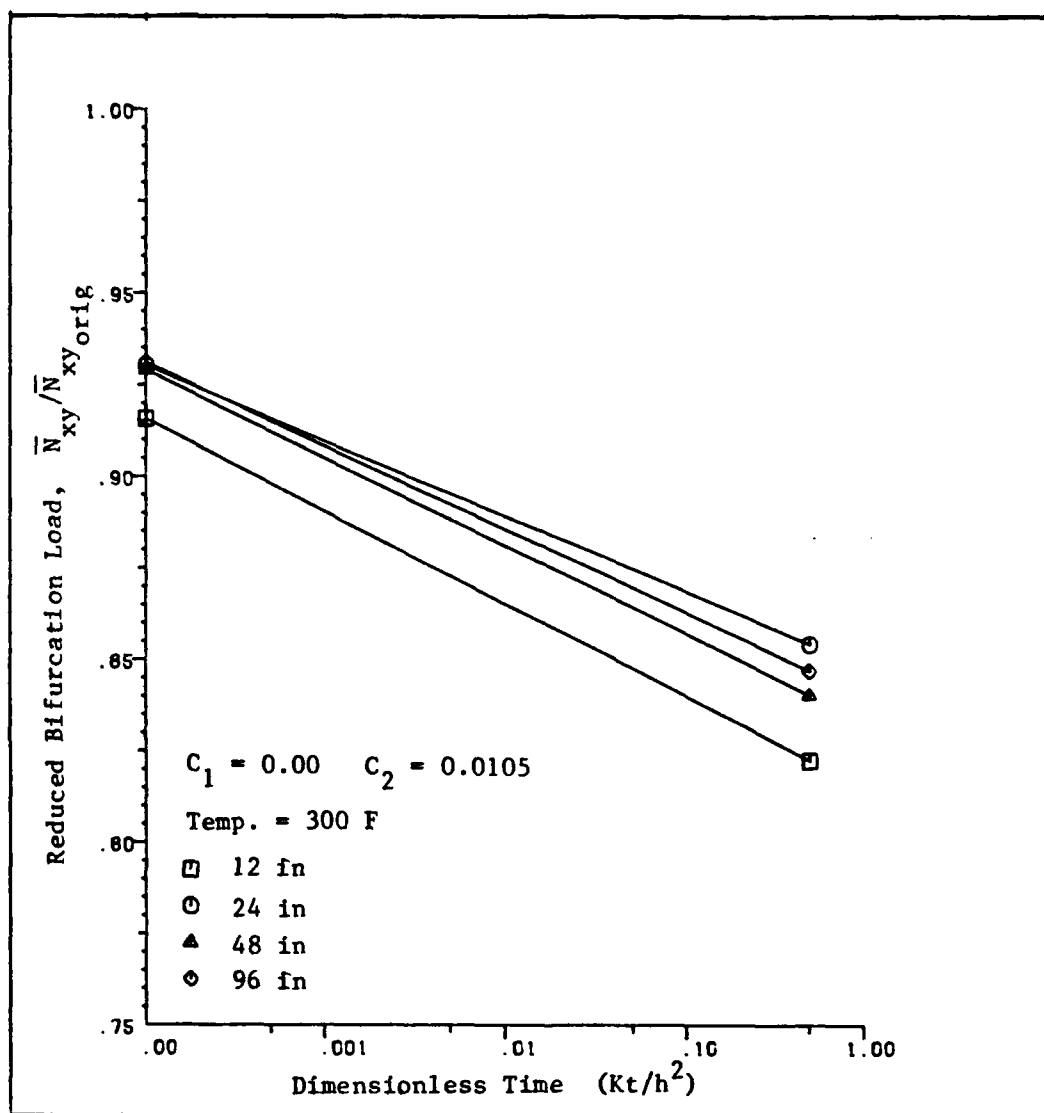
Figure 5.13 Effects of Curvature on Degradation in $\overline{N}_{xy}$ for the
$[45/-45]_{2s}$ Laminate, Moisture Condition 1

66

An interesting anomaly in Figure 5.10 is that the decrease in the reduced bifurcation load is not sequential in increasing radii. This can be seen by comparing the curves for 24, 36, and 48 in. at 300°F. The panel with a 24 in. radius falls above the panels with a 36 in. and 48 in. radius. This is contrary to what the theory indicates in Eq. (16), the strain-displacement relationships, where the curvature shows up as a linear dependent variable, which indicates that the curves should be sequential. Since Figure 5.10 is a plot for a normalized bifurcation load, $\bar{N}_{xy}/\bar{N}_{xy_{orig}}$, the question arose, "Is this anomaly actually in the bifurcation load or is it due to the normalizing factor?" Looking at the bifurcation load first, Figure 5.14 shows that as the radius increases the bifurcation load decreases for a given temperature and moisture condition. This was also shown in Figure 5.9. Both of these figures show that the bifurcation load is following the trend indicated by the theory. However, Figure 5.14 also shows that the rate of decrease is dependent on the moisture content for the given temperature. To correlate Figure 5.14 to Figure 5.10, the bifurcation loads were translated to a value of 150 lb/in so that each curve would have the same maximum (See Figure 5.15). This figure clearly shows that the plot of the bifurcation loads does not show the anomaly shown in Figure 5.10. Therefore, this anomaly must be due to the normalizing factor.

All the plots for the reduced bifurcation loads were normalized to the room temperature, 80°F and zero moisture concentration bifurcation load, $\bar{N}_{xy_{orig}}$. The bifurcation load is dependent, in general, on the prebuckled bending moments and membrane forces, with the curvature of

67
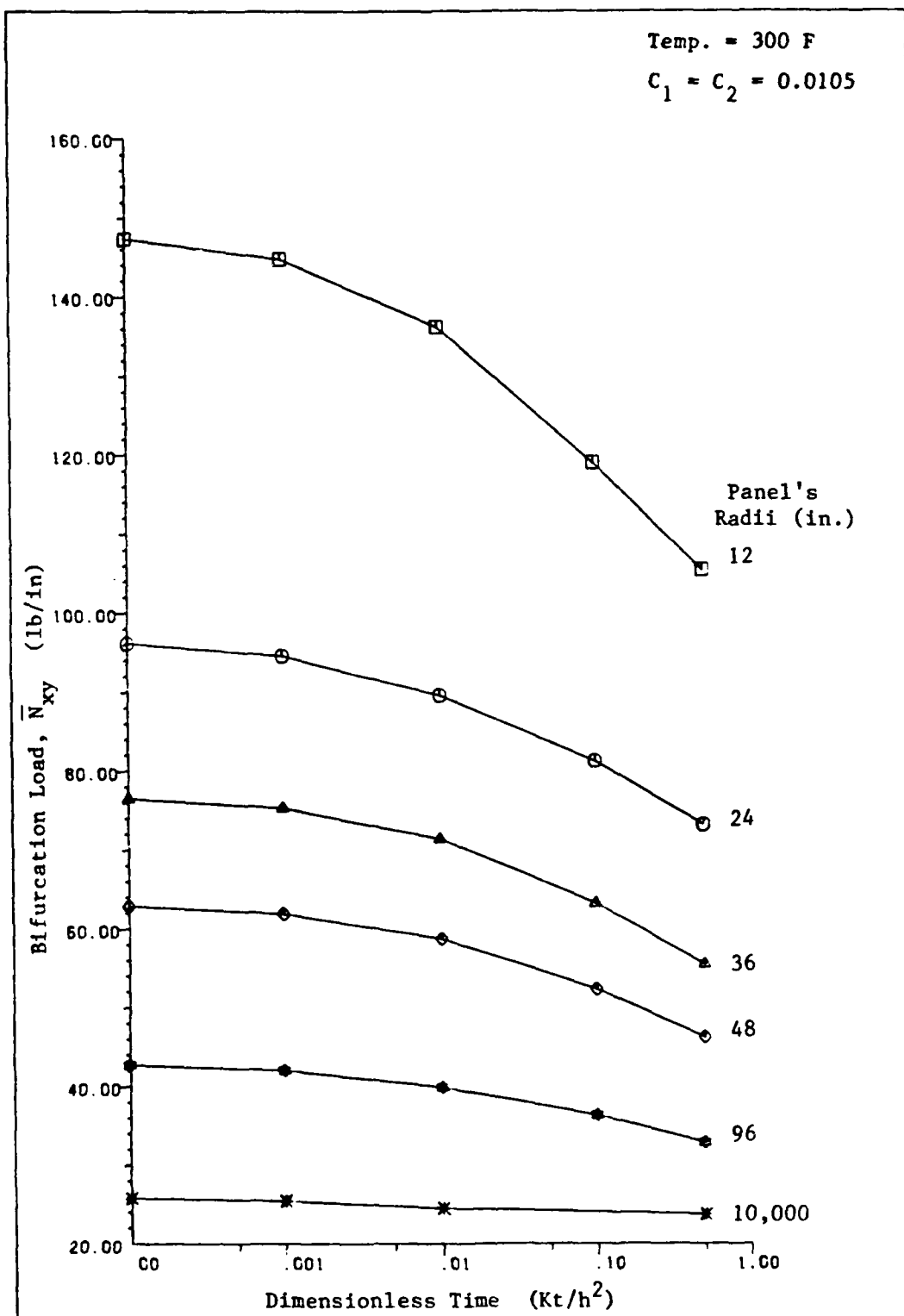
Figure 5.14 Effects of Curvature on the Bifurcation Load $\overline{N}_{xy}$, [45/-45]$_{2s}$ Panel
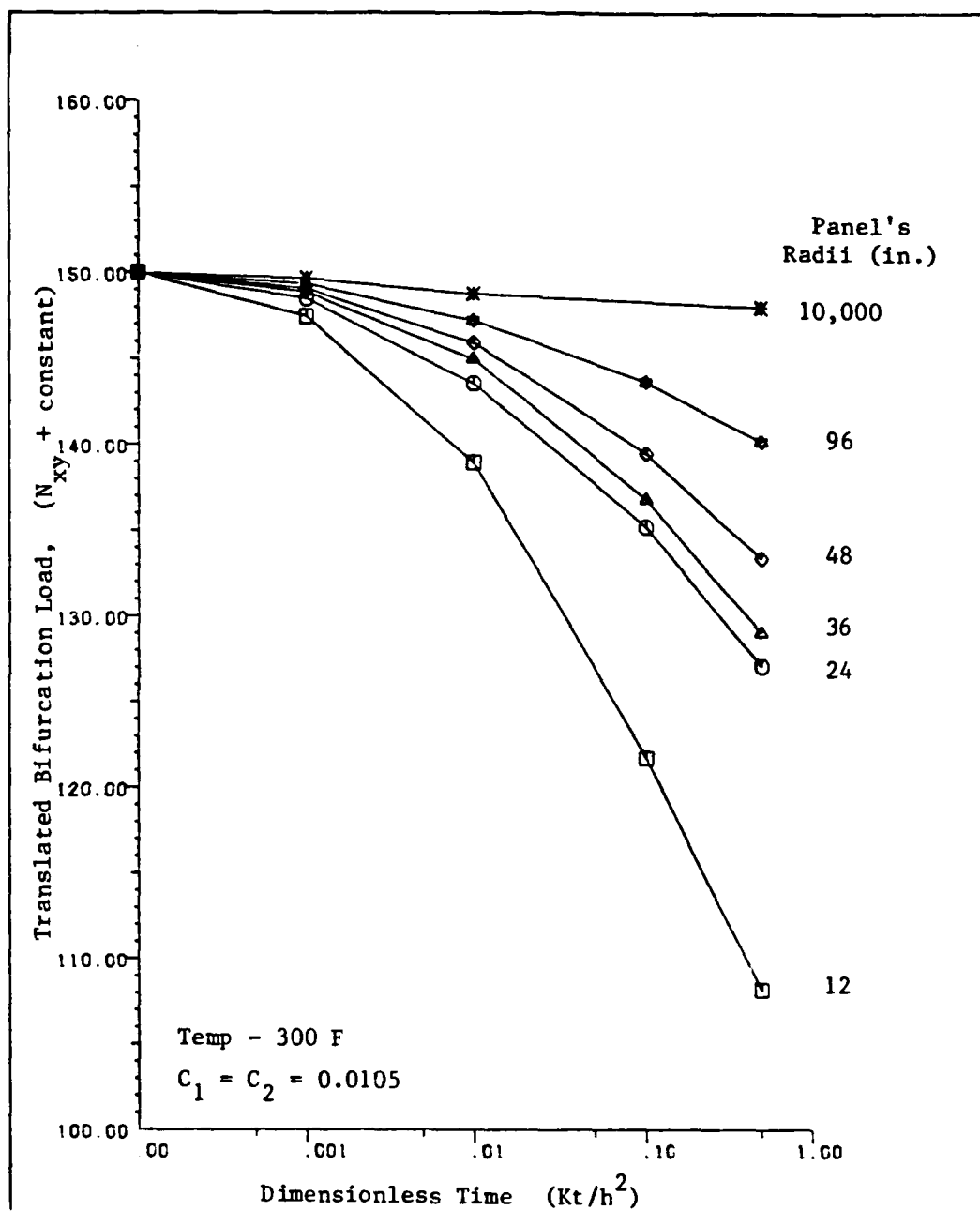
Figure 5.15 Effects of Curvature on the Translated Bifurcation Load $\bar{N}_{xy}$, $[45/-45]_{2s}$ Panel

the panel governing which load is more dominant. For a flat panel the dominant loads, which cause buckling, are the membrane forces and as the panels curvature increases the bending moments become important. What is being seen in Figure 5.10 is a transition in the dominant cause for buckling from membrane to bending. This is visiable since the normalizing factor is the relative shear bifurcation load.

Prebuckled Displacement, w and Eigenvector Characteristics

Figures 5.16, 5.17, and 5.18 show that there is a similarity in the appearance of the prebuckled displacements, w, when comparing the effects of temperature and moisture for a panel with a 12 in. radius. The primary difference being one of deflection magnitude. The terms 'Max.' and 'Min.' in these figures correspond to the maximum and minimum out-of-plane displacement caused by the unit line load N_{xy} applied on the panel's boundaries while the term 'Contour Step Size' indicates the increment between contour lines. As the radius increases there is a change in the panel's prebuckled displacement's, w, pattern. The area of negative displacement becomes greater, for increasing radii, due to decreasing effects of the prebuckle bending moments.

The eigenvectors, Figures 5.19 thru 5.21, are also not dependent on the moisture conditions and temperature, but they are dependent on the curvature, similar to the prebuckle displacement. The eigenvector for the panel with a 12 in. radius exhibits five half sine waves while a 10,000 in. radius exhibits two half sine waves. This also indicates

70

CASE 61

R = 12 in. $t^* = 0.0$ Temperature = 80 °F

Min.	Max.	Contour Step Size
-.1949E-5	.1863E-5	.1250E-6
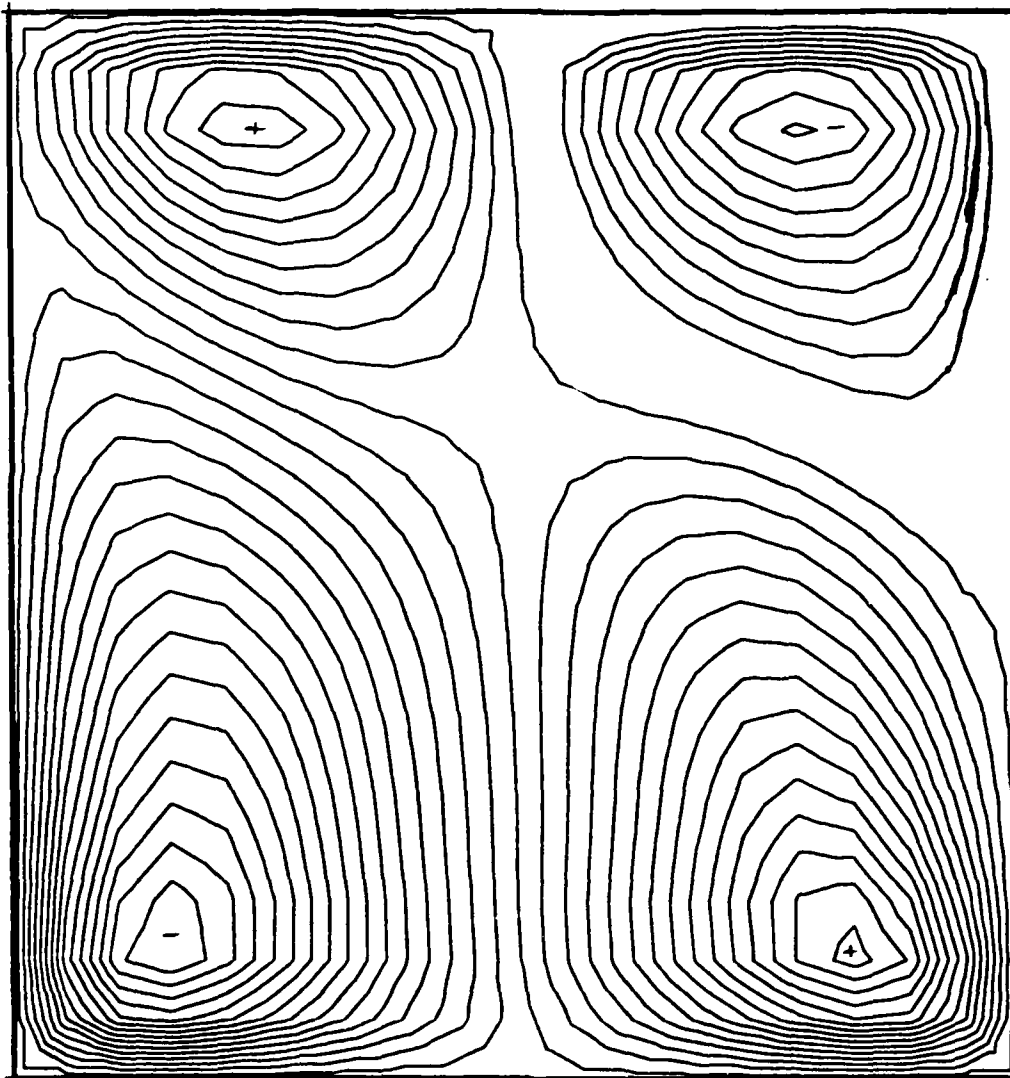
Figure 5.16 Contour Plots for the Prebuckled Displacement, w, [45/-45]2s at 80°F, t* = 0.0

71

R = 12 in. $t^* = 0.0$ Temperature = 300 °F

	Min.	Max.	Contour Step Size
	-.2397E-5	.2297E-5	.1540E-6
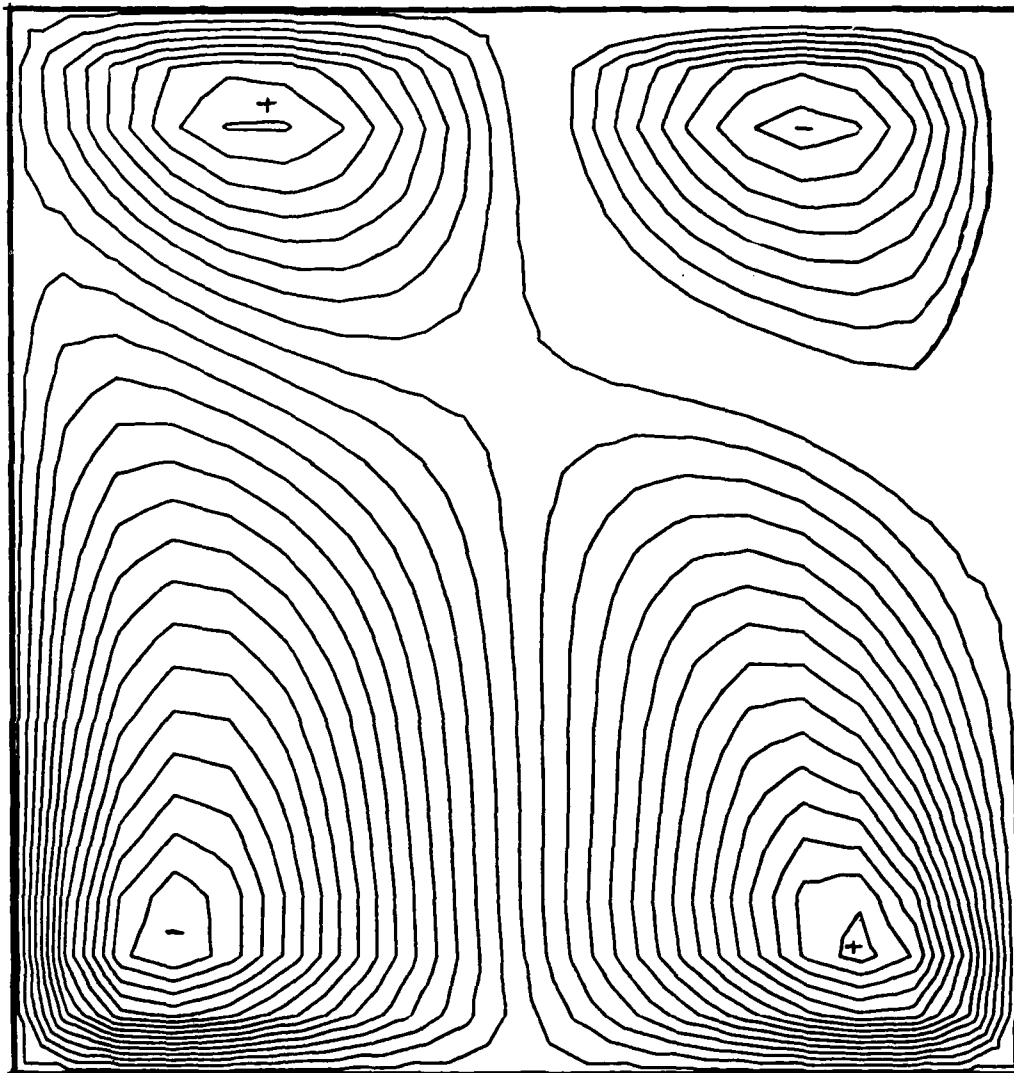
Figure 5.17 Contour Plots for the Prebuckled Displacement, w, $[45/-45]_{2s}$ at 300°F, $t^* = 0.0$

CASE 80

R = 12 in.   t* = 0.5   Temperature = 300 °F

	Min.	Max.	Contour Step Size
	-.6911E-5	.6691E-5	.4500E-6
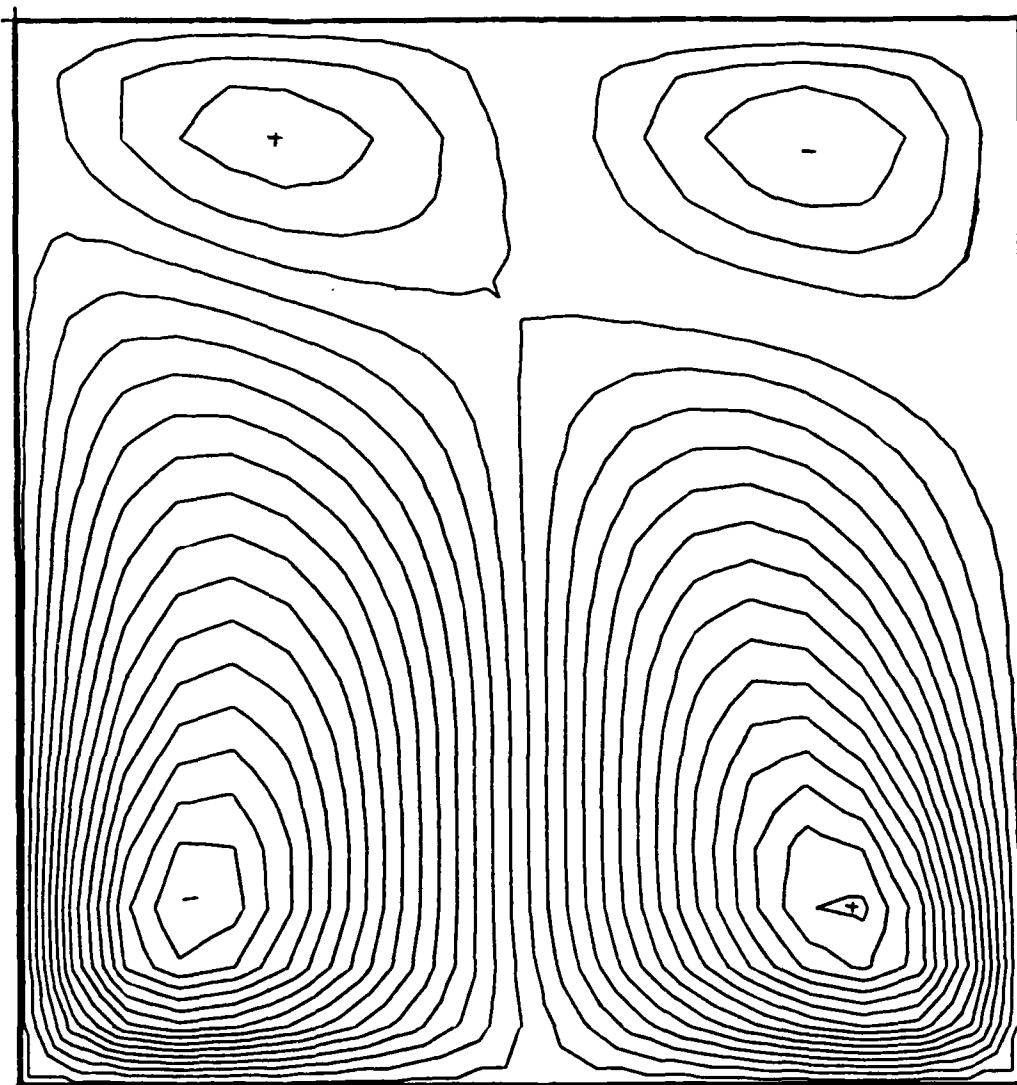
Figure 5.18 Contour Plots for the Prebuckled Displacement, w, [45/-45]$_{2s}$
at 300°F, t* = 0.5

73

CASE 61

$$R = 12 \text{ in.} \quad t^* = 0.0 \quad \text{Temperature} = 80 \text{ °F}$$

Min.	Max.	Contour Step Size
-.8537	.9231	.086
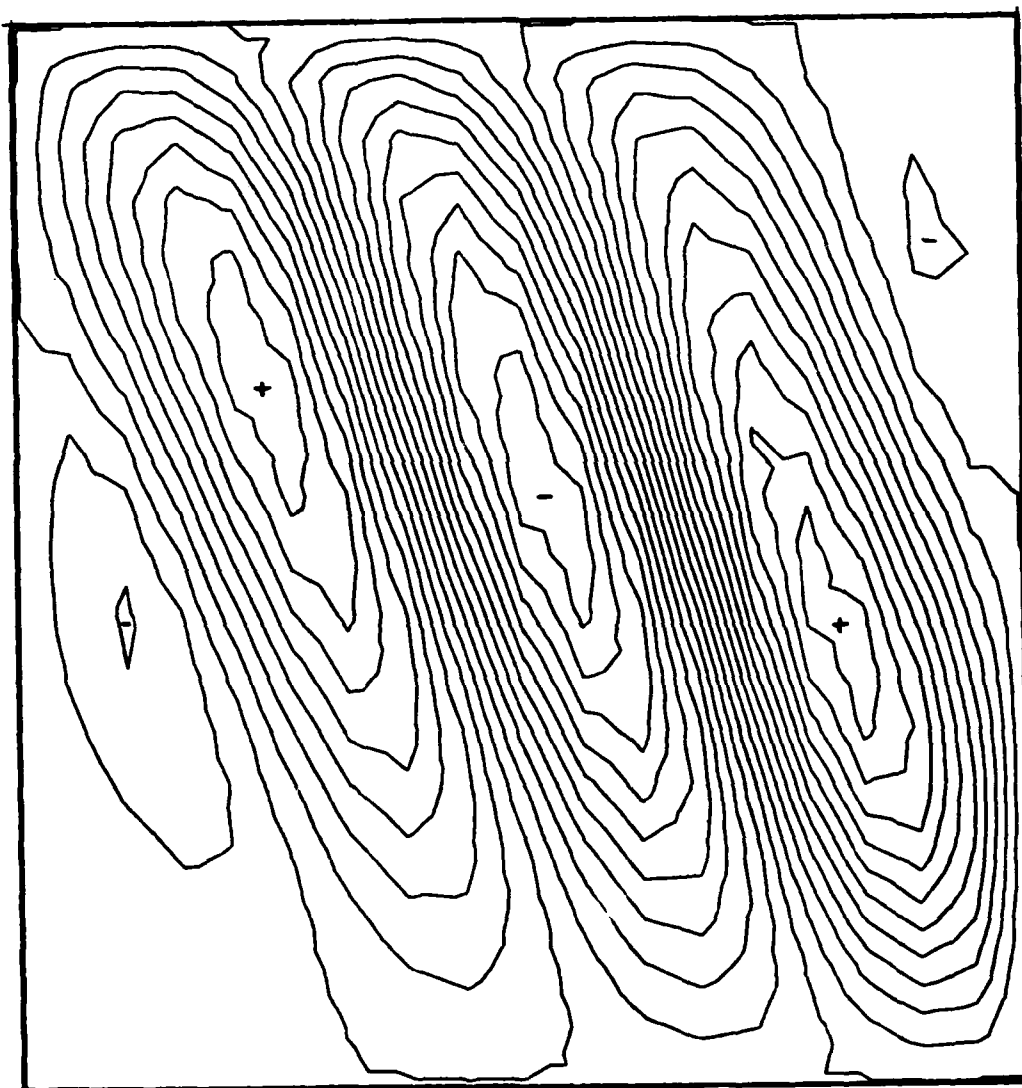
Figure 5.19 Contour Plots for the Eigenvector, w [45/-45]2s
at 80°F, t* = 0.0

R = 12 in.   t* = 0.0   Temperature = 300 °F

		Contour
Min.	Max.	Step Size
-.8808	.9417	.088
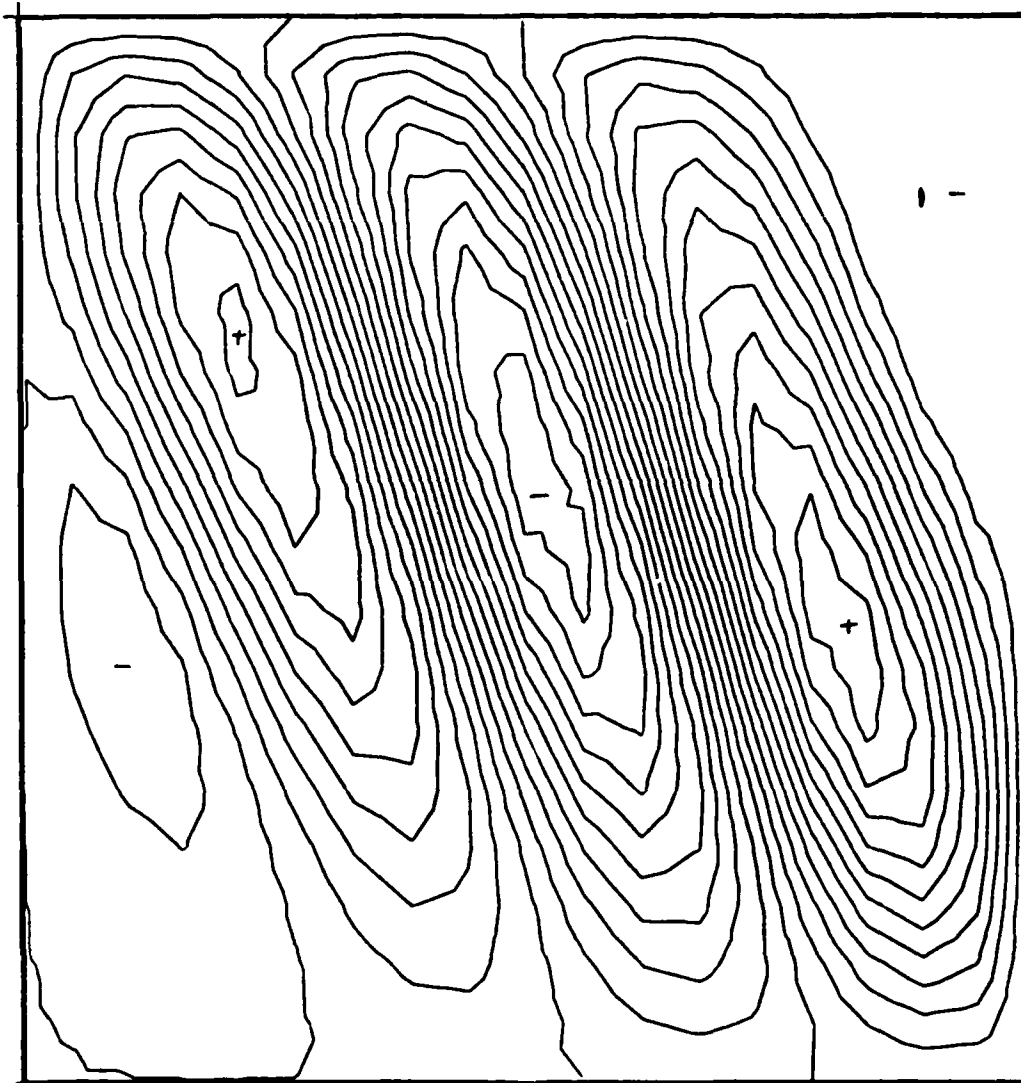
Figure 5.20 Contour Plots for the Eigenvector, w [45/-45]2s
at 300°F, t* = 0.0

R = 12 in.   t* = 0.5   Temperature = 300 °F

	Min.	Max.	Contour Step Size
	-.8469	1.0000	.090
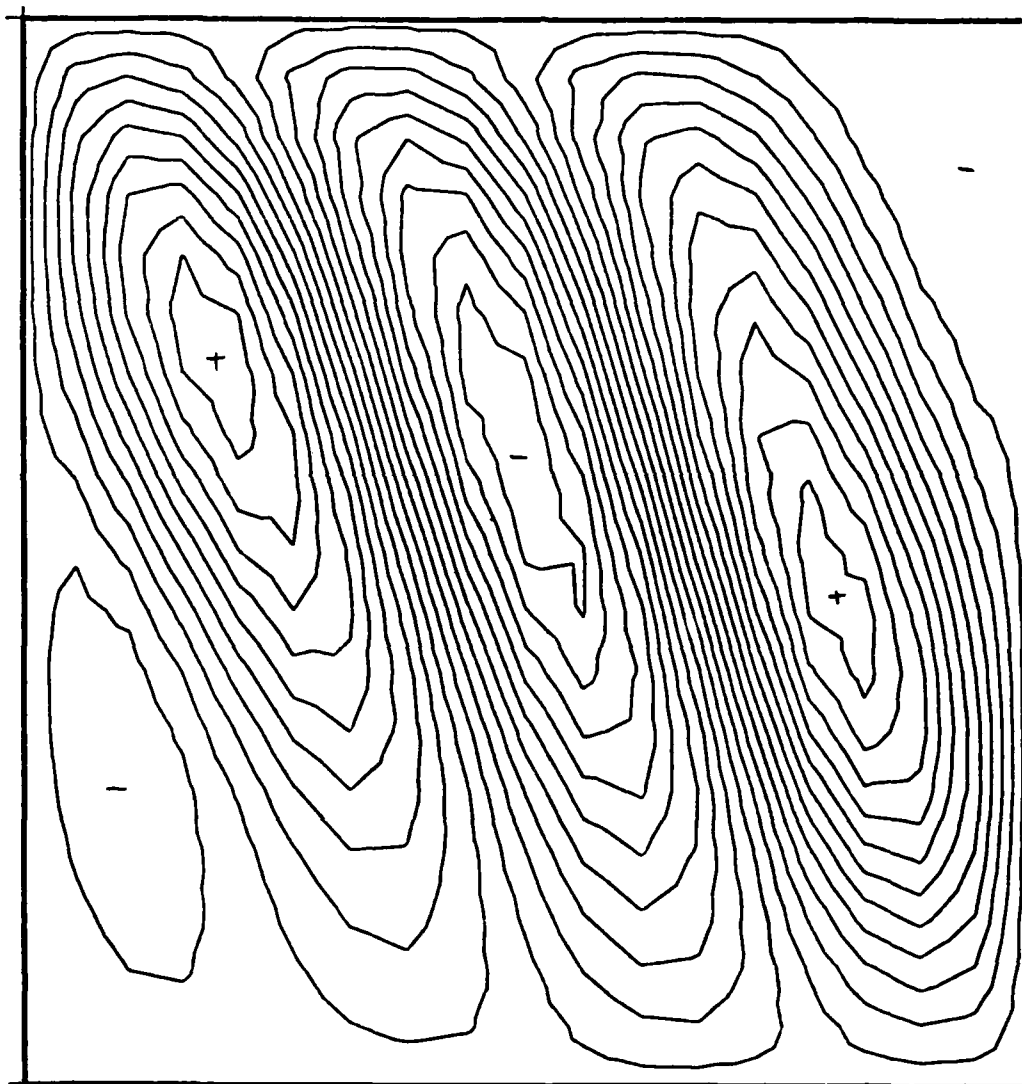
Figure 5.21 Contour Plots for the Eigenvector, w $[45/-45]_{2s}$
at 300°F, t* = 0.5

that the energy needed to buckle the panel, with a 12 in. radius, is greater than that for a 10,000 in. radius. Additional displacement, w, and eigenvector contour plots for representative cases of moisture, temperature, and curvature are included in Appendix C.

VI Conclusions

The following conclusions can be made for cylindrical, graphite/epoxy composite panels with various radii of curvature subject to moisture exposure and elevated temperatures, when loaded in simple shear.

1. The results for the STAGS-Cl finite element analysis, using flat plate elements, compare well to solutions obtained by Whitney[1], using the Galerkin method with the Donnell strain displacement relations, for relatively flat shells. (Radius/thicknest $\geq$ 1000)

2. The bifurcation load of a composite panel, with a resin material whose elastic moduli are reduced by absorbed moisture and elevated temperature, will degrade with increasing moisture concentrations and temperatures.

3. The trend for the reduction in bifurcation load of a composite panel subjected to a simple shear load is comparable to that found for an axial compression load at a given radius.

4. The extent of the degradation in the bifurcation load is influenced by the moisture concentration, the temperature, the panel's ply orientation, and panel's curvature. At 300°F, a radius of 12 in., and a symmetric moisture weight gain of 1.05 percent, the $[0/45/-45/90]_s$ panel experienced a 25.6 percent degradation and the $[45/-45]_{2s}$ panel experienced a 34.5 percent degradation.

5. The cylindrical panel's bifurcation load is influenced by the ply orientation, and curvature.

6. The bending – extension coupling induced by the unsymmetric initial moisture condition did not significantly influence the bifurcation load.

7. Increasing the cylindrical panel's radius decreased the panel's bifurcation load and can significantly change the moisture- and temperature-induced degradation characteristics for a given temperature.

8. If curvature is an important variable in a given problem, the use of the normalized bifurcation load, with respect to the membrane forces, can lead to conclusions that are invalid if one is trying to model the rate of change in the bifurcation load.

Appendix A

Computer Program

The main program calculates the moisture concentration at the mid-point of each lamina using Fick's Second Law of Diffusion. The main program calls the following subroutines.

Subroutine Header — Creates tape6 which contains the matrices A, B, and D and the $\bar{Q}_{ij}$'s.

Subroutine Calc1 — Calculates the reduced transverse and shear moduli and the value for ν_{21} for AS/3501-5, given the moisture concentration in the ply.

Subroutine Calc2 — Calculates the values for $\bar{Q}_{ij}$, A_{ij}, B_{ij}, and D_{ij}.

Subroutine Stags1
     and — Creates tape7 the input for STAGS-C1.
Subroutine Stags2

Computer Program

```
      PRCGRAM MC1C (INPUT,OUTPUT,TAFEE,TAPE7)
C
C
C ANTHONY D. STRAW, GAE-85D
C THIS PRCGRAM IS A MODIFICATICN OF CNE DEVELOPED BY JAMES M.
C SNEAD.
C
C
C THIS PRCGRAM CALCULATES THE MOISTURE CONCEATRATION THROUGH THE
C THICKNESS CF A COMPOSITE LAMINATE. THIS PRCGRAM ALSO CALCULATES THE
C PLY STIFFNESSES AND INVARIANT PRCPEFTIES, THE PLY'S REDUCED
C STIFFNESSES, AND THE LAMINATE'S [A!, [B!, ANC [D!.
C USING THE CALCULATED RECUCED MODULI, INPUT FILES FCR THE SJAGS
C FINITE ELEMENT BUCKLING LOAC PRCGRAM ARE WRITTEN  FCR A PANEL
C LOADED IN SIMPLE SHEAR.
C
C     REF. "THE MATHEMATICS OF DIFFUSION" BY JOHN CRANK, SECCND EDITICN,
C           CLAREDON PRESS, CXFCRD, 1975.
C     REF. "INTRODUCTION TC CCMPCSITE MATERIALS" BY STEPHEN W. TSAI AND
C           H. THCMAS HAHN, TECHNCPIC FUBLISHING CO., 1980.
C     REF. "MECHONICS OF COMPOSITE MATERIALS" BY ROBERT M. JCNES,
C           MCGRAW-HILL BCOK CCMPANY, 1975.
C
C     BASIC MOISTURE DIFFUSICN EQUATICN - FICK EQUATION (J. CRANK)
C
C           K*S.D. OF C WRT 2 = F.C. OF C WRT T
C           WHERE:
C             K = MOISTURE DIFFUSICN CCEFFICIENT
C             S.D. = SECCND PARITAL CERIVATIVE
C             F.C. = FIRST PARTIAL CERIVATIVE
C             WRT = WITH RESPECT TC
C             C = SPECIFIC MOISTURE CCNCENTRATION IN LAMINA
C             2 = SPACIAL CCORCINATE THRCUGH LAMINATE THICKNESS
C             T = TIME
C
C
C NOTES:
C     1. THIS PRCGRAM IS SET UP FOR AS/3501 GRAPHITE EPOXY USING
C        MATERIAL PRCPERTIES FCRM TSAI'S TEXT
C     2. THE TEMPERATURES ARE IN UNITS CF DEGREES KELVIN.
C     3. THE TEMPERATURE DISTRIBUTICN THRCUGH THE THICKNESS IS ASSUMEC
C        TO BE CONSTANT ANC EQUAL TO CNE OF THE FOUR SPECIFIED
C        TEMPERATURES DEFINED AS ELTEMP(4).
C     4. TAPEE CCNTAINS THE CUTPUT FILE ANC TAPE7 CCNTAINS THE INPUT
C        FILE FCR THE STAGS PRCGRAM.
      REAL K
      CCMMON/MAT/2(20),T(10),TNCNCIP(10),ELTEMP(4),L,NO,H,K,AL,LLL,TEMP,
     *C0,C1,C2,RAD,PI,TEMP2(20),C(4,5,8),E2(4,5,8),U21(4,5,8),
     *G12(4,5,8),THETA(8),Q11(4,5,8),G12(4,5,8),
     *Q22(4,5,8),Q66(4,5,8),U1(4,5,8),
     *U2(4,5,8),U3(4,5,8),U4(4,5,8),U5(4,5,8),
     *QR11(4,5,8),QR12(4,5,8),QR16(4,5,8),QR22(4,5,8),
     *QR26(4,5,8),QR66(4,5,8),E1,ICASE,HLAM,
     *A11(4,5),A12(4,5),A16(4,5),A22(4,5),A26(4,5),A66(4,5),
     *B11(4,5),B12(4,5),B16(4,5),B22(4,5),B26(4,5),B66(4,5),
     *D11(4,5),D12(4,5),D16(4,5),D22(4,5),D26(4,5),D66(4,5)
C THESE ARE THE FCUR TEMPERATURES AT WHICH TEST DATA FOR
```

```
C AS/3501 IS AVAILABLE IN TSAI'S TEXT
      ELTEMP(1)=300.
      ELTEMP(2)=366.
      ELTEMP(3)=394.
      ELTEMP(4)=422.
C AS/3501 E1 MODULI
      E1=18.85E06
C ZERO OUT THE ARRAYS
      DO 1 LLL=1,4
      DO 1 L=1,5
      DO 1 LL=1,8
      Z(LL)=THETA(LL)=0.0
      Q11(LLL,L,LL)=Q12(LLL,L,LL)=Q22(LLL,L,LL)=Q66(LLL,L,LL)=0.0
      U1(LLL,L,LL)=U2(LLL,L,LL)=U3(LLL,L,LL)=U4(LLL,L,LL)=U5(LLL,L,LL)
     *=0.0
      QR11(LLL,L,LL)=QR12(LLL,L,LL)=QR16(LLL,L,LL)=0.0
      QR22(LLL,L,LL)=QR26(LLL,L,LL)=QR66(LLL,L,LL)=0.0
    1 CONTINUE
      DO 4 L=1,10
    4 T(L)=TRCNDIP(L)=0.0
      PRINT *, ICASE,CO,C1,C2,H,HLAM,NC,K
C INPUT BEGINING CASE NO.(I5)
      PRINT *, " INPUT CASE NO. (I5) "
      READ *,ICASE
C INPUT CO,C1,C2 IN UNITS OF PERCENT/100 (EX.-1.0% = 0.01)
C   C1 IS THE CONCENTRATION ON THE INSIDE OF THE SHELL
C   C2 IS THE CONCENTRATION ON THE OUTSIDE OF THE SHELL
C   CO IS THE ORIGINAL CONCENTRATION IN THE LAMINATE
      PRINT *," INPUT CO,C1,C2 "
      READ *,CO,C1,C2
C INPUT LAMINAE THICKNESS AND NUMBER OF PLIES
      PRINT *, " INPUT LAMINAE THICKNESS AND NO. OF PLIES "
      READ *, HLAM,NO
C CALCULATE LAMINATE THICKNESS
      H=NC*HLAM
C CALCULATE THE CENTER OF EACH LAMINAE
      Z(1)=HLAM/2.0
      DO 2 L=2,NC
    2 Z(L)=Z(L-1)+HLAM
C INPUT THE PLY ORIENTATIONS FROM INSIDE TO OUTSIDE
      PRINT *, " INPUT PLY ORIENTATIONS FROM INSIDE TO OUTSIDE "
      DO 5 L=1,NC
      READ *,THETA(L)
    5 CONTINUE
C INPUT THE SHELL RADIUS IN INCHES
      PRINT *,"INPUT THE SHELL RADIUS IN INCHES"
      READ *, RAD
C DIFFUSION TEMPERATURE = 300 K (80 F)
      TEMP=300.
C REF. TSAI FOR EQUATION 8.40 TO CALCULATE K FOR GRAPHITE/EPOXY
C         K=KO*EXP(-ED/RT) (8.40)
C         K=6.51*EXP(-5722/TEMP(DEG KELVIN)) (FIG 8.7)
      K=6.51*EXP(-5722/TEMP)*0.03937**2
C INPUT NO. OF TIME INTERVALS AT WHICH MOISTURE DISTRIBUTION IN THE
C LAMINATE WILL BE CALCULATED
      PRINT *, " INPUT NO. OF TIME INTERVALS "
      READ *, NTIME
C INPUT NONDIMENSIONAL TIME INTERVALS (K*T/H**2)
      PRINT*, " INPUT TIME INTERVALS (K*T/H**2) "
      DO 3 L=1,NTIME
    3 READ *,TNONDIP(L)

      PI=3.14159265358979
      ICASE=ICASE-1
```

82

END

FILMED

DTIC
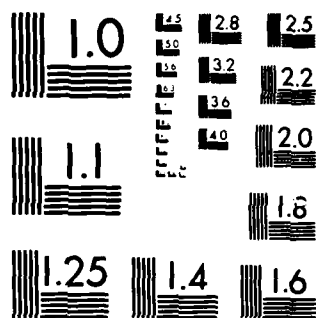
MICROCOPY RESOLUTION TEST CHART

NATIONAL BUREAU OF STANDARDS 1963-A

```
      DO 1009 LLL=1,4
      DO 1000 L=1,NTIME
      T(L)=TNONDIM(L)*H**2/K
      ICASE=ICASE+1
      CALL HEADER
      CALL STAGS1
      DO 2000 LL=1,NO
      TEMP2(LL)=ELTEMP(LLL)
      C(LLL,L,LL)=0.
      IF(T(L).EQ.0.) GO TC 12
      C(LLL,L,LL)=C1+(C2-C1)*Z(LL)/H
      CTEMP1=0.
      CTEMP2=0.
      N=0
   11 N=N+1
      IF(ABS(-K*N**2*PI**2*T(L)/H**2).GE.500.) GC TC 12
      CTEMP1=(2/PI)*((C2*CCS(N*PI)-C1)/N*SIN(N*PI*Z(LL)/H)
      CTEMP1=CTEMP1*EXP(-K*N**2*PI**2*T(L)/H**2)
      C(LLL,L,LL)=C(LLL,L,LL)+CTEMP1
      M=(N-1)/2
      CTEMP2=(4*CC/PI)/(2*M+1)*SIN((2*M+1)*PI*Z(LL)/H)
      CTEMP2=CTEMP2*EXP(-K*(2*M+1)**2*PI**2*T(L)/H**2)
      C(LLL,L,LL)=C(LLL,L,LL)+CTEMP2
      N=N+1
      CTEMP3=(2/PI)*((C2*CCS(N*PI)-C1)/N*SIN(N*PI*Z(LL)/H)
      CTEMP3=CTEMP3*EXP(-K*N**2*PI**2*T(L)/H**2)
      C(LLL,L,LL)=C(LLL,L,LL)+CTEMP3
      GO TO 11
   12 CONTINUE
      IF(C(LLL,L,LL).LT.0.0) C(LLL,L,LL)=0.0
      ZZ=Z(LL)/H
      CALL CALC1(C(LLL,L,LL),TEMP2(LL),E2(LLL,L,LL),U21(LLL,L,LL),
     * G12(LLL,L,LL))
  102 FORMAT(T10,I1,T30,"SI-1 DEFINES MATERIAL NC.")
      WRITE(7,102)LL
  100 FORMAT(4X,I1,2X,F6.4,2X,F6.4,1X,F7.5,1X,E11.5,1X,F8.5,1X,E11.5,1X,
     * I3,1X,I3)
  101 FORMAT(T3,"1R.85E06,",F10.7,",",F10.1,",.056,1.,",F10.4,",1.
     * SI-2")
      WRITE(7,101)U21(LLL,L,LL),G12(LLL,L,LL),E2(LLL,L,LL)
      WRITE(6,100)LL,ZZ,Z(LL),C(LLL,L,LL),E2(LLL,L,LL),U21(LLL,L,LL),
     *G12(LLL,L,LL),N,M
 2000 CONTINUE
      CALL CALC2
      CALL STAGS2
 1000 CONTINUE
      STCP
      END


      SUBROUTINE HEADER
      REAL K
      COMMON/MAT/Z(20),T(10),TNONDIM(10),ELTEMP(4),L,NO,H,K,LL,LLL,TEMP,
     *CO,C1,C2,RAD,PI,TEMP2(20),C(4,5,8),E2(4,5,8),U21(4,5,8),
     *G12(4,5,8),THETA(8),011(4,5,8),G12(4,5,8),
     *022(4,5,8),066(4,5,8),L1(4,5,8),
     *U2(4,5,8),U3(4,5,8),U4(4,5,8),U5(4,5,8),
     *QR11(4,5,8),QR12(4,5,8),QR16(4,5,8),QR22(4,5,8),
     *QR26(4,5,8),QR66(4,5,8),E1,ICASE,MLAM,
     *A11(4,5),A12(4,5),A16(4,5),A22(4,5),A26(4,5),A66(4,5),
     *B11(4,5),B12(4,5),B16(4,5),B22(4,5),B26(4,5),B66(4,5),
     *D11(4,5),D12(4,5),D16(4,5),D22(4,5),D26(4,5),D66(4,5)
  100 FORMAT(1H1,///)
```

83

```
101    FORMAT(T5,"PLY",T9,"Z/H",T17,"Z",T24,"C",T32,"E2",T44,"PU21",
      *T53,"G12",T64,"R",T68,"P",/,T17,"(IN.)",T32,"REDUCED",
      *T44,"REDUCED",T53,"REDUCED",/)
103    FORMAT(///)
104    FORMAT(T3,"CASE NC. ",I5," SHEAR INSTABILITY IN COMPOSITE PANELS"/
      *T5,"CALCULATION OF MOISTURE DISTRIBUTION IN ",I3,
      **PLY LAMINATE"/T5,"PLY ORIENTATION (",F5.1,",",F5.1,",",F5.1,",",
      *F5.1,",",F5.1,",",F5.1,",",F5.1,",",F5.1,")",/
      *T5,"MOISTURE DIFFUSION COEFFICIENT = ",
      *E11.5,/,T5,"DIFFUSION TEMPERATUE= ",F7.2," (KELVIN)",
      */,T5,"PLY THICKNESS = 0.005 IN.",/,T5,"CO = ",F9.5," C1 = ",
      *F9.5," C2 = ",F9.5,/,"     ORIGINAL MODULI",/,T5,"E1 = 18.85E06",
      ** E2=1.41375E06 U21=0.02250  G12=0.8555E06 (PSI)",/,T54
      **NONDIMENSICNAL TIME = ",E11.5,5X,"TIME (SEC) = ",E11.5,/)
  10   WRITE(6,100)
       WRITE(6,104)ICASE,NC,THETA(1),THETA(2),THETA(3),THETA(4),
      *THETA(5),THETA(6),THETA(7),THETA(8),K,TEMP,CO,C1,C2,
      *TNONDIM(L),T(L)
  20 CONTINUE
       WRITE(6,101)
       RETURN
       END

       SUBROUTINE CALC1(C,TEMP,E2,U21,G12)
       DIMENSION S(4,3),SS(4,2),X(3)
       N=0
       IF(TEMP.EQ.300.) N=1
       IF(TEMP.EQ.366.) N=2
       IF(TEMP.EQ.394.) N=3
       IF(TEMP.EQ.422.) N=4
       IF(N.EQ.0) PRINT *," ERROR IN CALC"
C  REF. TSAI FOR AS/3501 E2 AND G12 MODULI
       S(1,1)=1.41375E06
       S(1,2)=1.305E06
       S(1,3)=1.2615E06
       S(2,1)=1.05475E06
       S(2,2)=.9135E06
       S(2,3)=.841E06
       S(3,1)=1.015E06
       S(3,2)=.6235E06
       S(3,3)=.4705E06
       S(4,1)=1.015E06
       S(4,2)=.522E06
       S(4,3)=.290E06
       SS(1,1)=.8555E06
       SS(1,2)=.8555E06
       SS(2,1)=.7830E06
       SS(2,2)=.65975E06
       SS(3,1)=.6815E06
       SS(3,2)=.3915E06
       SS(4,1)=.6525E06
       SS(4,2)=.15225E06
       X(1)=0.00
       X(2)=0.005
       X(3)=0.0105
       U12=0.300
       IF(C.GE.0.005) GO TO 10
       SLOPE=(S(N,2)-S(N,1))/(X(2)-X(1))
       R=S(N,1)-SLOPE*X(1)
       E2=SLOPE*C+R
       U21= U12*E2/18.85E06
       GO TO 20
  10   CONTINUE
```

84

```
      SLOPE = (S(N,3)-S(N,2))/(X(3)-X(2))
      B=S(N,2)-SLOPE*X(2)
      E2=SLOPE*C+B
      U21=U12*E2/18.85E06
   20 CONTINUE
      SLOPE=(SS(N,2)-SS(N,1))/(X(3)-X(1))
      B=SS(N,1)-SLOPE*X(1)
      G12=SLOPE*C+B
      RETURN
      END

      SUBROUTINE STAGS1
      REAL K
      COMMON/MAT/Z(20),T(10),TNCADIM(10),ELTEMP(4),L,RO,H,K,AL,LLL,TEMP,
     *C0,C1,C2,RAD,PI,TEMP2(20),C(4,5,8),E2(4,5,8),L21(4,5,8),
     *G12(4,5,8),THETA(8),Q11(4,5,8),G12(4,5,8),
     *Q22(4,5,8),Q66(4,5,8),L1(4,5,8),
     *U2(4,5,8),U3(4,5,8),U4(4,5,8),U5(4,5,8),
     *QR11(4,5,8),QR12(4,5,8),QR1E(4,5,8),QR22(4,5,8),
     *QR2E(4,5,8),QR6E(4,5,8),E1,ICASE,HLAM,
     *A11(4,5),A12(4,5),A16(4,5),A22(4,5),A26(4,5),A66(4,5),
     *B11(4,5),B12(4,5),B16(4,5),B22(4,5),B26(4,5),B66(4,5),
     *D11(4,5),D12(4,5),D16(4,5),D22(4,5),D26(4,5),D66(4,5)
  100 FORMAT("/JCP",/"ACSTRAL,CP24000C. E851215,STRAL,EN,547,1",
     */"USER",/"CHARGE,*.*",
     */"RFL=240000.",/"SETTL(700).",/"ATTACH,STAGS1/UN=D820050.",
     */"ATTACH,STAGS2/UN=E820090.",/"STAGS1.",/"RETLRN,STAGS1.",
     */"RFL=240000.",/"STAGS2.",/
     *"RETURN,STAGS2.",/
     *"SWRITE,TAPE21,CASE",I4,"P,AC1=EF10472.",/
     *"SWRITE,TAPE22,CASE",I4,"S,AC1=E810472.",/
     *"/ECR")
      WRITE(7,100)ICASE+1000,ICASE+1000

  101 FORMAT(T3,"CASE NO. ",I5," SHEAR INSTABILITY IN COMPOSITE PANELS",
     */"C  PLY ORIENTATION (",F5.1,",",F5.1,",",F5.1,",",F5.1,",",
     *F5.1,",",F5.1,",",F5.1,",",F5.1,")",/
     *"C  BOUNDARY CONDITION - TOP - U,V,RV,RW FREE ",/
     *"C                       SIDES - U,V,RL,RW FREE ",/
     *"C                       BOTTOM - RV,RL  FREE ",/
     *"C  PANEL RADIUS = ",E9.3," INCHES",/
     *"C  ELEMENT TYPE = 410",/
     *"C",/
     *"C  TRANSVERSE AND SHEAR MODULI REDUCED DUE TO MOISTURE AND TEFF",
     */"C  ORIGINAL MODULI FOR AS/3501 GRAPHITE/EPOXY IS",/
     *"C  E1=18.85E06  E2=1.41375E06  U21=.0225  G12=0.8555E+6 (PSI)",/
     *"C  MOISTURE DIFFUSION COEFFICIENT = ",E11.5," AT ",F6.1," DEG
     * KELVIN",/"C  C0 = ",E11.5," C1 = ",E11.5," C2 = ",E11.5,/
     *"C  C1 IS INSIDE SHELL; C2 IS OUTSIDE SHELL",/
     *"C  NONDIMENSIONAL TIME = ",E11.5," TIME (SEC) = ",E11.5,/
     *"C  LAMINATE TEMPERATURE = ",F6.1," (KELVIN)")
      WRITE(7,101)ICASE,THETA(1),THETA(2),THETA(3),THETA(4),THETA(5),
     *THETA(6),THETA(7),THETA(8),RAD,K,TEMP,C0,C1,C2,TNONDIM(L),T(L),
     *ELTEMP(LLL)

  102 FORMAT(T10,"1,1,1,0,0",T30,"$B-1 LINEAR BIFURCATION ANAL",/
     *T10,"1",T30,"$B-2 1 SHELL UNIT USED",/
     *T10,"8,0,1,0",T30,"$B-3 8 MATERIALS; 1 SHELL WALL PROPERTY",/
     *T10,"1.",T30,"$C-1 STARTING LOAD FACTOR",/
     *T10,"1.0,E50",T30,"$D-2 NO. OF EIGENVALUES;MAX NO. CPU SECS",/
     *T10,"1",T30,"$D-3 EIGENVALUE PER CLUSTER TO BE COMPUTED",/
     *T10,"19,19",T30,"$F-1 19 ROWS, 19 COLUMNS")
```

```
      WRITE(7,102)

      RETURN
      END

      SUBROUTINE STAGS2
      REAL K
      COMMON/MAT/Z(20),T(10),TNCNDIP(10),ELTEPP(4),L,NO,H,K,AL,LLL,TEPP,
     *C0,C1,C2,RAD,PI,TEPF2(20),C(4,5,8),E2(4,5,8),U21(4,5,8),
     *G12(4,5,8),THETA(8),Q11(4,5,8),G12(4,5,8),
     *Q22(4,5,8),Q66(4,5,8),U1(4,5,8),
     *U2(4,5,8),U3(4,5,8),U4(4,5,8),L5(4,5,8),
     *QR11(4,5,8),QR12(4,5,8),QR16(4,5,8),QR22(4,5,8),
     *QR26(4,5,8),QR66(4,5,8),E1,ICASE,HLAM,
     *A11(4,5),A12(4,5),A16(4,5),A22(4,5),A26(4,5),A66(4,5),
     *B11(4,5),B12(4,5),B16(4,5),B22(4,5),B26(4,5),B66(4,5),
     *D11(4,5),D12(4,5),D16(4,5),D22(4,5),D26(4,5),D66(4,5)
  105 FORMAT(T10,"1,1,",I2,T25,"SK-1 1 WALL COEF. NO., GEN LAYER WALL,"
     *I2," PLIES",/T10,"1, .005, ",F6.2,"   SK-2")
      WRITE(7,105)NO,AO,THETA(1)
      NOTEPP=NO-1
      ANGB=12*180/(RAD*PI)
      DO 1 J=2,NOTEPP
    1 WRITE(7,106)J,THETA(J)
  106 FORMAT(T9,I2,", .005, ",F6.2)
  107 FORMAT(T9,I2,", .005, ",F6.2,"   SK-2")
      WRITE(7,107)NC,THETA(NC)
  108 FORMAT(T10,"5",T30,"SP-1 CYLINDRICAL SHELL GEOMETRY",/
     *T5,"0., 12., 0., ",F10.7,",",E5.3,"      SK-2A",/
     *T10,"1",T30,"SM-5 SHELL WALL COEF. NO. IN DATA TABLE",/
     *T10,"410",T30,"SN-1 ELEMENT TYPE",/
     *T10,"0,0,0,0",T30,"SP-1 BOUNDARY CONSTRAINTS DEFINED ON NEXT CARD"
     *,/T10,"110,C11",T30,"SP-2 TOP - L,V,RV,RW=FREE; W,RU=FIXED",/
     *T10,"110,101",T30,"SP-2 RIGHT SIDE - L,V,RU,RW=FREE",/
     *T10,"000,C11",T30,"SP-2 BOTTOM - RV,RW = FREE",/
     *T10,"110,101",T30,"SP-2 LEFT SIDE - U,V,RU,RW = FREE",/
     *T10,"1",T30,"SG-1 NO. OF LOAD SYSTEMS",/
     *T10,"1,4,0",T30,"SQ-2",/
     *T9,"-1.,2.,2,1,0",T30,"SQ-3   TOP LINE LOAD",/
     *T10,"1.,3,1,0,15",T30,"SQ-3   RIGHT LINE LOAD",/
     *T10,"1.,2,2,19,0",T30,"SQ-3   BOTTOM LINE LOAD",/
     *T9,"-1.,3,1,0,1",T30,"SG-3   LEFT LINE LOAD",/
     *T10,"1,1,1,0    ",T30,"SR-1   OUTPUT CONTROL",/
     *"*/EOR")
      WRITE(7,108) ANGB,RAD

      RETURN
      END

      SUBROUTINE CALC2
C THIS SUBROUTINE CALCULATES THE PLY AND LAMINATE STIFFNESSES

      REAL K
      DIMENSION TTHETA(20),ZZ(20)
      COMMON/MAT/Z(20),T(10),TNCNDIP(10),ELTEPP(4),L,NO,H,K,AL,LLL,TEPP,
     *C0,C1,C2,RAD,PI,TEPF2(20),C(4,5,8),E2(4,5,8),U21(4,5,8),
     *G12(4,5,8),THETA(8),Q11(4,5,8),G12(4,5,8),
     *Q22(4,5,8),Q66(4,5,8),L1(4,5,8),
     *U2(4,5,8),U3(4,5,8),U4(4,5,8),L5(4,5,8),
     *QR11(4,5,8),QR12(4,5,8),QR16(4,5,8),QR22(4,5,8),
     *QR26(4,5,8),QR66(4,5,8),E1,ICASE,HLAM,
     *A11(4,5),A12(4,5),A16(4,5),A22(4,5),A26(4,5),A66(4,5),
     *B11(4,5),B12(4,5),B16(4,5),B22(4,5),B26(4,5),B66(4,5),
     *D11(4,5),D12(4,5),D16(4,5),D22(4,5),D26(4,5),D66(4,5)
```

```
C   U12 FOR AS/3501 GRAPHITE/EPOXY
      U12=0.300
      DO 1 J=1,NC
C   CALCULATING PLY STIFFNESSES
      Q11(LLL,L,J)=E1/(1.-U12*U21(LLL,L,J))
      Q12(LLL,L,J)=U12*E2(LLL,L,J)/(1.-U12*U21(LLL,L,J))
      Q22(LLL,L,J)=E2(LLL,L,J)/(1.-U12*U21(LLL,L,J))
    1 Q66(LLL,L,J)=G12(LLL,L,J)

C   CALCULATING THE REDUCED PLY STIFFNESSES USING THE INVARIANT
C   PROPERTIES APPROACH OF TSAI AND PAGANO (REF. JONES)
      DO 2 J=1,NC
      U1(LLL,L,J)=(3.*Q11(LLL,L,J)+3.*Q22(LLL,L,J)+2.*Q12(LLL,L,J)+
     *4.*Q66(LLL,L,J))/8.
      U2(LLL,L,J)=(Q11(LLL,L,J)-Q22(LLL,L,J))/2.
      U3(LLL,L,J)=(Q11(LLL,L,J)+Q22(LLL,L,J)-2.*Q12(LLL,L,J)-4.*
     *Q66(LLL,L,J))/8.
      U4(LLL,L,J)=(Q11(LLL,L,J)+Q22(LLL,L,J)+6.*Q12(LLL,L,J)-4.*
     *Q66(LLL,L,J))/8.
    2 U5(LLL,L,J)=(Q11(LLL,L,J)+Q22(LLL,L,J)-2.*Q12(LLL,L,J)+4.*
     *Q66(LLL,L,J))/8.

C   CHANGING THE SIGN OF THETA TO BE CONSISTANT WITH THE TSAI/PAGANO
C   FORMULATION AS SHOWN IN JONES
      DO 3 J=1,NC
    3 TTHETA(J)=-THETA(J)*3.14159265441/180.

C   CALCULATING THE REDUCED STIFFNESSES
C
      DO 4 J=1,NC
      QR11(LLL,L,J)=U1(LLL,L,J)+U2(LLL,L,J)*COS(2.*TTHETA(J))+U3(LLL,
     *L,J)*COS(4.*TTHETA(J))
      QR12(LLL,L,J)=U4(LLL,L,J)-U3(LLL,L,J)*COS(4.*TTHETA(J))
      QR22(LLL,L,J)=U1(LLL,L,J)-U2(LLL,L,J)*COS(2.*TTHETA(J))+U3(LLL,
     *L,J)*COS(4.*TTHETA(J))
      QR16(LLL,L,J)=-.5*U2(LLL,L,J)*SIN(2.*TTHETA(J))-U3(LLL,L,J)*
     *SIN(4.*TTHETA(J))
      QR26(LLL,L,J)=-.5*U2(LLL,L,J)*SIN(2.*TTHETA(J))+U3(LLL,L,J)*
     *SIN(4.*TTHETA(J))
    4 QR66(LLL,L,J)=U5(LLL,L,J)-U3(LLL,L,J)*COS(4.*TTHETA(J))
C
C   CALCULATING THE Z COORDINATE PER FIG. 4-5 IN JONES
C
      ZZ(1)=-NO*HLAM/2.
      NOTEMP=NO+1
      DO 5 J=2,NOTEMP
    5 ZZ(J)=ZZ(J-1)+HLAM
C
C   CALCULATING THE [A], [B], AND [C]
C
      A11(LLL,L)=A12(LLL,L)=A16(LLL,L)=A22(LLL,L)=A26(LLL,L)=A66(LLL,L)
     *=0.0
      DO 6 J=1,NC
      ZTEMP=ZZ(J+1)-ZZ(J)
      A11(LLL,L)=A11(LLL,L)+QR11(LLL,L,J)*ZTEMP
      A12(LLL,L)=A12(LLL,L)+QR12(LLL,L,J)*ZTEMP
      A16(LLL,L)=A16(LLL,L)+QR16(LLL,L,J)*ZTEMP
      A22(LLL,L)=A22(LLL,L)+QR22(LLL,L,J)*ZTEMP
      A26(LLL,L)=A26(LLL,L)+QR26(LLL,L,J)*ZTEMP
      A66(LLL,L)=A66(LLL,L)+QR66(LLL,L,J)*ZTEMP
    6 CONTINUE
      B11(LLL,L)=B12(LLL,L)=B16(LLL,L)=B22(LLL,L)=B26(LLL,L)=B66(LLL,L)
     *=0.0
```

87

```fortran
      DO 7 J=1,NC
      ZTEMP=ZZ(J+1)**2-ZZ(J)**2
      A11(LLL,L)=A11(LLL,L)+QR11(LLL,L,J)*ZTEMP*.5
      A12(LLL,L)=A12(LLL,L)+QR12(LLL,L,J)*ZTEMP*.5
      A16(LLL,L)=A16(LLL,L)+QR16(LLL,L,J)*ZTEMP*.5
      A22(LLL,L)=A22(LLL,L)+QR22(LLL,L,J)*ZTEMP*.5
      A26(LLL,L)=A26(LLL,L)+QR26(LLL,L,J)*ZTEMP*.5
      A66(LLL,L)=A66(LLL,L)+QR66(LLL,L,J)*ZTEMP*.5
    7 CONTINUE
      D11(LLL,L)=D12(LLL,L)=D16(LLL,L)=D22(LLL,L)=D26(LLL,L)=D66(LLL,L)
     *=0.0
      DO 8 J=1,NC
      ZTEMP=ZZ(J+1)**3-ZZ(J)**3
      D11(LLL,L)=D11(LLL,L)+QR11(LLL,L,J)*ZTEMP/3.
      D12(LLL,L)=D12(LLL,L)+QR12(LLL,L,J)*ZTEMP/3.
      D16(LLL,L)=D16(LLL,L)+QR16(LLL,L,J)*ZTEMP/3.
      D22(LLL,L)=D22(LLL,L)+QR22(LLL,L,J)*ZTEMP/3.
      D26(LLL,L)=D26(LLL,L)+QR26(LLL,L,J)*ZTEMP/3.
      D66(LLL,L)=D66(LLL,L)+QR66(LLL,L,J)*ZTEMP/3.
    8 CONTINUE
  100 FORMAT(//,T6,"PLY",T10,"Q11",T22,"Q12",T34,"Q22",T46,"Q66",
     *T58,"THETA",T70,"TEMP"/)
      WRITE(6,100)
  101 FORMAT(T6,I2,T10,E11.5,T22,E11.5,T34,E11.5,T46,E11.5,T58,
     *E11.5,T70,F7.2)
      DO 9 J=1,NO
    9 WRITE(6,101)J,Q11(LLL,L,J),Q12(LLL,L,J),Q22(LLL,L,J),Q66(LLL,L,J),
     *THETA(J),TEMP2(J)
  102 FORMAT(//,T6,"PLY",T10,"U1",T22,"U2",T34,"U3",T46,"U4",T58,"U5"/)
      WRITE(6,102)
      DO 10 J=1,NC
   10 WRITE(6,101)J,U1(LLL,L,J),U2(LLL,L,J),U3(LLL,L,J),U4(LLL,L,J),U5(L
     *LL,L,J)
  103 FORMAT(1H1//,T6,"PLY",T10,"QR11",T22,"QR12",T34,"QR16",T46,"QR22",
     *T58,"QR26",T70,"QR66"/)
      WRITE(6,103)
  104 FORMAT(T6,I2,T10,E11.5,T22,E11.5,T34,E11.5,T46,E11.5,T58,E11.5,
     *T70,E11.5)
      DO 11 J=1,NC
   11 WRITE(6,104)J,QR11(LLL,L,J),QR12(LLL,L,J),QR16(LLL,L,J),QR22(LLL,L
     *,J),QR26(LLL,L,J),QR66(LLL,L,J)
  105 FORMAT(//,T6,"A11= ",E11.5,T30,"B11= ",E11.5,T54,"D11= ",E11.5,/
     *T6,"A12= ",E11.5,T30,"B12= ",E11.5,T54,"D12= ",E11.5,/
     *T6,"A16= ",E11.5,T30,"B16= ",E11.5,T54,"D16= ",E11.5,/
     *T6,"A22= ",E11.5,T30,"B22= ",E11.5,T54,"D22= ",E11.5,/
     *T6,"A26= ",E11.5,T30,"B26= ",E11.5,T54,"D26= ",E11.5,/
     *T6,"A66= ",E11.5,T30,"B66= ",E11.5,T54,"D66= ",E11.5)
      WRITE(6,105)A11(LLL,L),B11(LLL,L),D11(LLL,L),
     *A12(LLL,L),B12(LLL,L),C12(LLL,L),
     *A16(LLL,L),B16(LLL,L),C16(LLL,L),
     *A22(LLL,L),B22(LLL,L),C22(LLL,L),
     *A26(LLL,L),B26(LLL,L),D26(LLL,L),
     *A66(LLL,L),B66(LLL,L),D66(LLL,L)
      RETURN
      END
```

Apprndix B

Summary of STAGS-C1 Runs

Bifurcation Loads

Case No. 1-20 $[0/45/-45/90]_s$ R = 12.0 in.

Laminate Temperature (Deg. F)	Nondimensional Time (Kt/h^2)				
	0.00	0.001	0.01	0.1	0.5
$\overline{N}_{xy}/\overline{N}_{xy_{orig}}$					
80.0	123.3802	123.15182	122.51071	121.93600	121.58738
	1.00000	.9982	.99295	.98829	.9864
200.0	116.44961	116.05624	114.87964	113.69288	113.10469
	.94386	.94064	.93109	.92148	.91672
250.0	113.20656	112.57167	109.80117	107.42864	105.83039
	.91933	.91240	.89167	.87071	.86026
300.0	112.97977	111.88204	108.44757	104.72933	102.39487
	.91571	.90681	.87897	.84883	.83315

Case No. 21-40 $[45/-45]_{2s}$ R = 12.0 in.

Laminate Temperature (Deg. F)	Nondimensional Time (Kt/h^2)				
	0.00	0.001	0.01	0.1	0.5
$\overline{N}_{xy}/\overline{N}_{xy_{orig}}$					
80.0	160.85196	160.68808	160.23854	159.84078	159.68968
	1.00000	.99898	.99619	.99379	.99277
200.0	154.14556	153.828690	152.88125	151.38482	150.40302
	.95831	.95634	.95045	.94114	.93511
250.0	148.69028	147.99595	145.89194	142.20926	139.64275
	.92439	.92008	.90699	.88410	.86815
300.0	147.30035	146.36451	143.33539	137.08092	132.76267
	.91575	.90993	.89110	.85222	.82242

Bifurcation Loads

Case No. 41-60 $[0/45/-45/90]_s$ R = 12.0 in.

Laminate Temperature (Deg. F)	Nondimensional Time (Kt/h^2)				
	0.00	0.001	0.01	0.1	0.5

$\overline{N}_{xy}/\overline{N}_{xy_{orig}}$

	0.00	0.001	0.01	0.1	0.5
80.0	123.38024	122.97095	121.79026	120.87806	120.61371
	1.00000	.99668	.98711	.97972	.97758
200.0	116.44962	115.62477	113.09808	110.77044	109.90825
	.94383	.93714	.91666	.89780	.89081
250.0	113.20656	111.61128	106.05130	100.93193	99.04338
	.91933	.90461	.85955	.81806	.80275
300.0	112.97977	110.54358	102.73265	94.94916	91.77837
	.91570	.89596	.83265	.76957	.74387

Case No. 61-80 $[45/-45]_{2s}$ R = 12.0 in.

Laminate Temperature (Deg. F)	Nondimensional Time (Kt/h^2)				
	0.00	0.001	0.01	0.1	0.5

$\overline{N}_{xy}/\overline{N}_{xy_{orig}}$

	0.00	0.001	0.01	0.1	0.5
80.0	160.85196	160.42377	159.69079	159.10577	158.92862
	1.00000	.99828	.99382	.99008	.98898
200.0	154.14556	153.27435	150.94923	147.48502	145.60686
	.95831	.95379	.93933	.91777	.90608
250.0	148.69028	146.89746	141.47279	132.37836	126.76072
	.92439	.91411	.88036	.82376	.78881
300.0	147.30035	144.73534	136.19195	118.99368	105.48780
	.91575	.90066	.84749	.73977	.65519

Bifurcation Load

Case No. 81-91 $[45/-45]_{2s}$ R = 24.0 in.

Laminate Temperature (Deg. F)	Nondimensional Time (Kt/h^2)				
	0.00	0.001	0.01	0.1	0.5

$\overline{N}_{xy}/\overline{N}_{xy_{orig}}$

	0.00	0.001	0.01	0.1	0.5
80.0	103.33830	103.12701	102.57902	-----	102.07056
	1.00000	.99796	.99265	-----	.98773
200.0	99.36737	-----	-----	-----	.96157
	.96157	-----	-----	-----	.91910
300.0	96.12327	94.59905	89.63421	81.26078	73.17607
	.93018	.91543	.86739	.78636	.70812

Case No. 92-93 $[45/-45]_{2s}$ R = 24.0 in.

Laminate Temperature (Deg. F)	Nondimensional Time (Kt/h^2)				
	0.00	0.001	0.01	0.1	0.5

$\overline{N}_{xy}/\overline{N}_{xy_{orig}}$

	0.00	0.001	0.01	0.1	0.5
80.0	103.33830	(from case 81)			
	1.00000				
300.0	96.12327	-----	-----	-----	88.27289
	.93018	-----	-----	-----	.85421

Case No. 300-305 $[45/-45]_{2s}$ R = 36.0 in.

Laminate Temperature (Deg. F)	Nondimensional Time (Kt/h^2)				
	0.00	0.001	0.01	0.1	0.5

$\overline{N}_{xy}/\overline{N}_{xy_{orig}}$

	0.00	0.001	0.01	0.1	0.5
80.0	82.45344	-----	-----	-----	-----
	1.00000	-----	-----	-----	-----
300.0	76.47433	75.32610	71.41175	63.21319	55.46706
	.92749	.91356	.86609	.76665	.67271

Bifurcation Load

Case No. 100-110 $[45/-45]_{2s}$ R = 48.0 in.

Laminate Temperature (Deg. F)	Nondimensional Time (Kt/h^2)				
	0.00	0.001	0.01	0.1	0.5

$\overline{N}_{xy}/\overline{N}_{xy_{orig}}$

Laminate Temperature (Deg. F)	0.00	0.001	0.01	0.1	0.5
80.0	67.68884	67.55834	67.21995	-----	66.89306
	1.00000	.99807	.99307	-----	.98824
200.0	65.12717	-----	-----	-----	62.13212
	.96216	-----	-----	-----	.91791
300.0	62.88856	61.94464	58.77294	52.30344	46.22196
	.92908	.91514	.86828	.77270	.68286

Case No. 111-112 $[45/-45]_{2s}$ R = 48.0 in.

Laminate Temperature (Deg. F)	Nondimensional Time (Kt/h^2)				
	0.00	0.001	0.01	0.1	0.5

$\overline{N}_{xy}/\overline{N}_{xy_{orig}}$

Laminate Temperature (Deg. F)	0.00	0.001	0.01	0.1	0.5
80.0	67.68884	(from case 100)			
	1.00000				
300.0	62.88856	-----	-----	-----	56.88047
	.92908	-----	-----	-----	.84032

Case No. 121-128 $[45/-45]_{2s}$ R = 96.0 in.

Laminate Temperature (Deg. F)	Nondimensional Time (Kt/h^2)				
	0.00	0.001	0.01	0.1	0.5

$\overline{N}_{xy}/\overline{N}_{xy_{orig}}$

Laminate Temperature (Deg. F)	0.00	0.001	0.01	0.1	0.5
80.0	45.87038	-----	-----	-----	-----
	1.00000	-----	-----	-----	-----
200.0	44.11947	-----	-----	-----	42.14792
	.96183	-----	-----	-----	.91885
300.0	42.71049	42.04119	39.88750	36.29267	32.82597
	.93111	.91652	.86957	.79120	.71562

Bifurcation Load

Case No. 131-132 $[45/-45]_{2s}$ R = 96.0 in.

Laminate Temperature (Deg. F)	Nondimensional Time (Kt/h^2)				
	0.00	0.001	0.01	0.1	0.5
$\overline{N}_{xy}/\overline{N}_{xy_{orig}}$					
80.0	45.87038	(from case 121)			
	1.00000				
300.0	42.71049	-----	-----	-----	38.84975
	.93111	-----	-----	-----	.84695

Case No. 141-147 $[45/-45]_{2s}$ R = 10,000.0 in.

Laminate Temperature (Deg. F)	Nondimensional Time (Kt/h^2)				
	0.00	0.001	0.01	0.1	0.5
$\overline{N}_{xy}/\overline{N}_{xy_{orig}}$					
80.0	26.89203	-----	-----	-----	-----
	1.00000	-----	-----	-----	-----
200.0	26.04990	-----	-----	-----	25.34861
	.96869	-----	-----	-----	.94261
300.0	25.78407	25.43476	24.50785	-----	23.68764
	.95880	.94581	.91134	-----	.88084

93
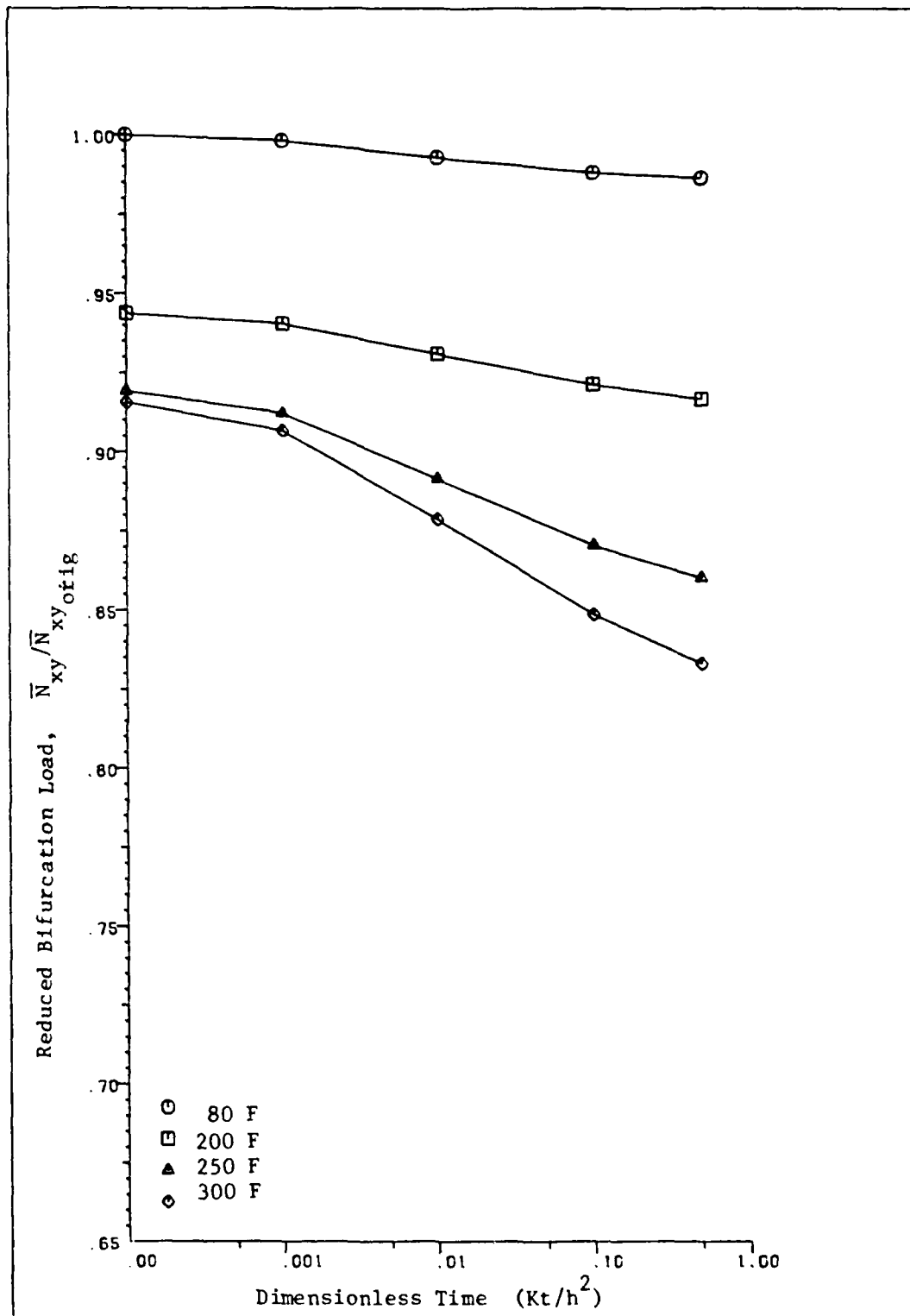
Figure B.1   Case No. 1 - 20; $[0/45/-45/90]_s$

94
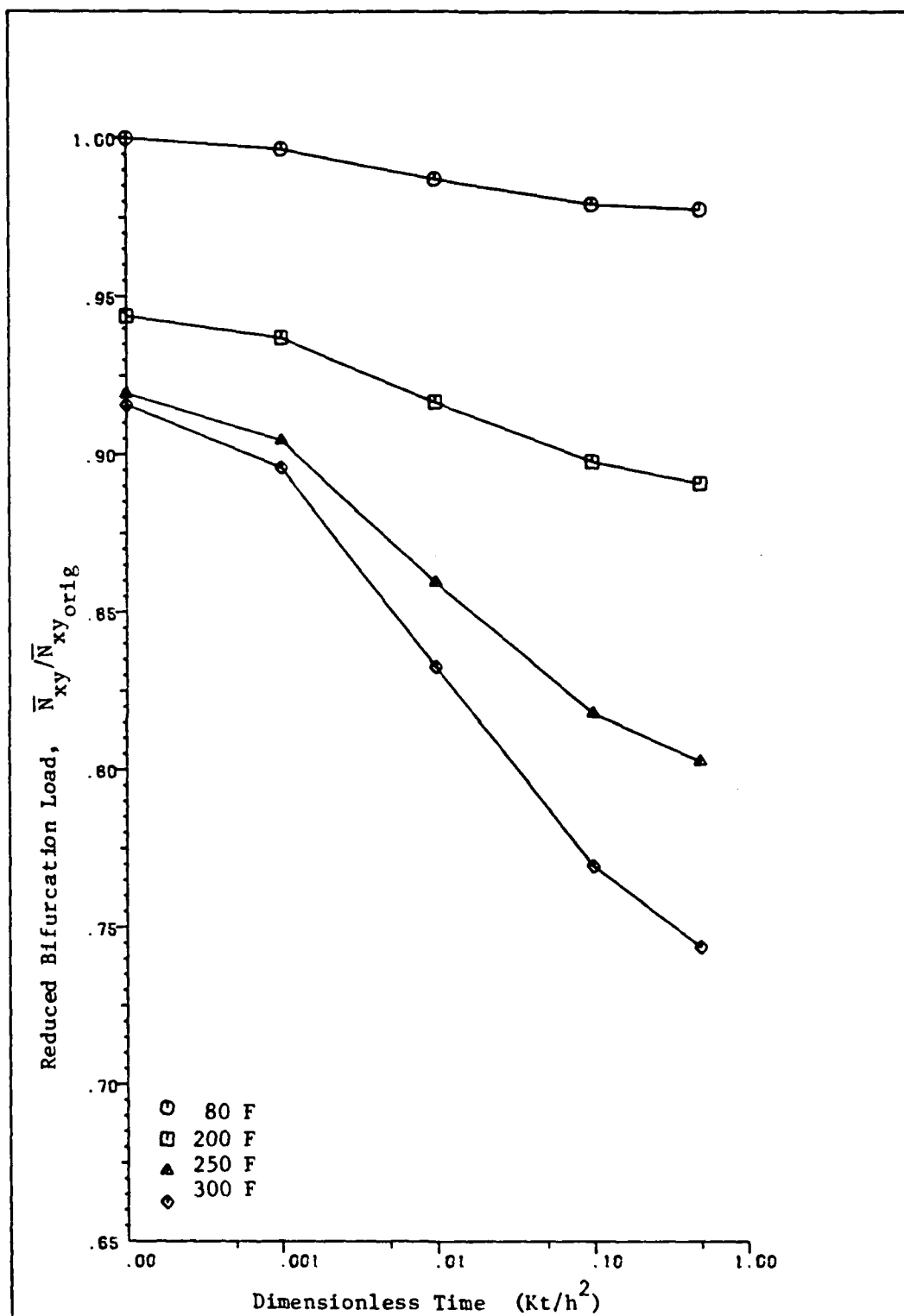
Figure B.2   Case No. 41 - 60; $[0/45/-45/90]_s$

95
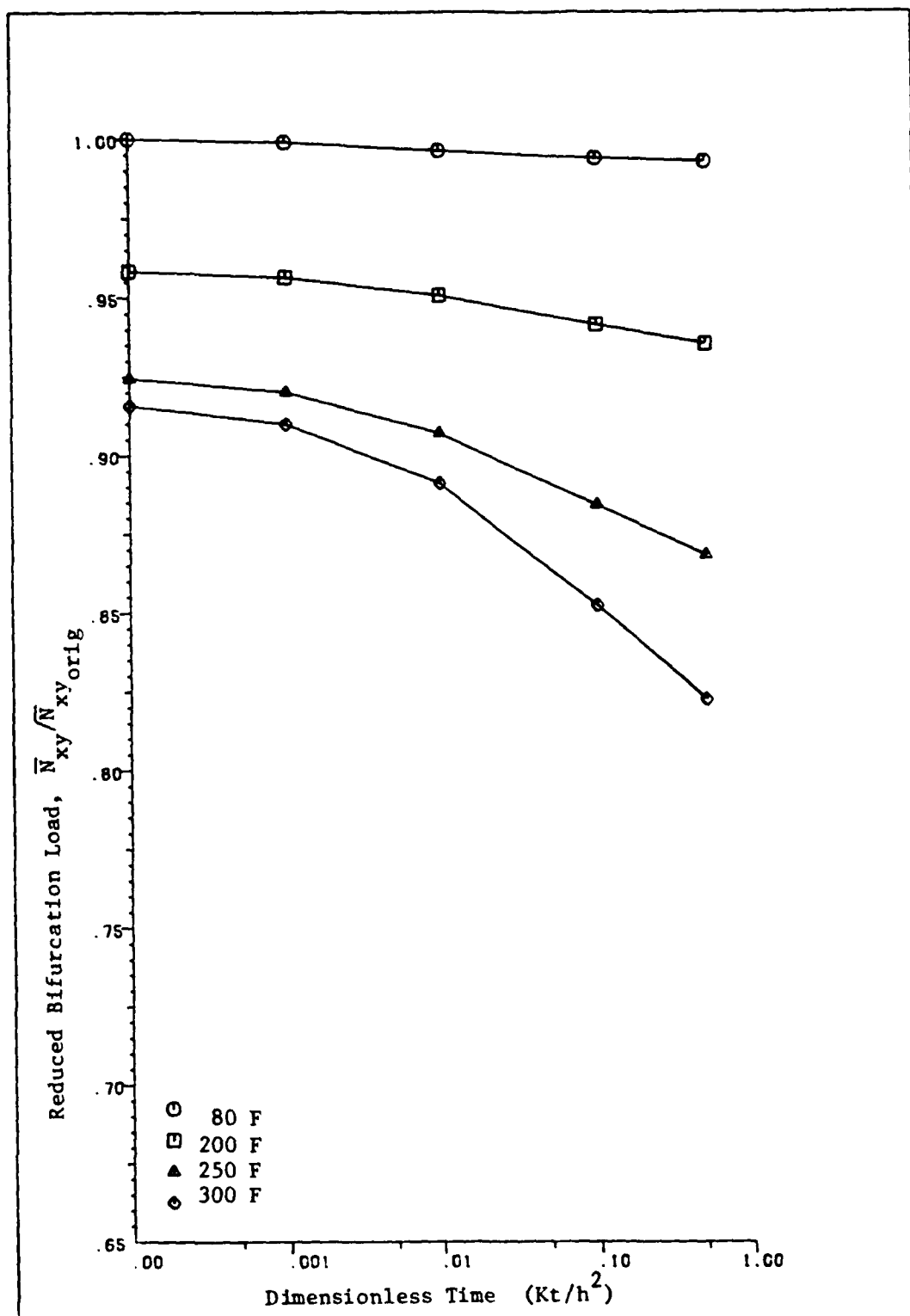
Figure B.3   Case No. 21 – 40; $[45/-45]_s$

96
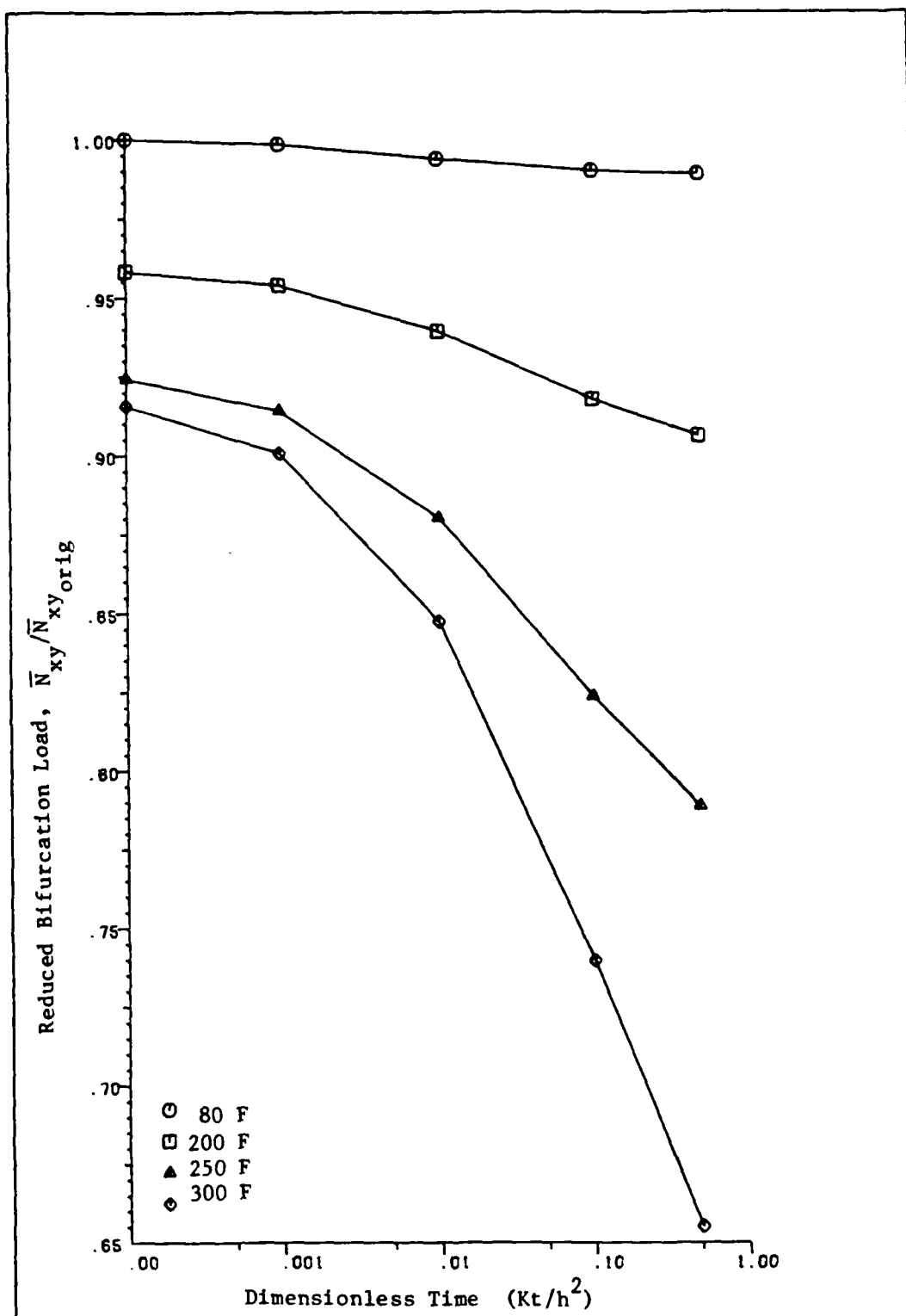
Figure B.4 Case No. 61 - 80; [45/-45]s

97

APPENDIX C
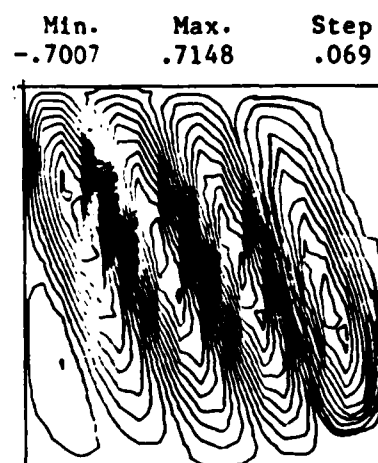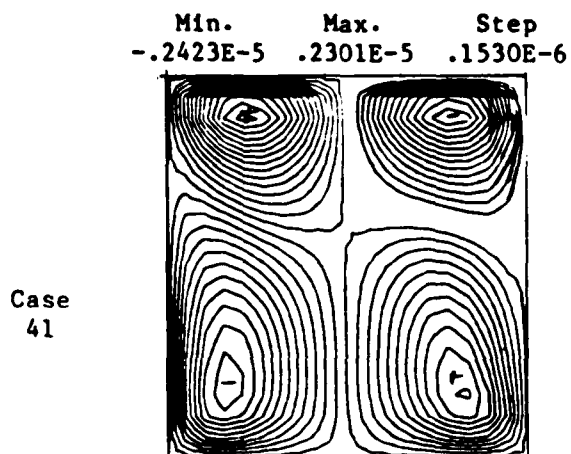
Prebuckled Displacement, w and

Eigenvector Contour Plots

The terms 'Max.' and 'Min.' in this appendix correspond to the
maximum and minimum out-of-plane displacement. For the prebuckled
displacement, w, this out-of-plane displacement was caused by a unit
line load, N_{xy}, applied at the panel's boundaries. The term 'Step'
indicates the increments between the contour lines.

98

Min.	Max.	Step
-.2423E-5	.2301E-5	.1550E-6

Min.	Max.	Step
-.7007	.7148	.069

Case 1

Min.	Max.	Step
-.2564E-5	.2431E-5	.164E-6

Min.	Max.	Step
-.6940	.7114	.068

Case 16

Min.	Max.	Step
-.3059E-5	.2402E-5	.179E-6

Min.	Max.	Step
-.6858	.7067	.068

Case 20
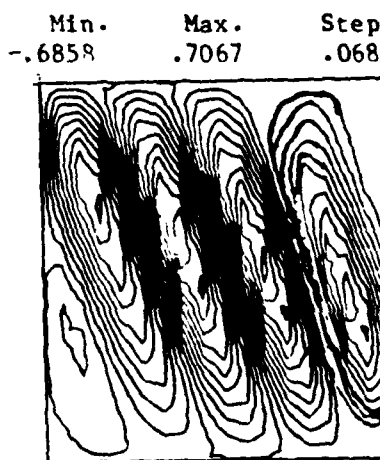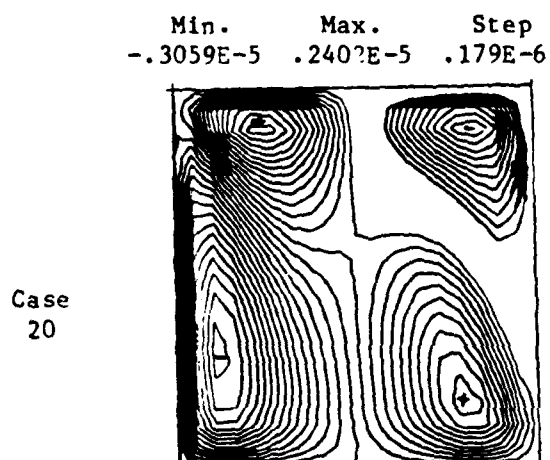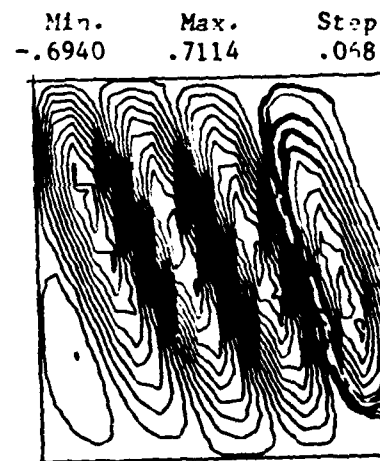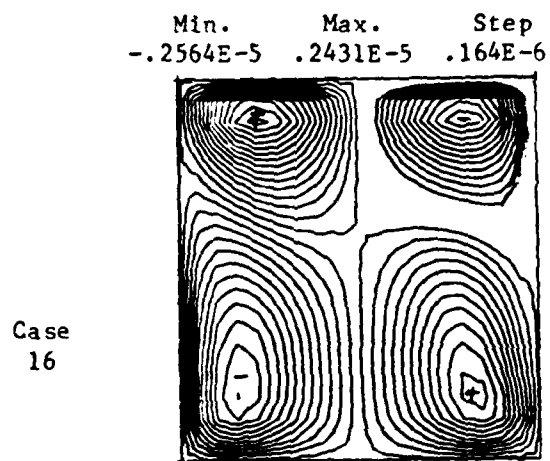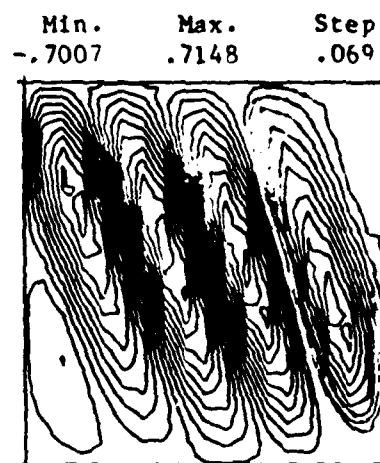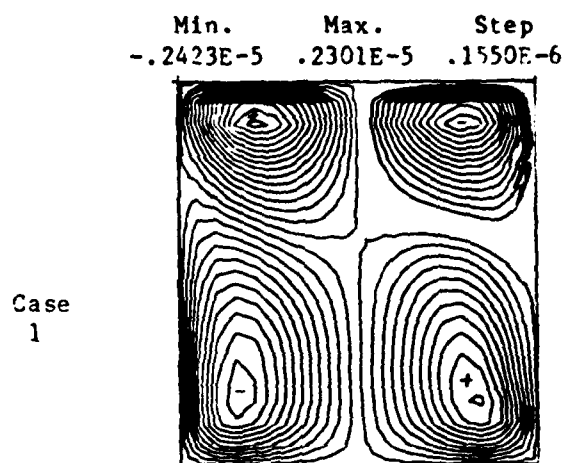
Prebuckle Displacements,w   Eigenvectors, w

Figure C-1 Case 1, 16, and 20 Contour Plots [0/45/-45/90]$_s$

99

Min.	Max.	Step		Min.	Max.	Step
-.2423E-5	.2301E-5	.1530E-6		-.7007	.7148	.069

Case
41

Min.	Max.	Step		Min.	Max.	Step
-.2564E-5	.2431E-5	.164E-6		-.6940	.7114	.068

Case
56

Min.	Max.	Step		Min.	Max.	Step
-.2942E-5	.2782E-5	.187E-6		-.6789	.7016	.067
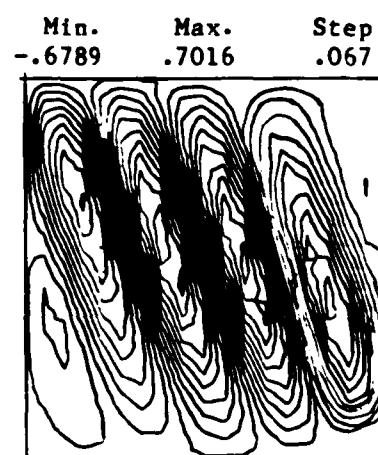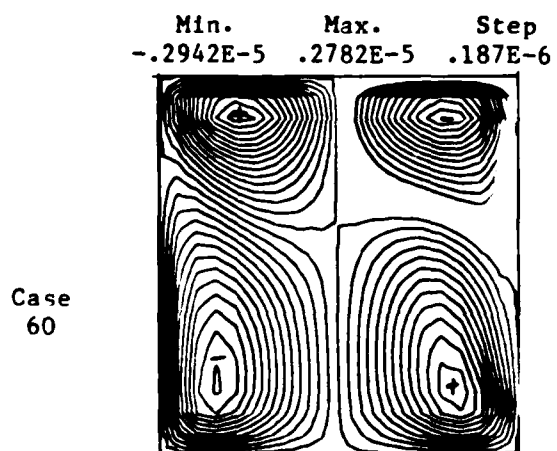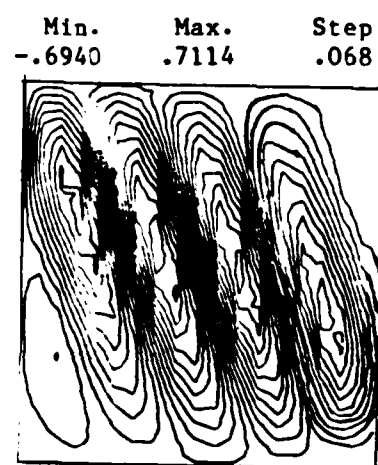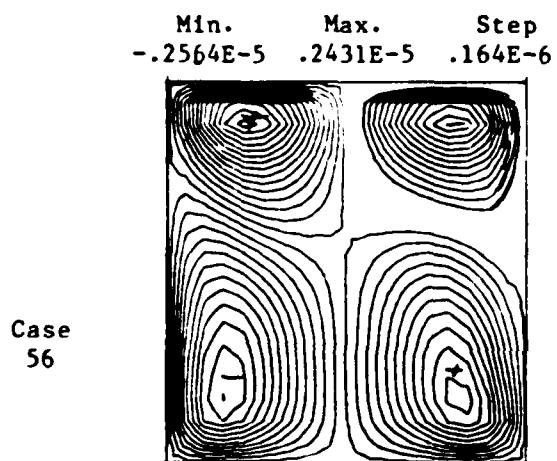
Case
60

Prebuckle Displacements,w   Eigenvectors, w

Figure C-2   Case 41, 56, and 60 Contour Plots [0/45/-45/90]$_s$

100

	Min.	Max.	Step
	-.1949E-5	.1863E-5	.1250E-6

	Min.	Max.	Step
	-.8537	.9231	.086

Case 21

	Min.	Max.	Step
	-.2397E-5	.2297E-5	.154E-6

	Min.	Max.	Step
	-.8808	.9417	.088

Case 36

	Min.	Max.	Step
	-.3830E-5	.3159E-5	.230E-6

	Min.	Max.	Step
	-.9107	.9811	.090

Case 40
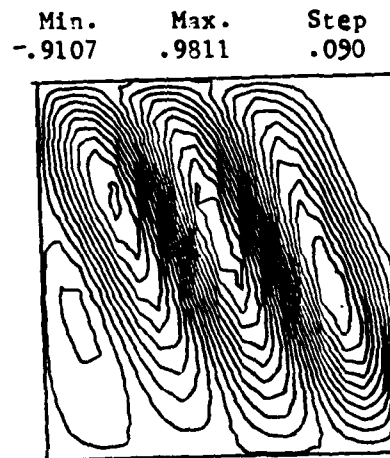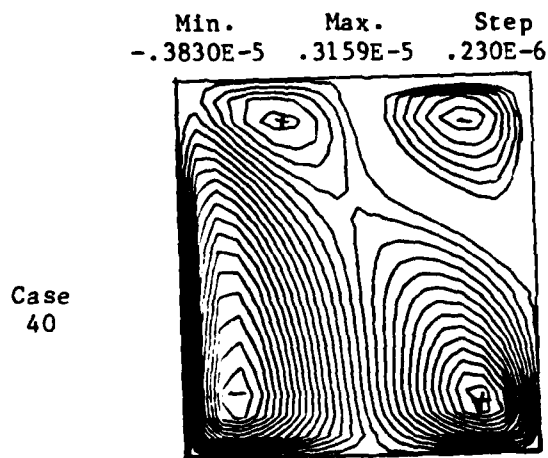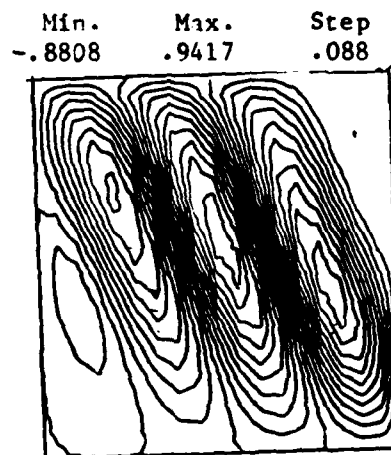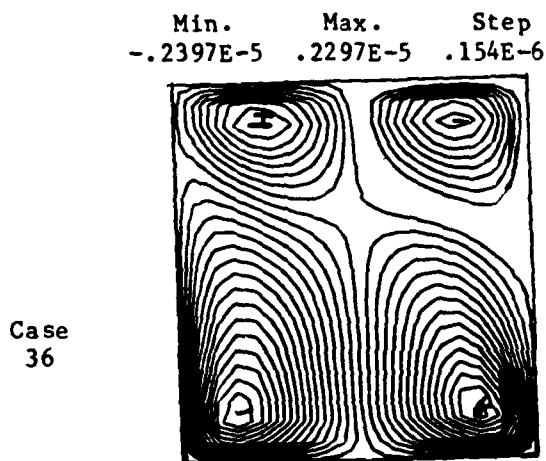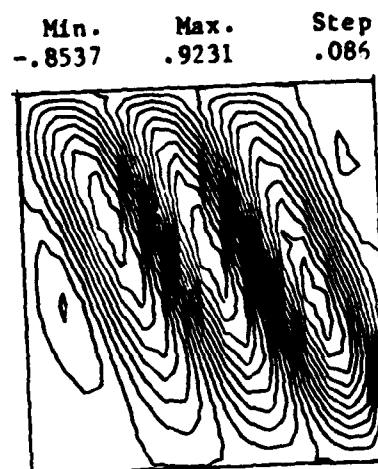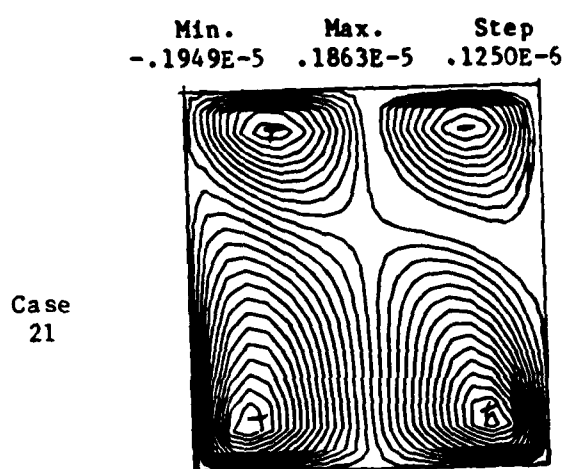
Prebuckle Displacements,w   Eigenvectors, w

Figure C-3 Case 21, 36, and 40 Contour Plots [45/-45]₂ₛ

101

Min.	Max.	Step		Min.	Max.	Step
-.1949E-5	.1863E-5	.1250E-6		-.8537	.9231	.086

Case
61

Min.	Max.	Step		Min.	Max.	Step
-.2397E-5	.2297E-5	.154E-6		-.8808	.9417	.088

Case
76

Min.	Max.	Step		Min.	Max.	Step
-.6911E-5	.6691E-5	.450E-6		-.8969	1.000	.090
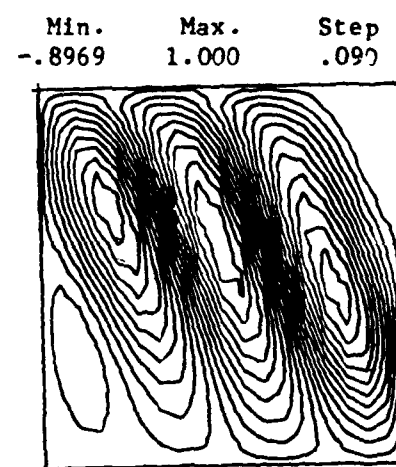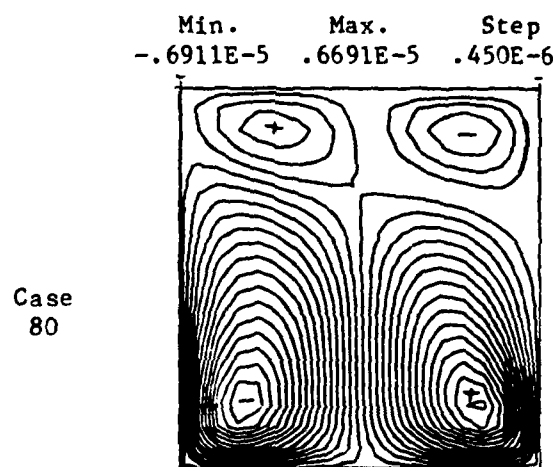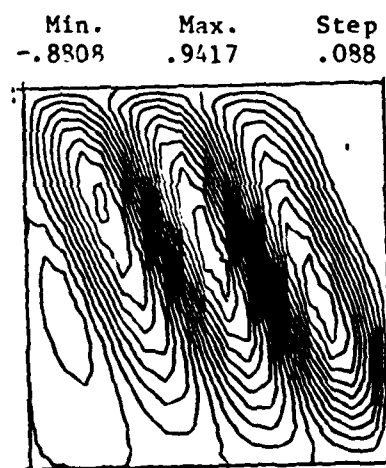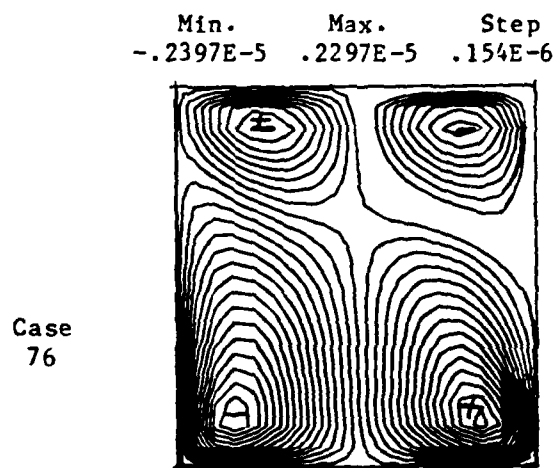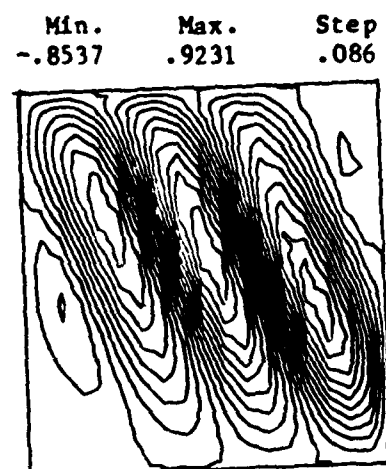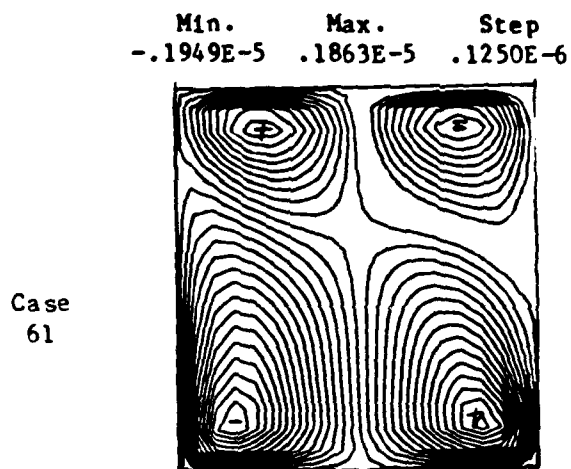
Case
80

Prebuckle Displacements,w   Eigenvectors, w

Figure C-4 Case 61, 76, and 80 Contour Plots [45/-45]2s

102

	Min.	Max.	Step		Min.	Max.	Step
	-.8395E-6	.7586E-6	.5200E-7		-.8702	1.000	.090
Case 81							
	Min.	Max.	Step		Min.	Max.	Step
	-.1031E-5	.9390E-6	.65E-7		-.8415	1.000	.090
Case 87							
	Min.	Max.	Step		Min.	Max.	Step
	-.2926E-5	.2745E-5	.185E-6		-.6981	1.000	.082
Case 91							
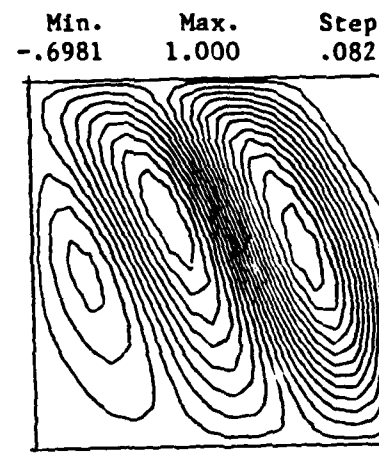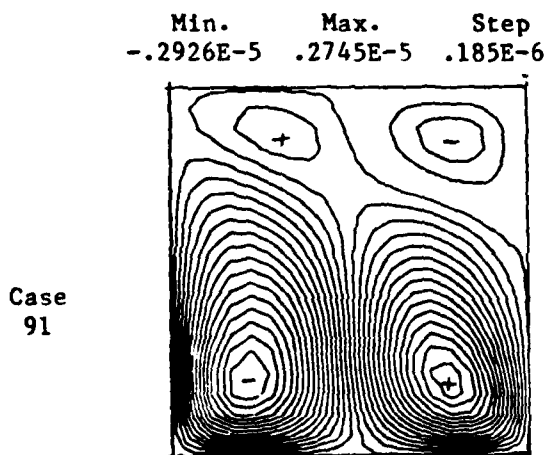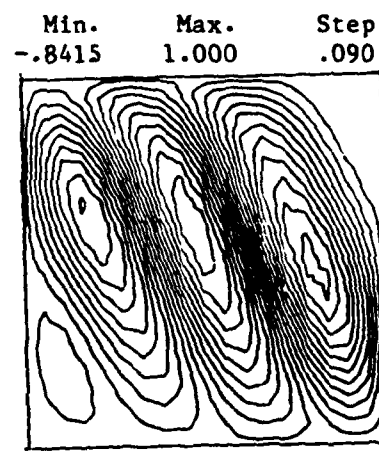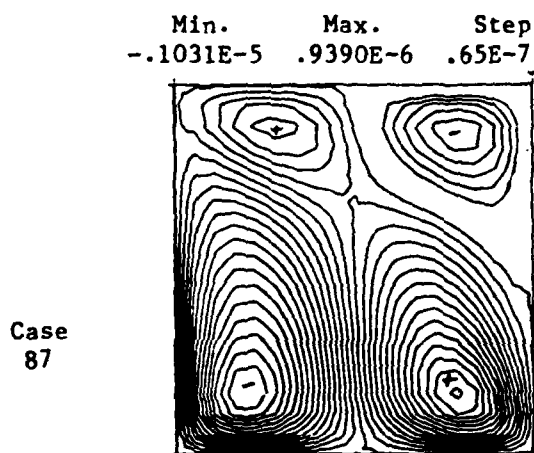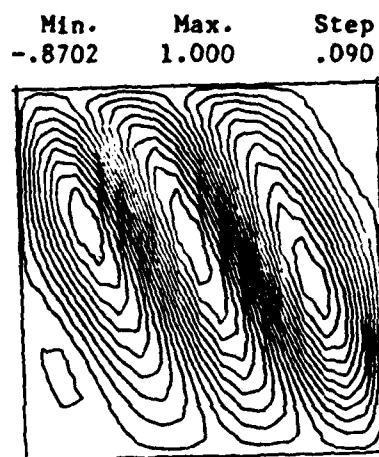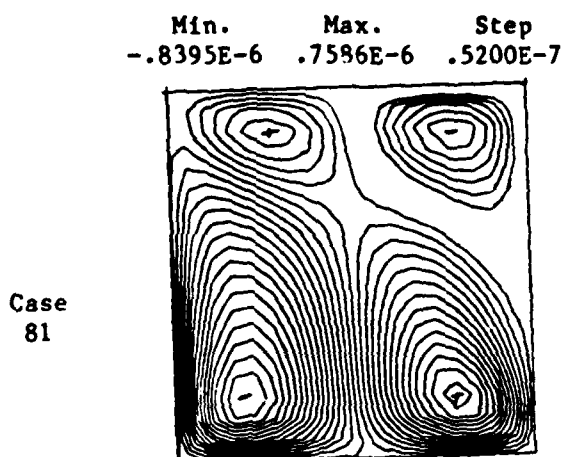
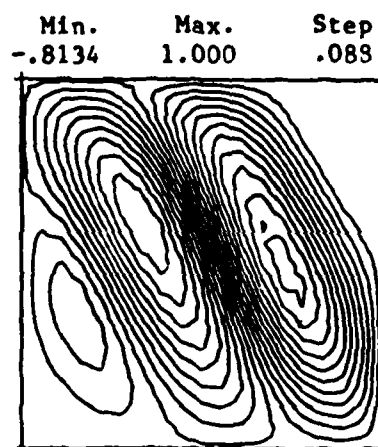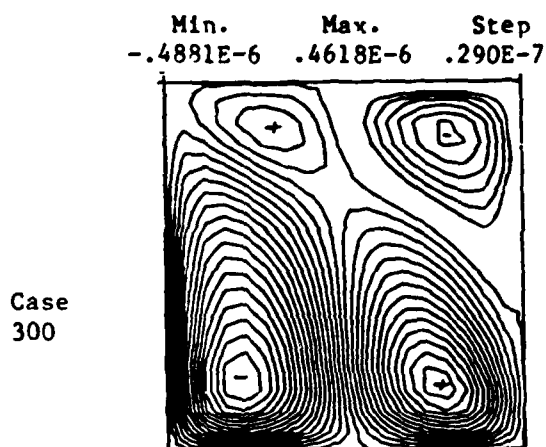Prebuckle Displacements,w   Eigenvectors, w

Figure C-5   Case 81, 87, and 91 Contour Plots [45/-45]2s

103
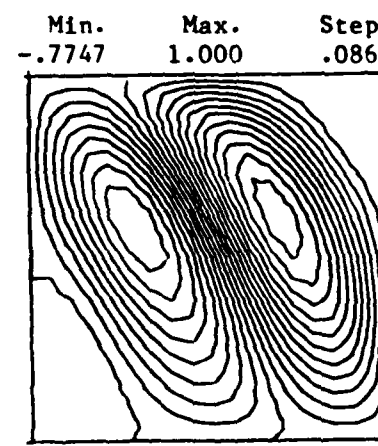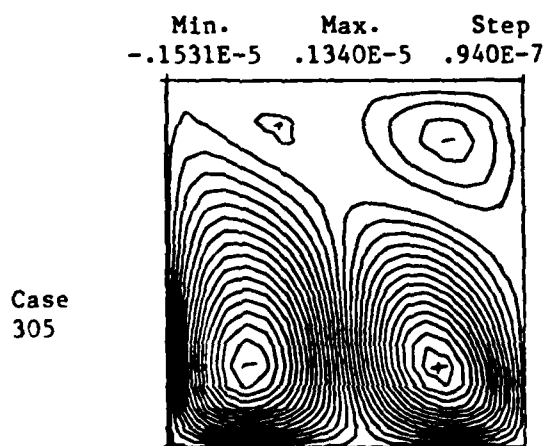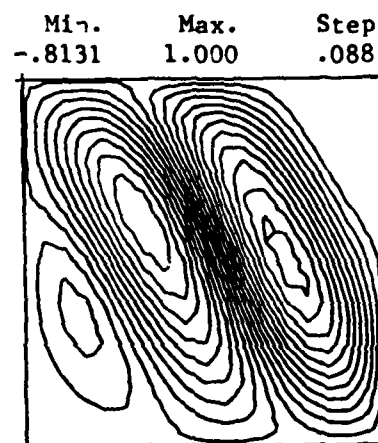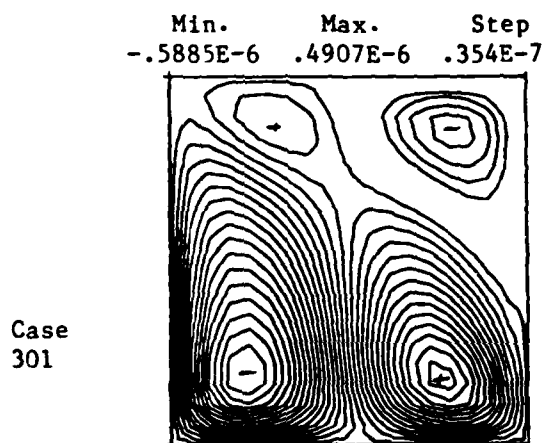
Prebuckle Displacements,w   Eigenvectors, w
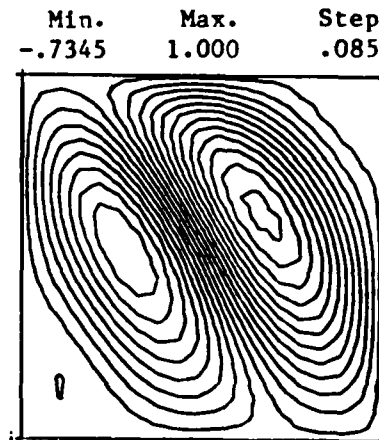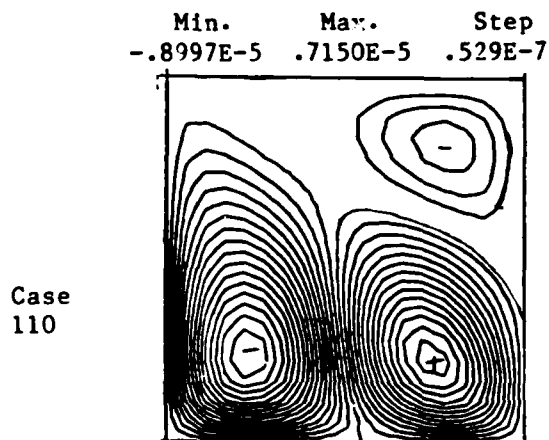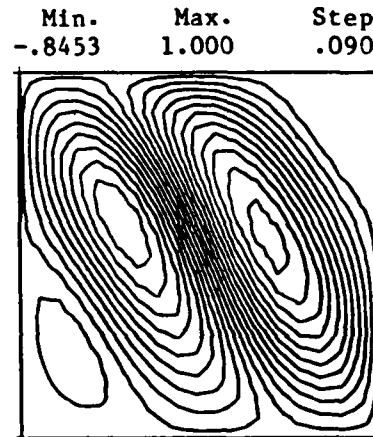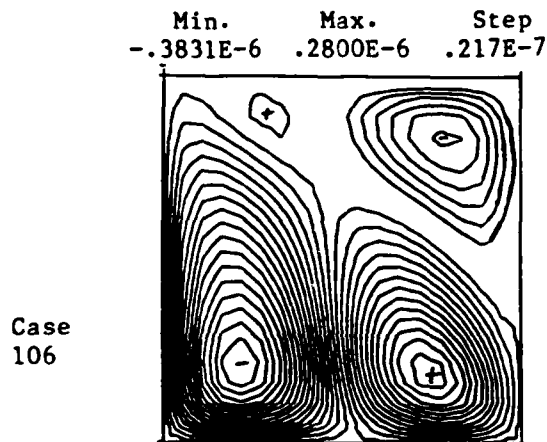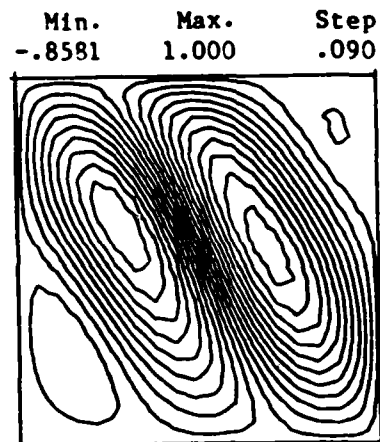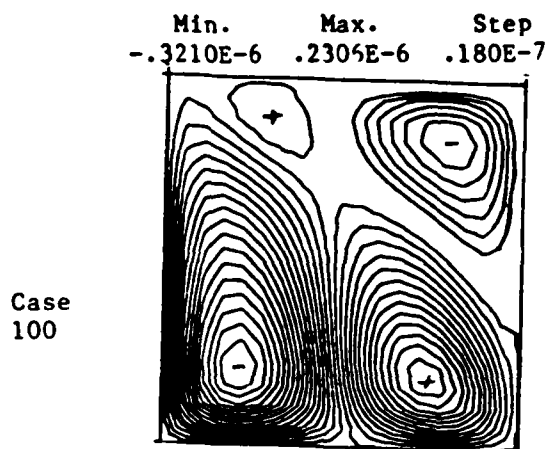
Figure C-6   Case 300, 301, and 305 Contour Plots [45/-45]$_{2s}$

Min.	Max.	Step		Min.	Max.	Step
-.3210E-6	.2305E-6	.180E-7		-.8581	1.000	.090

Case
100

Min.	Max.	Step		Min.	Max.	Step
-.3831E-6	.2800E-6	.217E-7		-.8453	1.000	.090

Case
106

Min.	Max.	Step		Min.	Max.	Step
-.8997E-5	.7150E-5	.529E-7		-.7345	1.000	.085

Case
110

Prebuckle Displacements,w   Eigenvectors, w

Figure C-7   Case 100, 106, and 112 Contour Plots [45/-45]2s

105

Min.	Max.	Step
−.1116E−6	.2297E−6	.441E−7

Min.	Max.	Step
−.7185	1.000	.089

Case
121

Min.	Max.	Step
−.1286E−6	.2730E−7	.50E−8

Min.	Max.	Step
−.7023	1.000	.083

Case
124

Min.	Max.	Step
−.2441E−6	.6179E−7	.100E−7

Min.	Max.	Step
−.6543	1.000	.081
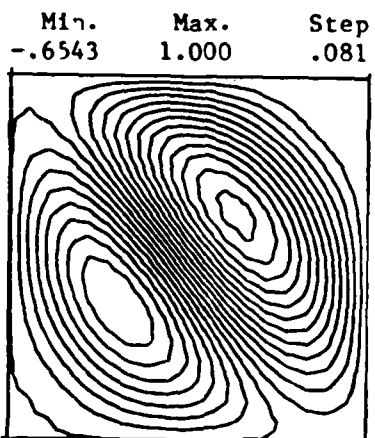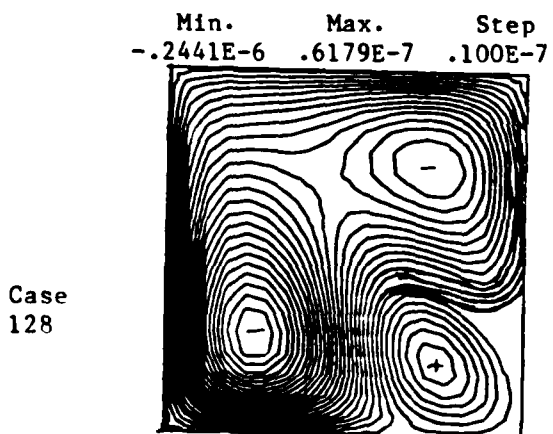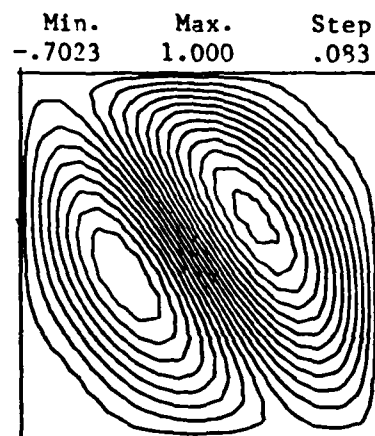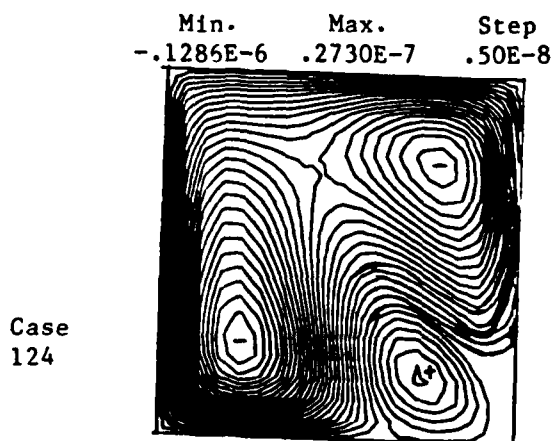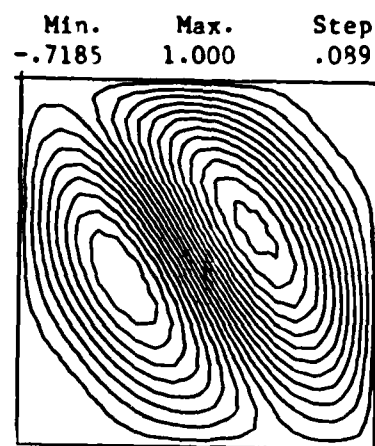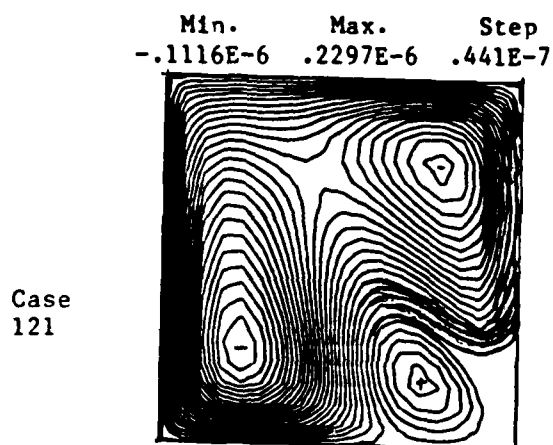
Case
128

Prebuckle Displacements,w   Eigenvectors, w

Figure C-8   Case 121, 124, and 128 Contour Plots $[45/-45]_{2s}$

106

Min.	Max.	Step		Min.	Max.	Step
-.2563E-6	.0000	.84E-7		-.4079	1.000	.050

Case
141

Min.	Max.	Step		Min.	Max.	Step
-.2700E-6	.00000	.08E-8		-.4380E-1	1.000	.070

Case
144

Min.	Max.	Step		Min.	Max.	Step
-.3050E-6	.0000	.10E-7		-.5171E-1	1.000	.074
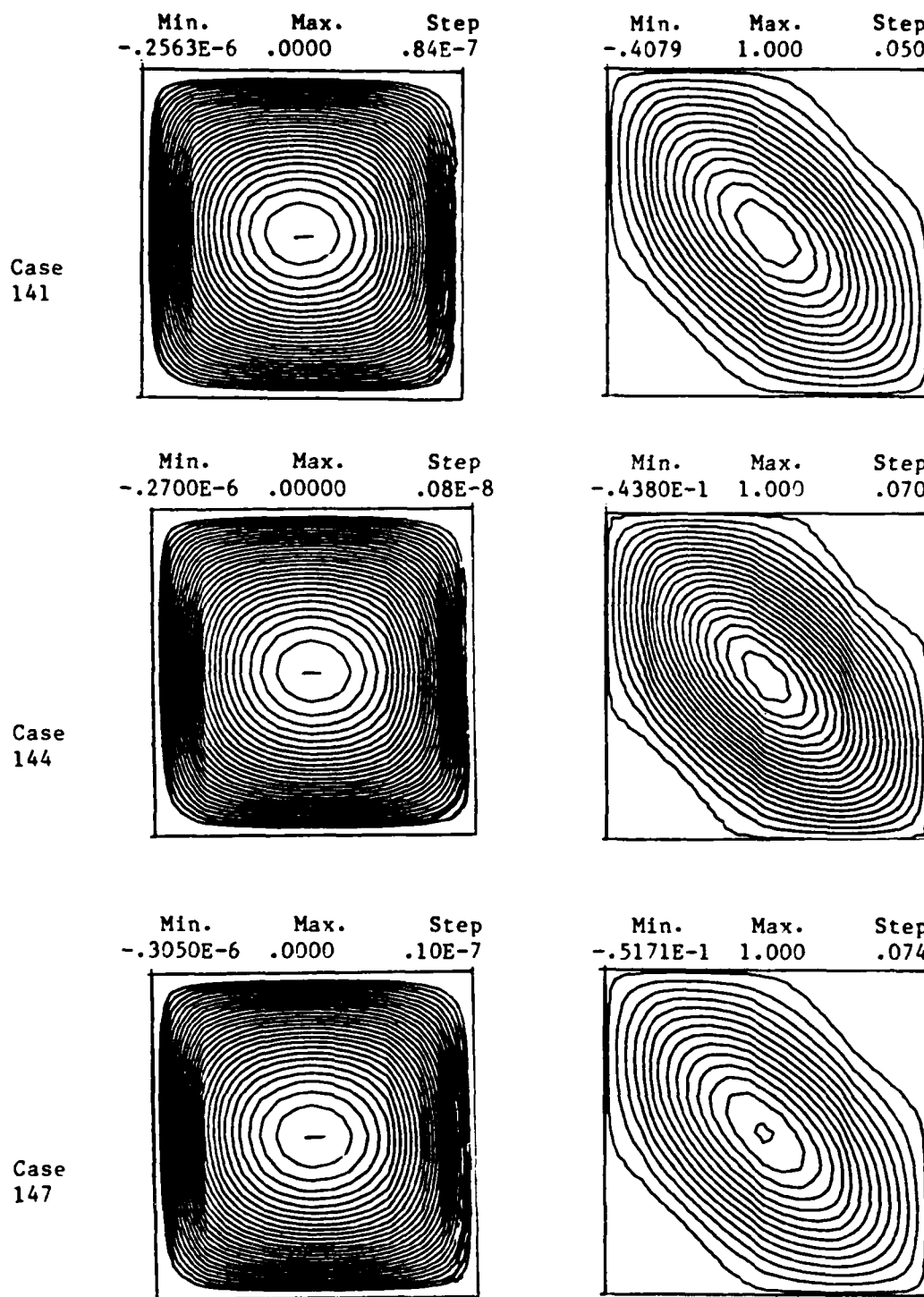
Case
147

Prebuckle Displacements,w   Eigenvectors, w

Figure C-9   Case 151, 144, and 147 Contour Plots [45/-45]$_{2s}$

107

Bibliography

1. Whitney, J. M., "Buckling of Anisotropic Laminated Cylindrical Plates," *AIAA Journal*, 22, 1641-1645 (November 1984).

2. Becker, M. L., Palazotto, A. N., and Khot, N. S., "Instability of Composite Panels," *AIAA, Journal of Aircraft*, 18, 739-743 (September 1981).

3. Herbert, J. S., and Palazotto, A. N., "Comparison Between Experimental and Numerical Bucklin gof Curved Cylindrical Composite Panels," Proceedings of the Southeastern Conference on Theoretical and Applied Mechanics, SECTAM XII Vol II, 124-129 (May 1984).

4. Janisse, T. C., Palazotto, A. N., "Callapse Analysis of Cylindrical Composite Panel with Cutouts," *AIAA, Journal of Aircaft*, 21, 731-733 (September 1984).

5. Lee, C. E., and Palazotto, A. N., "Collapse Analysis of Composite Cylindrical Panels with Small Cutouts," *Composite Structures*, 4, 217-229 (1985).

6. Harper, J. G., *Buckling Analysis of Laminate Composite Circular Cylindrical Shells*, MS Thesis, AFIT/GAE/AA/78D-8, School of Engineering, Air Force Institute of Technology (AU), Wright-Patterson AFB, OH, December 1978.

7. Snead, J. M., and Palazotto, A. N., "Moisture and Temperature Effects on the Instability of Cylindrical Composite Panels," *AIAA, Journal of Aircraft*, 20, 777-783 (Setember 1983)

8. Blikstad, M., Sjoblom, P. O. W., and Johannesson, T. R., "Long-Term Moisture Absorption in Graphite/Epoxy Angle-Ply Laminates," *Journal of Composite Materials*, 18, 32-46 (January 1984).

9. Loos, A C., and Springer, G. S., "Moisture Absorption of Graphite/Epoxy Composites Immersed in Liquids and in Humid Air," *Journal of Composite Materials*, 13: 131-147 (April 1979).

10. Kondo, K., and Taki, T., "Moisture Diffusivity of Unidirectional Composites," *Journal of Composite Materials*, 16, 82-93 (March 1982).

11. Browning, C. E. "The Mechanisms of Elevated Temperature Property Losses in High Performance Structural Epoxy Matrix Materials After Exposures to High Humidity Environments," *Polymer Engineering and Science*, 18, 16-24 (January 1978).

12. Browning, C. E., Husman, G. E., and Whitney, J. M., "Moisture Effects in Epoxy Matrix Composites," _Composite Materials: Testing and Design (Fourth Conference), ASTM STP 617:_ 481-496, American Society for Testing and Materials (1977).

13. Chi-Hund S., and Springer, G. S., "Efects of Moisture and Temperature on the Tensile Strength of Composite Materials," _Journal of Composite Materials_, 11, 2-16 (January 1977).

14. Vinson, J. R., Pipes, R. B., Walker, W. J., Ulrich, D. R., _The Effects of Relative Humidity and Elevated Temperature on Composite Structures, Transactions of the Workshop on_, Sponsored by the Air Force Office of Scientific Research and the Center for Composite Materials, University of Delaware, March 30-31, 1976.

15. Chi-Hung S., and Springer, G. S. "Enviromental Effects on the Elastic Moduli of Composite Materials," _Journal of Composite Materials_, 11, 250-264 (July 1977).

16. Pipes, R. B., Vinson, J. R., and Tsu-Wei C., "On the Hygrothermal Response of Laminated Systems," _Journal of Composite Materials_, 10, 129-148 (April 1976).

17. McKague, E. L., Halkias, J. E., and Reynolds, J. D., "Moisture in Composites: The Effect of Supersonic Service on Diffusion," _Journal of Composite Materials_, 9, 2-9 (January 1975).

18. Chi-Hung S., and Springer, G. S., "Moisture Absorption and Desorption of Composite Materials," _Journal of Composite Materials_, 10, 2-20 (January 1976).

19. Shirrell, C. D., Halpin, J. C., and Browning, C. E., "Moisture – An Assessment of its Impact on the Design of Resin Based Advanced Composites," NASA Technical Memorandum, NASA TM X-3377: 405-425 (April 1976).

20. _Environmental Effects on Advanced Composite Materials_, 78th Annual Meeting American Society for Testing and Materials, ASTM, 22-27 (June 1975).

21. Whitney, J. M. and Ashton, J. E., "Effect of Environment on the Elastic Response of Layered Composite Plates," _AIAA Journal_, 9: 1708-1712 (December 1971).

22. Tsai, S. W. and Hahn, H. T., _Introducing to Composite Materials_. Westport, Connecticut: Technomic Publishing Company, 1980.

23. Jones, R. M. _Mechanics of Composite Materials_. New York: McGraw-Hill, 1975.

24. Bauld, N. R., Jr. and Satyamurthy, D., Collapse Load Analysis for Plates and Panels, AFFDL-TR-79-3038, WPAFB, Ohio: Air Force Flight Dynamics Laboratory, 1979.

25. Almroth, B. O., Brogan, F. A., and Stanley, G. M., Structural Analysis of General Shells, Volume II User Instructions for STAGSC-1, LMSC-D633873, Lockheed Palo Alto Research Laboratory, California, January 1983.

26. Sobel, L. H. and Thomas, Kevin, Evaluation of the STAGSC-1 Shell Analysis Computer Program, WARD-10881. Westinghouse Advanced Reactors Division, Madison PA, August 1981.

27. Cook, Robert D., Concepts and Applications of Finite Element Analysis (Second Edition), New York: John Wiley and Sons, 1981.

28. Brush, D. O., and Almroth, B. O., Buckling of Bars, Plates, and Shells, New York: McGraw-Hill, 1975.

29. Nelson, D. A., Buckling of Axially Compressed Stringer Stiffened Cylindrical Shells With and Without Cutouts, MS Thesis, AFIT/GAE/AA/77D-8, School of Engineering, Air Force Institute of Technology, Wright-Patterson AFB, OH, December 1977.

30. Almroth, B. O. and Brogan, F. A., Numerical Procedures for Analysis of Structural Shells. AFWAL-TR-80-3129, March 1981.

31. Almroth, B. O. and Brogan, F. A., Users Manual for STAGS, Volume 1, Theory. Structrual Mechanics Laboratory, Lockheed Palo Alto Research Laboratory, March 1978.

32. Crank, J., The Mathematics of Diffusion (Second Edition), Clarendon Press, Oxford, 1975.

Vita

Mr. Anthony D. Straw was born on April 8, 1952 in Decatur, Indiana. Anthony graduated form Crestview High School,in Convoy, Ohio, in Jun 1970 and then attended The Ohio State University from which he received the degree Bachelor of Science in Aeronautical and Astronautical Engineering in March of 1975.

He began his professional career as an intelligence analyst, investigating foreign structural mechanics research, with the Foreign Technology Division in June of 1977. Anthony married Barbara Trager in Van Wert County, Ohio in July of 1980. In June of 1984, he entered the School of Engineering, Air Force Institute of Technology, under the Long Term Full Time Training program.

Permanent address: 4948 Harwick Ct.

Kettering, Ohio 45440

AD-A163878

REPORT DOCUMENTATION PAGE

1a. REPORT SECURITY CLASSIFICATION	1b. RESTRICTIVE MARKINGS
UNCLASSIFIED	

2a. SECURITY CLASSIFICATION AUTHORITY	3 DISTRIBUTION/AVAILABILITY OF REPORT
	Approved for public release;
2b. DECLASSIFICATION/DOWNGRADING SCHEDULE	distribution unlimited

4. PERFORMING ORGANIZATION REPORT NUMBER(S)	5. MONITORING ORGANIZATION REPORT NUMBER(S)
AFIT/GAE/AA/85D-15	

6a. NAME OF PERFORMING ORGANIZATION	6b. OFFICE SYMBOL (If applicable)	7a. NAME OF MONITORING ORGANIZATION
School of Engineering	AFIT/EN	

6c. ADDRESS (City, State and ZIP Code)	7b. ADDRESS (City, State and ZIP Code)
Air Force Institute of Technology Wright-Patterson AFB, OH 45433	

8a. NAME OF FUNDING/SPONSORING ORGANIZATION	8b. OFFICE SYMBOL (If applicable)	9. PROCUREMENT INSTRUMENT IDENTIFICATION NUMBER

8c. ADDRESS (City, State and ZIP Code)	10. SOURCE OF FUNDING NOS			
	PROGRAM ELEMENT NO	PROJECT NO.	TASK NO.	WORK UNIT NO

11. TITLE (Include Security Classification)
See Box 19

12. PERSONAL AUTHOR(S)
STRAW, Anthony D.

13a. TYPE OF REPORT	13b. TIME COVERED	14. DATE OF REPORT (Yr., Mo., Day)	15. PAGE COUNT
MS Thesis	FROM _____ TO _____	1985 December	

16. SUPPLEMENTARY NOTATION

17	COSATI CODES		18 SUBJECT TERMS (Continue on reverse if necessary and identify by block number)
FIELD	GROUP	SUB GR	Composite Materials, Shear Buckling, Finite Elements,
11	04		Bifurcation Analysis, Hygrothermal Effects, Curved Panels
13	13		

19 ABSTRACT (Continue on reverse if necessary and identify by block number)

Title: The Buckling of Composite Cylindrical Panels Considering Environmental Effects

Thesis Chairman: Dr. Anthony Palazotto
Professor, Aeronautics and Astronautics

See Back for Abstract

20 DISTRIBUTION/AVAILABILITY OF ABSTRACT	21 ABSTRACT SECURITY CLASSIFICATION
UNCLASSIFIED/UNLIMITED ☒ SAME AS RPT ☐ DTIC USERS ☐	UNCLASSIFIED

22a. NAME OF RESPONSIBLE INDIVIDUAL	22b. TELEPHONE NUMBER (Include Area Code)	22c. OFFICE SYMBOL
Dr. Anthony Palazotto	513-255-3517	AFIT/ENY

DD FORM 1473, 83 APR EDITION OF 1 JAN 73 IS OBSOLETE

Abstract

An analytical study was conducted to determine the influence of moisture, temperature, and curvature on the bifurcation load of cylindrical, composite panels subjected to a simple shear loading. Two laminate ply orientations, $[0/45/-45/90]_s$ and $[45/-45]_{2s}$, were analyzed for six radii, four temperatures, and two initial moisture conditions. The eight-ply composite panels were assumed to be manufactured from a graphite/epoxy, AS/3501-5. To evaluate the influence of moisture and temperature, the transverse modulus, E_2, and shear modulus, G_{12}, were degraded based on experimental test data for the AS/3501-5 system. Each ply orientation, for a 12 in. panel radius, was evaluated at 20 time/temperature conditions that ranged from 80 to 300°F, and moisture concentrations ranging from a zero moisture content to an equilibrium moisture distribution. The investigation of curvature was conducted only for the $[45/-45]_{2s}$ laminate and at a limited number of time/temperature conditions.

The bifurcation loads were determined using the STAGS-C1 finite elements shell analysis program. This analysis used the prebuckled linear displacement option to calculate the bifurcation loads. An increase in temperature and moisture absorption was found to cause a reduction in the panels bifurcation load ranging from a maximum of 25.6 percent for the $[0/45/-45/90]_s$ laminate to 34.5 percent for the $[45/-45]_{2s}$ laminate for the panels with a 12 in. radius. This reduction in the bifurcation load is significantly influenced by the change in curvature at elevated temperatures and moisture content. The maximum reduction in the bifurcation load varied from 34.5 percent for a 12 in. panel radius to 11.9 percent for a 10,000 in. panel radius a decrease of 22.6 percent for the $[45/-45]_{2s}$ laminate.

END

FILMED

3-86

DTIC